SPATIAL AND TEMPORAL TRENDS AND CONTROLLING FACTORS OF CARBONATE CHEMISTRY IN THE ESTUARIES OF THE NORTHWESTERN GULF OF MEXICO

A Dissertation

by

MELISSA RAE MCCUTCHEON

BS, Slippery Rock University, 2013
MS, Texas A&M University-Corpus Christi, 2015

Submitted in Partial Fulfillment of the Requirements for the Degree of

DOCTOR OF PHILOSOPHY

in

COASTAL AND MARINE SYSTEM SCIENCE

Texas A&M University-Corpus Christi
Corpus Christi, Texas

May 2021

May 2021

SPATIAL AND TEMPORAL TRENDS AND CONTROLLING FACTORS OF CARBONATE CHEMISTRY IN THE ESTUARIES OF THE NORTHWESTERN GULF OF MEXICO

A Dissertation

by

MELISSA RAE MCCUTCHEON

This dissertation meets the standards for scope and quality of
Texas A&M University-Corpus Christi and is hereby approved.

Xinping Hu, Ph.D.
Chair

Jennifer Beseres Pollack, Ph.D.
Committee Member

Benjamin Walther, Ph.D.
Committee Member

J. David Felix, Ph.D.
Committee Member

Barbara Szczerbinska, Ph.D.
Graduate Faculty Representative

May 2021

ABSTRACT

Estuarine carbonate chemistry is an important field of study because of its ties to coastal acidification (and associated ecological and economic impacts) as well as regional carbon budgets. This dissertation investigated the temporal and spatial variability in carbonate chemistry in estuaries of the northwestern Gulf of Mexico (nwGOM) as well as the relationships between the carbonate system and other environmental parameters. First, a four-decade dataset that spans seven estuaries along a latitudinal gradient was used investigate long-term trends in calculated carbonate system parameters. Partial pressure of CO_2 (pCO_2) was generally increasing, and rates indicated that the estuaries have become an increasing source of CO_2 to the atmosphere. Saturation state of aragonite (Ω_{Ar}) was generally decreasing across the region, suggesting that carbonate chemistry has become less suitable to calcifying organisms. Next diel and seasonal variability in pH and pCO_2 at a tidal inlet was assessed; variability was substantial over both timescales, though fluctuations were smaller than many other regions. Data from co-located environmental sensors suggested that temperature, net community metabolism, tidal fluctuations, and freshwater inflow all exerted important controls on the carbonate system, and pCO_2 was among the most important of many environmental parameters to distinguish between seasons and between day/night conditions. Finally, the last chapter investigated carbonate system dynamics in an estuary that experiences periodic summertime hypoxia. There was a positive relationship between pH and dissolved oxygen concentration; however, hypoxic conditions did not result in critically low pH as it has in other coastal systems. The high buffer capacity was attributed to strong evaporation and high productivity in adjacent seagrass meadows, highlighting the importance of intrinsic buffer capacity on the extent of hypoxia-induced acidification.

DEDICATION

This dissertation is dedicated to my grandma, “Gram”, a very special contributor to my life that passed away during the last year of my Ph.D. It is in large part because of the encouragement and support that I received from her and my grandpa, “Pa”, that I was able to pursue and achieve my goal of getting a Ph.D., and I will be forever grateful.

ACKNOWLEDGEMENTS

I would like to thank Texas A&M University-Corpus Christi (TAMUCC), the Harte Research Institute for Gulf of Mexico Studies, National Oceanic and Atmospheric Administration's (NOAA's) National Center for Coastal Ocean Science and Ocean Acidification Program, the National Science Foundation, the Coastal Bend Bays and Estuaries Program, the Mission-Aransas National Estuarine Research Reserve, the Texas General Land Office's Coastal Management Program, Texas Sea Grant's Grants-in-Aid of Graduate Research Program, TAMUCC's Center for Coastal Studies, the U.S. Geological Survey, and the Texas Commission on Environmental Quality for providing financial support, other research support, or data that made this dissertation possible.

I would like to extend my sincerest gratitude to my advisor, Dr. Xinping Hu, for being such a supportive mentor. I credit his guidance for much of my development as a scientist and independent researcher. I am also grateful that he not only allowed, but encouraged, me to pursue professional development opportunities that were outside of the realm of my dissertation research along the way. I regard those opportunities as some of my most rewarding professional experiences, and I know they will continue to shape my career path. I faced several personal hardships throughout the course of my Ph.D., and Dr. Hu always went beyond expectations in offering personal support or allowing special accommodations. It has been wonderful to work for someone that truly cares for the wellbeing of his lab members.

I also would like to extend my gratitude to my committee members, Drs. Jennifer Pollack, David Felix, and Ben Walther for their guidance and support. During the formation of my research direction and through the qualifying exams process, their varying expertise helped to expand my understanding of the interdisciplinary nature of coastal environmental science. I

especially appreciate the mentorship that I have received from Dr. Pollack, and I will always remember her encouraging me to be confident in myself and the fact that I can "build the plane while I am flying it".

I am grateful to have had wonderful lab mates throughout my time in the Hu lab. I would like to thank Hongjie Wang, Hongming Yao, Cory Staryk, Qiyuan Liu, Larissa Dias, Corrie Clark, and Eva Jundt for their collaboration and support over the years. I am especially thankful for the friendships that I build with Hongjie, Hongming, and Larissa, who I spent a lot of time traveling to conferences with and C.J., who I spent a lot of time conducting field work or lab work with. Throughout the course of grad school, I have also made many other friends at TAMUCC that I would like to acknowledge as being essential in getting me through these years.

I would also like to thank Dr. Sarah Cooley and Ryan Ono for allowing me the opportunity to work at Ocean Conservancy and guiding the work that I did there for my NSF-Funded non-academic research internship. Dr. Cooley—who I have always admired as a female scientist who has shaped a successful scientific career through a non-traditional career path—was a wonderful mentor who helped shape the way that I think about coastal environmental issues and science-backed management and policy.

Finally, I also need to extend gratitude to my family for their support throughout my education. My brother Ryan, as the first in the family to pursue a graduate degree in the sciences, has provided a lot of guidance and moral support along the way. Finally, my parents—despite having very little understanding of the process of graduate education or my field of study—have always encouraged me to pursue my dreams, and they have been critical in getting me through.

TABLE OF CONTENTS

LIST OF FIGURES

FIGURES PAGE

LIST OF TABLES

TABLES PAGE

CHAPTER I: INTRODUCTION

1.1 Defining ocean carbonate chemistry and its importance in marine environments

Humans have a strong connection, culturally and economically, to marine environments; however, humans' interaction with the environment and reliance on marine resources has led to several notable stressors faced by marine environments. These stressors include overfishing – including immense pressure on top ocean predators and the associated ecosystem disruption, pollution – including marine plastics and microplastics and mercury pollution, coastal eutrophication (i.e., the loading of excess nutrients), increases in harmful algal blooms, ocean warming, ocean deoxygenation, and ocean acidification. The later three of these challenges—warming, deoxygenation, and ocean acidification, all of which are primarily driven by increasing atmospheric carbon dioxide (CO_2) or the resulting climate change—are expected together to stress ocean environments in the coming decades and increasingly lead to changes to the ocean's ecosystems and biogeochemical cycles (Gruber, 2011).

Ocean acidification (OA) is the global increase in ocean acidity (i.e., increase in proton concentration or $[H^+]$ and decrease in pH) that results from the absorption of atmospheric CO_2 by surface waters (Cao et al. 2007; Doney et al. 2009; Feely et al. 2009; Orr et al. 2005). Ocean acidification is innately tied to carbonate chemistry, or the speciation of dissolved inorganic carbon (DIC). Equation 1.1 shows the sequence of equilibria reactions that alter the speciation of DIC in water (Zeebe and Wolf-Gladrow, 2003). Unlike most other gases absorbed in Earth's waters, CO_2 does not simply dissolve, but reacts with the water to form carbonic acid (H_2CO_3), which then dissociates and produces bicarbonate (HCO_3^-) and a proton (H^+). At seawater pH levels (~8), protons then react with carbonate (CO_3^{2-}) ions, decreasing CO_3^{2-} concentration and

further increasing that of HCO_3^-. Due to these reactions, an increase in atmospheric CO_2 by a certain factor does not result in the same factor of increase in DIC, but rather ~10% increase under current oceanic conditions (Zeebe and Wolf-Gladrow, 2003).

$$CO_{2(aq)} + H_2O \leftrightarrow H_2CO_3 \leftrightarrow H^+ + HCO_3^- \leftrightarrow 2H^+ + CO_3^- \qquad (1.1)$$

There are two primary reasons for scientific and stakeholder interest in marine carbonate chemistry, each of which is discussed in detail in the following sections. The first is that carbonate chemistry, especially acidification of natural waters, has important biological and subsequent economic implications. The second is that carbonate chemistry plays a large role in determining how a body of water contributes to carbon budgets through the flux of carbon between reservoirs. Carbonate chemistry can vary drastically between water bodies, so the following sections include descriptions of the open ocean, coastal ocean, and estuaries (i.e., coastal, semi-enclosed bodies of water where seawater is diluted by freshwater runoff from land).

1.2 Ocean, Coastal, and Estuarine Acidification: Causes and Implications

Acidification of the global surface oceans resulting from absorption of atmospheric CO_2 is occurring at a rate of 0.0017 – 0.0021 pH units per year (Carstensen and Duarte, 2019). Average global surface ocean pH has declined by approximately 0.1 units since the industrial revolution, which equates to ~30% increase in $[H^+]$ (Doney et al. 2020). There are many examples of coastal and estuarine waters that are also acidifying, though rates of change are more widely varying (Bauer et al. 2013; Feely et al. 2010; Hu and Cai, 2013).While atmospheric CO_2 drives OA on a global scale, it is not the only process altering carbonate chemistry in coastal waters and estuarine waters. Processes including altered net community metabolism (often caused by eutrophication), substantial river inputs, upwelling, or delivery of deep waters to the

surface by storm activity can all play an important role in the coastal oceans. Of the factors that can locally worsen acidification, eutrophication is likely the most globally prevalent, occurring in many areas of the coastal ocean as well as estuaries. Though high nutrient input intensifies community primary production, it is often followed by increases in bacterial respiration that consumes oxygen, often resulting in hypoxia, while producing CO_2 (i.e., lowering pH). This type of respiration-driven acidification has been observed in many places, including the GOM (Cai et al. 2011; Hu et al. 2018).

Estuarine carbonate chemistry is much more heterogeneous than the open ocean or even the majority of the coastal ocean, varying temporally and seasonally due to a myriad of biogeochemical processes which may locally exacerbate or alleviate OA (Hofmann et al. 2011). Changing land and resource use practices in the watershed, river geochemistry, volume of river input, net community metabolism, net calcification or $CaCO_3$ dissolution, submarine groundwater discharge, anaerobic activity in the sediment column, tidal fluctuations, estuarine circulation patterns, changing residence times, and atmospheric deposition from boat emissions all contribute to variability in carbonate chemistry (Mongin and Baird, 2014; Hofmann et al. 2011, Cyronak et al. 2013; De Weys et al. 2011; Jeffrey et al. 2016; Liu et al. 2014; Hassellov et al. 2013).

Temporal variability in coastal and estuarine pH far exceeds variability in the open ocean (Carstensen and Duarte, 2019). It is important to note that acidification effects, no matter the source of acidification, can be compounded by the short periods of more acidified conditions that occur with natural, biologically driven, diel fluctuations in the carbonate system (Gobler et al. 2017). Daily fluctuations in the carbonate system often exceed 0.1 pH units in coastal/estuarine environments, with some documented fluctuations exceeding 1 pH unit (Challener et al. 2016;

Cyronak et al. 2018; Schulz and Riebesell, 2013; Semesi et al. 2009; Yates et al. 2007). The largest fluctuations have been noted in regions that are less well buffered or already experience extremes in mean conditions due to biological activity, such as seagrass beds, oyster reefs, and coral reefs. Estuaries generally have less buffer capacity than ocean waters (Hu and Cai, 2013) as well as high biological activity, resulting in relatively large fluctuations in carbonate system speciation. Carbonate system fluctuations across all timescales are expected to intensify, resulting in continually lower minima, as ocean acidification further reduces the buffer capacity of the seawater endmember (Shaw et al. 2013). There have been few investigations of long-term acidification in estuaries due to a lack of long-term estuarine data. Of those studies that exist, estuarine waters are just as likely to have long-term increases in pH as long-term acidification, but rates of acidification have generally exceeded that of the open ocean (Carstensen and Duarte, 2019).

Many studies have indicated that various aspects of acidification—including increasing pCO_2, decreasing pH, and decreasing saturation state of calcium carbonate (Ω, Equation 1.2)—are linked to negative impacts to organismal and ecosystem health as well as loss of associated ecosystem services (Cooley et al. 2009; Ekstrom et al. 2015; Kleypas and Yates, 2009; Lemasson et al. 2017; Waldbusser and Salisbury, 2014; Yates and Halley, 2006). Organisms that form their shells or skeletons out of calcium carbonate ($CaCO_3$) have received particular focus in OA studies, as they are typically highly sensitive to changing carbonate chemistry. The calcification process (Equation 1.3), despite the direct utilization of HCO_3^-, is less thermodynamically favorable under lower CO_3^{2-} concentrations (i.e., lower Ω).

$$\Omega = \frac{[CO_3^{2-}][Ca^{2+}]}{K_{sp}} \qquad (1.2)$$

where K_{sp} is the apparent equilibrium solubility product at a given temperature, salinity, and pressure.

$$Ca^{2+} + 2HCO_3^- \rightarrow CaCO_3 + H_2O + CO_2 \qquad (1.3)$$

Calcareous organisms (e.g., oysters, clams, corals, and pteropods) often play important roles in marine ecosystems, serving as ecosystem engineers or occupying bottom trophic levels, so reduction of net calcification can have serious consequences for marine ecosystems (Andersson and Gledhill, 2013; Kleypas and Yates, 2009; Waldbusser et al. 2015; Wang et al. 2017). One calcareous organism that is especially economically and ecologically important in the region of this study is the Eastern Oyster, *Crassostrea virginica* (Culbertson et al. 2004). While oyster populations are still considered to be in "fair" condition in the GOM region compared to the dwindling populations around the world, the GOM has experienced 50%-89% loss from historical levels (Beck et al. 2009), and acidification in the region could serve as a secondary stressor and further reduce oyster population sizes. The impact to oysters is especially pertinent in the Texas estuaries, given the passage of Senate Bill 682 in 2019, which permitted oyster aquaculture on the Texas coast for the first time. This new industry will rely heavily on the suitable water chemistry for oyster growth.

OA may also have important physiological impacts on non-calcifiers. Many fish species have shown effective pH compensation strategies, however that does not necessarily translate to tolerance for acidification (Heuer and Grosell, 2014). Current and near-future CO_2 effects have been shown to manifest through many aspects of fish physiology, including metabolic rates, mitochondrial function, otolith development, larval yolk consumption, larval settlement, olfactory senses, chemical cue recognition, and behavior (Espinel-velasco et al. 2018; Heuer and Grosell, 2014). While OA is primarily regarded as a secondary threat to marine organisms, it has

been suggested that continued OA will impact phytoplankton community function more than other anticipated ocean changes like warming or nutrient supply, favoring diazotrophs (nitrogen fixers) and large phytoplankton like dinoflagellates over smaller taxa (Dutkiewicz et al. 2015). OA is also likely to improve the competitive fitness of harmful algal bloom (HAB) species, allowing them to outcompete other taxa (Brandenburg et al. 2019). This increased fitness along with expected increases in toxin production in high CO_2 environments has the potential to exacerbate the negative effects of HABs on humans and marine ecosystems.

1.3 Global Carbon Budget Contribution of Marine Waters

Since the start of the industrial revolution, anthropogenic CO_2 emissions from fossil fuel combustion, cement production, and deforestation have led to an increase in atmospheric CO_2—currently at a rate of 5.1 Pg C yr^{-1}—that has resulted in global climate change (Friedlingstein et al. 2020). The global oceans are the largest single reservoir for carbon, holding more than 98% of the CO_2 in the ocean-atmosphere system is in the form of DIC (Friedlingstein et al. 2020). Oceanic stores of organic carbon are considerably less than DIC, yet they are still on the same order of magnitude as atmospheric carbon stores (Friedlingstein et al. 2020).

There is considerable CO_2 exchange between water and the atmosphere; the global oceans have absorbed nearly one third of anthropogenic CO_2 emissions. The net air-sea exchange of CO_2 (CO_2 flux) is a function of the gradient between the atmospheric partial pressure of CO_2 (pCO_2) and the pCO_2 of the surface water, as can be seen in the most broadly used flux calculation (Eq 1.4, Wanninkhof, 1992). Over the past several decades, increasing atmospheric CO_2 has maintained a relatively constant air-sea pCO_2 gradient, causing the ocean act as a CO_2 sink (absorbing CO_2 from the atmosphere). Open ocean CO_2 flux is relatively well constrained, occurring at a rate of ~2.5 Pg C yr^{-1} (Friedlingstein et al. 2020).

$$F = k K_0 (pCO_{2(w)} - pCO_{2(a)}) \qquad (1.4)$$

where k is the gas transfer velocity (which changes with turbulence), K_0 is the aqueous phase solubility of CO_2, and $pCO_{2,w}$ and $pCO_{2,a}$ are the pCO_2 in the water and air, respectively.

While the open ocean is a relatively stable sink for atmospheric CO_2, coastal areas vary. Subtropical to tropical marginal seas are generally net CO_2 sources, i.e., outgas CO_2, while high and temperature latitude areas are generally CO_2 sinks (Borges et al. 2005). The magnitude of the sink/source often fluctuates on a seasonal basis. Large river plumes often act as CO_2 sinks due to nutrient-stimulated high algal biomass and primary productivity; the Amazon and Mississippi river plumes are some of the most substantial marine CO_2 sinks (Cooley et al. 2007; Guo et al. 2012).

If the rate of change of pCO_2 in water differs from that of the atmosphere, the capacity for the water to absorb CO_2 or emit CO_2 will be altered, causing strengthening of a sink/source or even reversal between sink/source (Landschützer et al. 2016, 2014). Model simulations indicate that global coastal oceans have recently switched from a net CO_2 source (which they were over most of the past 300 years) to a CO_2 sink, with the shift primarily driven by rising atmospheric CO_2 as well as increasing nutrient loading (Andersson et al. 2005). Direct warming effects and upwelling also have the potential to alter coastal pCO_2 trends so that they may not mirror atmospheric pCO_2 trends, as has been noted in the eastern boundary current and western boundary current regions, respectively (Wang et al. 2017). Even within smaller geographic regions, long-term trends in surface pCO_2 may vary; for example, pCO_2 trends are higher than atmospheric rates in the northwestern Gulf of Mexico (nwGOM) and West Florida Shelf but lower than atmospheric rates in central GOM (Kealoha et al. 2020).

The contribution of estuaries to the global carbon budget is believed to be significant despite their relatively small surface area (Bauer et al. 2013; Cai, 2011). On a global scale, estuaries are believed to be a source of CO_2 to the atmosphere, though the magnitude of this source is not well-quantified because of data gaps and substantial heterogeneity within and between estuaries (Cai, 2011; Chen et al. 2013). Net ecosystem metabolism is often the most important driving factor of estuarine pCO_2 and CO_2 flux. Estuarine outgassing of CO_2 is primarily driven by net heterotrophy (respiration exceeding photosynthesis), which is common in estuaries due to organic matter loading from the land (Bauer et al. 2013; Cai et al. 1999; Raymond et al. 2000). Some cases of net heterotrophy can cause severe separation between atmospheric and estuarine pCO_2; for example the Scheldt estuary in the Netherlands can have a pCO_2 as high as 8500 μatm compared to a much lower level in the atmosphere (Frankignoulle and Borges, 2001).

More freshwater-influenced regions of the estuaries are generally more net heterotrophic than the rest of the estuary due to direct allochthonous carbon input (Caffrey, 2004), creating a gradient of pCO_2 and CO_2 flux along the salinity gradient within an estuary. On average, the upper extent of an estuary with low salinity is usually a strong source of CO_2 to the atmosphere, the mid-estuary with salinities ranging from 2 to 25 acts as a moderate source, and the lower, more saline extent of the estuary acts as a weak source (Chen et al. 2013). Temperature is often the most important controlling factor of local variability of net community metabolism, producing strong seasonal shifts that may cause net autotrophy for a portion of the year in estuaries that annually exhibit net heterotrophy (Caffrey, 2004). High-frequency data suggest that this switch between autotrophic and heterotrophic can occur at fairly frequent intervals (Shadwick et al. 2019).

Aside from respiration of allochthonous (and autochthonous) organic carbon, other biogeochemical processes also serve as a source of DIC to estuaries and lead to elevated CO_2 flux. Among these are DIC inputs from rivers and intertidal marshes and submarine groundwater discharge of high-pCO_2 water (Bianchi, 2007; Cai et al. 2003). Additionally, the process of calcification may increase water pCO_2, contributing to the CO_2 outgassing experienced at most oyster reefs (Frankignoulle et al. 1994; Lejart et al. 2011). While one study reported long-term decreases in pCO_2 in two low-salinity areas of Chesapeake Bay (Prasad et al. 2013), there has been only one published study reporting values for annual rates of change in estuarine pCO_2. Three Danish fjords have had increasing pCO_2 at rates ~4 times higher than ocean and atmospheric rates, indicating that Danish fjords are becoming an increasing source of CO_2 (Carstensen et al. 2018).

1.4 Contributions of this dissertation

Sufficient carbonate chemistry data are still lacking in the global coastal zones, especially in the Gulf of Mexico region and its estuaries. Texas Commission on Environmental Quality (TCEQ) has sustained one of the longest-running estuarine water quality monitoring efforts to include two carbonate system parameters (pH and TA). These data are used in Chapter II for calculations of the full carbonate system and long-term trends in seven estuaries along the northwestern Gulf of Mexico (nwGOM) coast. This is only the second investigation to date of long-term trends in any estuarine environment in the most biologically relevant carbonate system parameters (pCO_2 and Ω) and the most carbon budget-relevant parameters (pCO_2 and DIC). Chapter II also investigates long-term trends in the buffer factor, β_{DIC}, providing insight to the way the pH response of the nwGOM estuaries to DIC addition has changed over time.

High temporal frequency carbonate chemistry data from sensors are especially rare in estuaries. The first relatively large-scale deployment of sensors to monitor carbonate chemistry in estuarine environments began in 2015 when the U.S. Environmental Protection Agency (EPA) funded the purchase of autonomous sensors for pH and pCO_2 to be deployed in seven estuaries around the United States. Data from one of these estuaries, the Mission-Aransas Estuary in the nwGOM, is investigated in Chapter III. Hourly sensor data are used to investigate daily variability in the carbonate system at the Aransas Ship Channel, the outlet of the Mission-Aransas Estuary to the Gulf of Mexico. Carbonate chemistry data are also combined with data from other co-located environmental sensors to investigate the driving factors in carbonate system variability. Sensor data are also used in combination with 5+ years of monthly, laboratory-analyzed, discrete water samples to investigate seasonal variability and air-sea CO_2 fluxes, and results from the two methods are compared.

There is a known correlation between oxygen and DIC concentrations in coastal water, as respiration can drive both deoxygenation and acidification. Chapter IV investigates the intensity of respiration-induced acidification in an area that experiences periodic summertime hypoxia (Corpus Christi Bay, nwGOM). The changes in the pH and Ω associated with hypoxic conditions are explored and compared to other coastal and estuarine systems. Local influences on carbonate chemistry including seagrass beds, strong evaporation, and hydrologic fluctuation are discussed, and a conceptual model is developed to explain the unique carbonate system response to hypoxia in the region. All chapters together, this dissertation will serve to further the field of estuarine carbonate chemistry in a way that is applicable to coastal ecosystem health.

References

Andersson, A.J., Gledhill, D. 2013. Ocean acidification and coral reefs: effects on breakdown, dissolution, and net ecosystem calcification. *Annual Review of Marine Science* 5: 321–48.

Andersson, A.J., Mackenzie, F.T., Lerman, A. 2005. Coastal ocean and carbonate systems in the high CO_2 world of the Anthropocene. *American Journal of Science* 305: 875–918.

Bauer, J.E., Cai, W.-J., Raymond, P. a., Bianchi, T.S., Hopkinson, C.S., Regnier, P. A. G. 2013. The changing carbon cycle of the coastal ocean. *Nature* 504: 61–70.

Beck, M.W., Brumbaugh, R.D., Airoldi, L., Carranza, A., Coen, L.D., Crawford, C., Defeo, O., Edgar, G.J., Hancock, B., Kay, M., Lenihan, H., Luckenbach, M.W., Toropova, C.L., Zhang, G. 2009. Shellfish reefs at risk: A global analysis of problems and solutions. The Nature Conservancy, Arlington VA. *pp* 1-52.

Bianchi, T.S. 2007. Biogeochemistry of Estuaries. New York.

Borges, A. V, Delille, B., Frankignoulle, M. 2005. Budgeting sinks and sources of CO_2 in the coastal ocean: Diversity of ecosystems counts. *Geophysical Research Letters* 32: 2–5.

Brandenburg, K.M., Velthuis, M., Van de Waal, D.B. 2019. Meta□analysis reveals enhanced growth of marine harmful algae from temperate regions with warming and elevated CO_2 levels . *Global Change Biology* 25: 2607–2618.

Caffrey, J.M. 2004. Factors controlling net ecosystem metabolism in U.S. estuaries. *Estuaries* 27: 90–101.

Cai, W.-J. 2011. Estuarine and coastal ocean carbon paradox: CO_2 sinks or sites of terrestrial carbon incineration? *Annual Review of Marine Science* 3: 123–45.

Cai, W.-J., Hu, X., Huang, W.-J., Murrell, M.C., Lehrter, J.C., Lohrenz, S.E., Chou, W.-C., Zhai, W., Hollibaugh, J.T., Wang, Y., Zhao, P., Guo, X., Gundersen, K., Dai, M., Gong, G.-C. 2011. Acidification of subsurface coastal waters enhanced by eutrophication. *Nature Geoscience* 4: 766–770.

Cai, W.-J., Pomeroy, L.R., Moran, M.A., Wang, Y. 1999. Oxygen and carbon dioxide mass balance for the estuarine-intertidal marsh complex of five rivers in the southeastern U.S. *Limnology and Oceanography* 44: 639–649.

Cai, W.J., Wang, Y., Krest, J., Moore, W.S. 2003. The geochemistry of dissolved inorganic carbon in a surficial groundwater aquifer in North Inlet, South Carolina, and the carbon fluxes to the coastal ocean. *Geochimica et Cosmochimica Acta* 67: 631–637.

Cao, L., Caldeira, K., Jain, A.K. 2007. Effects of carbon dioxide and climate change on ocean acidification and carbonate mineral saturation. *Geophysical Research Letters* 34: 1-5.

Carstensen, J., Chierici, M., Gustafsson, B.G., Gustafsson, E. 2018. Long-term and seasonal trends in estuarine and coastal carbonate systems. *Global Biogeochemical Cycles* 32: 1271–1288.

Carstensen, J., Duarte, C.M. 2019. Drivers of pH variability in coastal ecosystems. *Environmental Science & Technology* 53: 4020–4029.

Challener, R.C., Robbins, L.L., Mcclintock, J.B. 2016. Variability of the carbonate chemistry in a shallow, seagrass-dominated ecosystem: Implications for ocean acidification experiments. *Marine and Freshwater Research* 67: 163–172.

Chen, C.T.A., Huang, T.H., Chen, Y.C., Bai, Y., He, X., Kang, Y. 2013. Air-sea exchanges of

CO_2 in the world's coastal seas. *Biogeosciences* 10: 6509–6544.

Cooley, S.R., Coles, V.J., Subramaniam, A., Yager, P.L. 2007. Seasonal variations in the Amazon plume-related atmospheric carbon sink. *Global Biogeochemical Cycles* 21, 1–15.

Cooley, S.R., Kite-Powell, H.L., Doney, S.C. 2009. Ocean acidification's potential to alter global marine ecosystem services. *Oceanography* 22: 172–181.

Culbertson, J., Robinson, L., Campbell, P., Butler, L. 2004. Trends in Texas commercial fishery landing, 1972-1996, Texas Parks & Wildlife Management Data Series.

Cyronak, T., Andersson, A.J., D'Angelo, S., Bresnahan, P., Davidson, C., Griffin, A., Kindeberg, T., Pennise, J., Takeshita, Y., White, M. 2018. Short-term spatial and temporal carbonate chemistry variability in two contrasting seagrass meadows: Implications for pH buffering capacities. *Estuaries and Coasts* 41: 1282–1296.

Doney, S.C., Busch, D.S., Cooley, S.R., Kroeker, K.J. 2020. The impacts of ocean acidification on marine ecosystems and reliant human communities. *The Annual Review of Environmental Resources* 45: 83–112.

Doney, S.C., Fabry, V.J., Feely, R. A., Kleypas, J. A. 2009. Ocean acidification: the other CO_2 problem. *Annual Review of Marine Science* 1: 169–192.

Dutkiewicz, S., Morris, J.J., Follows, M.J., Scott, J., Levitan, O., Dyhrman, S.T., Berman-Frank, I. 2015. Impact of ocean acidification on the structure of future phytoplankton communities. *Nature Climate Change* 5: 1002–1006.

Ekstrom, J. a., Suatoni, L., Cooley, S.R., Pendleton, L.H., Waldbusser, G.G., Cinner, J.E., Ritter, J., Langdon, C., van Hooidonk, R., Gledhill, D., Wellman, K., Beck, M.W., Brander, L.M.,

Rittschof, D., Doherty, C., Edwards, P.E.T., Portela, R. 2015. Vulnerability and adaptation of US shellfisheries to ocean acidification. *Nature Climate Change* 5: 3: 207-214.

Espinel-velasco, N., Hoffmann, L., Agüera, A., Byrne, M., Dupont, S., Uthicke, S., Webster, N.S., Lamare, M. 2018. Effects of ocean acidification on the settlement and metamorphosis of marine invertebrate and fish larvae : a review. *Marine Ecology Progress Series* 606: 237–257.

Feely, R. A., Alin, S.R., Newton, J., Sabine, C.L., Warner, M., Devol, A., Krembs, C., Maloy, C. 2010. The combined effects of ocean acidification, mixing, and respiration on pH and carbonate saturation in an urbanized estuary. *Estuarine, Coastal, and Shelf Science* 88: 442–449.

Feely, R., Doney, S., Cooley, S. 2009. Ocean acidification: Present conditions and future changes in a high-CO_2 world. *Oceanography* 22: 36-47.

Frankignoulle, M., Borges, A.V. 2001. Direct and indirect pCO_2 measurements in a wide range of pCO_2 and salinity values (The Scheldt Estuary). *Aquatic Geochemistry* 7: 267–273.

Frankignoulle, M., Canon, C., Gattuso, J.-P. 1994. Marine calcification as a source of carbon dioxide: Positive feedback of increasing atmospheric CO_2. *Limnology and Oceanography* 39: 458–462.

Friedlingstein, P., Sullivan, M.O., Jones, M.W., Andrew, R.M., Hauck, J. 2020. Global Carbon Budget 2020: 3269–3340.

Gobler, C.J., Clark, H.R., Griffith, A.W., Lusty, M.W. 2017. Diurnal fluctuations in acidification and hypoxia reduce growth and survival of larval and juvenile bay scallops (*Argopecten*

irradians) and hard clams (*Mercenaria mercenaria*). *Frontiers in Marine Science* 3: 282: 1–13.

Gruber, N. 2011. Warming up, turning sour, losing breath: Ocean biogeochemistry under global change. *Philosophical Transaction of the Royal Society, Mathematical, Physical and Engineering Sciences* 369: 1980–1996.

Guo, X., Cai, W.-J., Huang, W.-J., Wang, Y., Chen, F., Murrell, M.C., Lohrenz, S.E., Jiang, L.-Q., Dai, M., Hartmann, J., Lin, Q., Culp, R. 2012. Carbon dynamics and community production in the Mississippi River plume. *Limnology and Oceanography* 57: 1–17.

Heuer, R.M., Grosell, M. 2014. Physiological impacts of elevated carbon dioxide and ocean acidification on fish. *American Journal of Physiology - Regulatory Integrative and Comparative Physiology*, R1061 - R1084

Hofmann, G.E., Smith, J.E., Johnson, K.S., Send, U., Levin, L. a, Micheli, F., Paytan, A., Price, N.N., Peterson, B., Takeshita, Y., Matson, P.G., Crook, E.D., Kroeker, K.J., Gambi, M.C., Rivest, E.B., Frieder, C. a, Yu, P.C., Martz, T.R. 2011. High-frequency dynamics of ocean pH: a multi-ecosystem comparison. *PLoS One* 6: 12: e28983.

Hu, X., Beseres Pollack, J., McCutcheon, M.R., Montagna, P. a., Ouyang, Z. 2015. Long-term alkalinity decrease and acidification of estuaries in Northwestern Gulf of Mexico. *Environmental Science and Technology* 49: 3401–3409.

Hu, X., Cai, W.-J. 2013. Estuarine acidification and minimum buffer zone-A conceptual study. *Geophysical Research Letters* 40: 5176–5181.

Hu, X., Nuttall, M.F., Wang, H., Yao, H., Staryk, C.J., McCutcheon, M.R., Eckert, R.J., Embesi,

J.A., Johnston, M.A., Hickerson, E.L., Schmahl, G.P., Manzello, D., Enochs, I.C., DiMarco, S., Barbero, L. 2018. Seasonal variability of carbonate chemistry and decadal changes in waters of a marine sanctuary in the Northwestern Gulf of Mexico. *Marine Chemistry* 205: 16–28.

Kealoha, A.K., Shamberger, K.E.F., DiMarco, S.F., Thyng, K.M., Hetland, R.D., Manzello, D.P., Slowey, N.C., Enochs, I.C. 2020. Surface water CO_2 variability in the Gulf of Mexico (1996–2017). *Scientific Reports* 10: 1–13.

Kleypas, J.A., Yates, K.K. 2009. Coral reefs and ocean acidification. *Oceanography* 22: 108–117.

Landschützer, P., Gruber, N., Bakker, D.C.E. 2016. Decadal variations and trends of the global ocean carbon sink. *Global Biogeochemical Cycles* 30: 1396–1417.

Landschützer, P., Gruber, N., Bakker, D.C.E., Schuster, U. 2014. Recent variability of the global ocean carbon sink. *Global Biogeochemical Cycles* 28: 927–949.

Lejart, M., Clavier, J., Chauvaud, L., Hily, C. 2011. Respiration and calcification of *Crassostrea gigas*: Contribution of an intertidal invasive species to coastal ecosystem CO_2 fluxes. *Estuaries and Coasts* 35: 622–632.

Lemasson, A.J., Fletcher, S., Hall-Spencer, J.M., Knights, A.M. 2017. Linking the biological impacts of ocean acidification on oysters to changes in ecosystem services: A review. *Journal of Experimental Marine Biology and Ecology* 492: 49-62.

Orr, J.C., Fabry, V.J., Aumont, O., Bopp, L., Doney, S.C., Feely, R. A, Gnanadesikan, A., Gruber, N., Ishida, A., Joos, F., Key, R.M., Lindsay, K., Maier-Reimer, E., Matear, R.,

Monfray, P., Mouchet, A., Najjar, R.G., Plattner, G.-K., Rodgers, K.B., Sabine, C.L., Sarmiento, J.L., Schlitzer, R., Slater, R.D., Totterdell, I.J., Weirig, M.-F., Yamanaka, Y., Yool, A. 2005. Anthropogenic ocean acidification over the twenty-first century and its impact on calcifying organisms. *Nature* 437: 681–686.

Prasad, M.B.K., Kaushal, S.S., Murtugudde, R. 2013. Long-term pCO_2 dynamics in rivers in the Chesapeake Bay watershed. *Applied Geochemistry* 31: 209–215.

Pritchard, D. W. (1967) *What is an estuary: physical viewpoint*. p. 3–5 *in:* G. H. Lauf (ed.) *Estuaries*, A.A.A.S. Publ. No. 83, Washington, D.C.

Raymond, P. a., Bauer, J.E., Cole, J.J. 2000. Atmospheric CO_2 evasion, dissolved inorganic carbon production, and net heterotrophy in the York River estuary. *Limnology and Oceanography*. 45: 1707–1717.

Robbins, L.L., Lisle, J.T. 2018. Regional acidification trends in Florida shellfish estuaries: a 20+ year look at pH, oxygen, temperature, and salinity. *Estuaries and Coasts* 41: 1268–1281.

Schulz, K.G., Riebesell, U. 2013. Diurnal changes in seawater carbonate chemistry speciation at increasing atmospheric carbon dioxide. *Marine Biology* 160: 1889–1899.

Semesi, I.S., Beer, S., Björk, M. 2009. Seagrass photosynthesis controls rates of calcification and photosynthesis of calcareous macroalgae in a tropical seagrass meadow. *Marine Ecological Progress Series*. 382: 41–47.

Shadwick, E.H., Friedrichs, M.A.M., Najjar, R.G., De Meo, O.A., Friedman, J.R., Da, F., Reay, W.G. 2019. High-frequency CO_2 system variability over the winter-to-spring transition in a coastal plain estuary. *Journal of Geophysical Research* 124: 11: 7646–7642.

Waldbusser, G.G., Hales, B., Langdon, C.J., Haley, B.A., Schrader, P., Brunner, E.L., Gray, M.W., Miller, C.A., Gimenez, I. 2015. Saturation-state sensitivity of marine bivalve larvae to ocean acidification. *Nature Climate Change* 5: 273–280.

Waldbusser, G.G., Salisbury, J.E. 2014. Ocean acidification in the coastal zone from an organism's perspective: multiple system parameters, frequency domains, and habitats. *Annual Review of Marine Science* 6: 221–47.

Wang, H., Hu, X., Cai, W.J., Sterba-Boatwright, B. 2017. Decadal fCO_2 trends in global ocean margins and adjacent boundary current-influenced areas. *Geophysical Research Letters* 44: 8962–8970.

Wang, Z.A., Lawson, G.L., Pilskaln, C., Maas, A. 2017. Seasonal control of aragonite saturation states in the Gulf of Maine. *Journal of Geophysical Research*: *Oceans* 122: 372–389.

Wanninkhof, R.H. 1992. Relationship between wind speed and gas exchange. *Journal of Geophysical Research*: *Oceans* 97: 7373–7382.

Yates, K.K., Dufore, C., Smiley, N., Jackson, C., Halley, R.B. 2007. Diurnal variation of oxygen and carbonate system parameters in Tampa Bay and Florida Bay. *Marine Chemistry* 104: 110–124.

Yates, K.K., and R.B. Halley. 2006. CO_3^{2-} concentration and pCO_2 thresholds for calcification and dissolution on the Molokai reef flat, Hawaii. *Biogeosciences* 3: 357-369.

Zeebe, R.E., Wolf-Gladrow, D. 2003. CO_2 in Seawater: Equilibrium, Kinetics, Isotopes.

CHAPTER II: LONG-TERM TRENDS IN THE CARBONATE CHEMISTRY OF THE ESTUARIES OF THE NORTHWESTERN GULF OF MEXICO

Abstract

A four-decade dataset that spans seven estuaries along a latitudinal gradient in the northwestern Gulf of Mexico and includes measurements of pH and total alkalinity was used to calculate partial pressure of CO_2 (pCO_2), dissolved inorganic carbon (DIC), saturation state of aragonite (Ω_{Ar}), and the buffer factor β_{DIC} and examine long-term trends and spatial patterns in these parameters. With the notable exception of the northernmost and southernmost estuaries (and select stations near freshwater input), these estuaries have generally experienced long-term increases in pCO_2 and decreases in DIC, Ω_{Ar}, and β_{DIC}, with the magnitude of change generally increasing from north to south.

At all stations with increasing pCO_2, the rate of increase exceeded the rate of increase in atmospheric pCO_2, indicating that these estuaries have become a greater source of CO_2 to the atmosphere over the last decades. The decreases in Ω_{Ar} have yet to cause Ω_{Ar} to reach undersaturation, but even the observed decreases may have the potential to decrease calcification rates in important estuarine calcifiers like oysters. The decreases in β_{DIC} directly indicate for the first time in any estuarine environment that these estuaries have experienced continually greater change in pH with a given addition of DIC over past decades.

2.1 Introduction

Unlike the acidification of the open oceans that is driven almost solely by the ocean's uptake of atmospheric CO_2, the changing carbonate chemistry of coastal and estuarine environments is modulated by several regional to local factors that are superimposed on global

trends. The high temporal and spatial heterogeneity in estuarine carbonate chemistry is driven by the complex interactions between watershed dynamics, riverine input of nutrients and organic matter, changing net ecosystem metabolism, changes to upwelling, mixing between and within reservoirs, and reservoir residence time (Frankignoulle et al. 1994; Cai et al. 2003; Feely et al. 2010; Hofmann et al. 2011; Lejart et al. 2011; Mongin and Baird 2014; Wallace et al. 2014; Challener et al. 2016).

Of all contributing biogeochemical processes, net ecosystem metabolism (NEM) is often the major driver of the carbonate system in estuaries (Wallace et al. 2014), with the exception of the river-dominated upper reaches of some estuaries where riverine CO_2 inputs become dominant (Joesoef et al. 2015; Van Dam et al. 2018). The majority of the world's estuaries are net heterotrophic because of terrestrial organic matter loading, and as a result they generally have elevated partial pressure of CO_2 (pCO_2) and act as a source of CO_2 to the atmosphere (Cai et al. 1999; Raymond et al. 2000; Bauer et al. 2013). For example, the Scheldt estuary in the Netherlands can have a pCO_2 as high as 8500 μatm (Frankignoulle and Borges 2001), which is substantially higher than open ocean pCO_2 that is usually near equilibrium with atmospheric pCO_2. Subsequently, estuaries can substantially contribute to global carbon cycles, with studies estimating that the magnitude of estuarine air-water CO_2 flux is nearly the same as that of continental shelves, even though the latter occupy ~24 times more surface area (Cai 2011; Bauer et al. 2013).

Several regional studies have demonstrated long-term trends in carbonate system parameters, primarily pH and total alkalinity (TA), in estuarine and coastal environments (Waldbusser et al. 2011b; Hu et al. 2015; Carstensen et al. 2018; Robbins and Lisle 2018; Carstensen and Duarte 2019; Najjar et al. 2019). It was previously demonstrated that the bays in

the nwGOM (our study area) have experienced long-term declines in pH and TA, which was hypothesized to be caused by long-term decreases in freshwater inflow of high-alkalinity rivers and accompanying decreases in TA delivery to the bays (Hu et al. 2015). While the identification of pH and TA trends was an important first step in understanding the system and defining management strategies, several other carbonate system parameters may be more informative about the effect of these symptoms of acidification on an estuary and its biological communities. In this chapter long-term trends in pCO_2 are first explored, which is the most important factor to understand carbon budget and air-sea flux implications. Long-term trends in total dissolved inorganic carbon (DIC) are next explored, another carbon budget-relevant parameter. Trends in saturation state of aragonite (Ω_{Ar}) are next explored, which is likely the most important factor to understand biological implications, particularly the potential difficulty for calcifiers (e.g., oysters) to build and maintain their calcium carbonate skeletons (de Putron et al. 2011; Waldbusser et al. 2015). Finally, long-term trends in β_{DIC} ($(\partial \ln[H^+]/\partial DIC)^{-1}$), a buffer factor that represents the amount of change in pH that occurs with a given addition of DIC (Egleston et al. 2010), are explored. Long-term trends in pH and TA will also be reported for each station (as stations were not aggregated into bay entities as was done in Hu et al. (2015) and an additional five years of data (2010-2015) were available in addition to the earlier analysis). Differences over geographic space in long-term trends, potential drivers of trends, and implications of trends are discussed.

2.2 Methods

2.2.1 Study site

The studied region includes seven estuaries that border the Texas coast in the northwestern Gulf of Mexico (nwGOM)—spanning north to south they are Sabine-Neches

Estuary (SNE), Trinity-San Jacinto Estuary (TSJ), Lavaca-Colorado Estuary (LCE), Guadalupe Estuary (GE), Mission-Aransas Estuary (MAE), Nueces Estuary (NE), and Laguna Madre Estuary (LM) (Fig. 1). This region hosts 595 km of coastline that lies between 26° N and 30° N in a subtropical climate. The nwGOM estuaries are relatively shallow (rarely exceeding 3 m deep), and they are classified as lagoons due to their connectivity and the barrier island system that separates them from the Gulf of Mexico and limits water exchange (Russell et al. 2007; Montagna et al. 2011b). Along with other lagoonal bays that span the majority of the Gulf of Mexico coast, these estuaries make up part of the largest lagoonal system in the world (Dürr et al. 2011).

The area closest to the Louisiana border experiences twice the rate of precipitation as the area closest to the Mexico border. Together with an evaporation gradient, this yields a freshwater balance (sum of all freshwater input via rivers, runoff, and direct precipitation minus evaporation) that is two orders of magnitude higher in the northernmost estuary, i.e., SNE, than in the southernmost estuary, i.e., LM (Montagna et al. 2011a). The differing freshwater balance as well as different in land use and land cover between estuaries yields differing chemical properties, making these seven estuaries chemically unique despite their physical similarities.

2.2.2 Data sources and statistical treatment

Historical water quality data were obtained from the Texas Commission on Environmental Quality's (TCEQ's) Surface Water Quality Monitoring (SWQM) program. TCEQ has collected and compiled water quality data on a quarterly basis across the nwGOM estuaries since 1969, though years of monitoring have varied between stations. Only those stations with 20+ years of data (including one station in SNE, 10 in TSJ, 13 in LCE, two in GE, five in MAE, 13 in NE, and 10 in LM) and only those stations with 60+ simultaneous measurements for

temperature, salinity (or working salinity as defined below), pH, and TA were used for our analyses. Filtering to remove missing data necessary for carbonate system calculations resulted in removal of all data from 1969-1973; hence the earliest data used in this study were from 1974.

Measurement of TA by TCEQ involved titration to a pH of 4.5 and was monitored using a pH electrode with calibrated acid (H_2SO_4 or HCl) in accordance with EPA Protocol 310.1. Analytical precision of this type of interlaboratory methodology would be expected to have a precision of around 5% (Hu et al. 2015). TA is reported by TCEQ in mg-$CaCO_3$ L^{-1}, but it was converted to μmol kg^{-1} by multiplying by a factor of 20 and dividing by sample density (derived from salinity and room temperature at 22˚C) for this analysis. Measurement of pH by TCEQ involved pH sensors that were calibrated daily using a two-point calibration approach with National Institute of Standards and Technology pH 7.00 and 10.00 buffers, and the values were temperature compensated to reflect in situ conditions. Analytical precision was not reported by TCEQ for the pH measurements, although protocol did require measurements to be rounded to the tenth decimal place, so an uncertainty of up to 0.1 can be assumed. McLaughlin et al. (2017) reported that potentiometric pH sensors in coastal monitoring have error of ±0.2 pH units, but this is within deployed SeaBird instruments that may have additional sources of error (e.g., much deeper depth). For those observations that salinity data were missing but specific conductance data were available, a working salinity value was calculated using the linear relationship between specific conductance and salinity (R^2= 0.98, as calculated from those records with both salinity and specific conductance data). Working salinity values that were calculated to be ≤ 0 (3% of the 2747 calculated values) were removed from the analysis.

We used an intensive outlier removal approach that aimed to remove occurrences of falsely reported data due to any human or instrument error coming from the multiple laboratories

that analyze TCEQ SWQM samples. Outliers were defined as measurements that were three times the interquartile range (IQR) above quartile three (Q3) or three times the IQR below Q1 within bracketed subsets. This approach assumes that some outliers are representative of the system and therefore removes fewer data than the standard outlier calculation. Temperature outliers were removed within seasonal brackets (eight observations removed). There were no salinity observations that were deemed outliers.

A two-step approach for outlier removal based on both bracketed time and salinity intervals was conducted for pH and TA measurements, as was done by Hu et al. (2015). Seven time brackets were established (5-year intervals) and nine salinity brackets were established (with a range of 5 salinity units for salinity < 35 and 35-49.99 and 50+ to encompass the relatively limited observations at hypersalinity). Those observations of each parameter that were deemed outliers within either a time bracket or a salinity bracket were removed.

2.2.3 Calculation of carbonate system parameters

TCEQ's measured *in situ* temperature, salinity (or specific conductance that can be converted to working salinity), pH (converted from NBS scale to total scale), and TA were used as inputs to the Seacarb package in R for calculation of other carbonate system parameters, propagated error associated with carbonate system parameters, and the β_{DIC} buffer factor (R Core Team, 2020; Gattuso et al. 2021). For speciation calculations, the carbonic acid dissociation constants K_1 and K_2 were from Millero (2010), the HF dissociation constant was from Perez and Fraga (1987), the HSO_4^- dissociation constant was from Dickson (1990), and boron concentration was from Uppström (1974). Nutrient contributions (phosphate, silica, ammonium) to TA were not included in speciation calculations, as they were not consistently measured and are assumed to be negligible to TA. Propagated error was calculated using the Gaussian method

1st order, 2nd moment analysis using analytical precision as the standard deviation associated with each of the measured variables (temp= 0.1, Sal = 0.1, pH = 0.1, TA= 115 μmol kg^{-1}). The β_{DIC} buffer factor was calculated using the appropriately corrected equation from Egleston et al. (2010).

The calculated Ω_{Ar} was corrected to account for non-zero calcium concentrations ($[Ca^{2+}]$) in the river end members. Separate corrections were performed for each estuary to reflect different river chemistries. For those estuaries that TCEQ had sufficient $[Ca^{2+}]$ data—TSJ, LCE, NE, and LM (59, 26, 58, and 9 aligning $[Ca^{2+}]$ and salinity observations, respectively)—a linear regression between TCEQ measured $[Ca^{2+}]$ and salinity within each estuary was used to estimate $[Ca^{2+}]$ for every date/station observation. A correction to Ω_{Ar} was then conducted based on the difference between theoretical $[Ca^{2+}]$ (with freshwater endmember having zero $[Ca^{2+}]$) and the actual (i.e., estimated) $[Ca^{2+}]$, similar to the Ω_{Ar} correction in McCutcheon et al. (2019). GE, MAE, and SNE all had insufficient $[Ca^{2+}]$ data from TCEQ, so Ω_{Ar} corrections differed. For GE and MAE, similar estuary-wide $[Ca^{2+}]$/Sal regressions were used for correction, using $[Ca^{2+}]$ and salinity data from our own lab from 2013 – 2015 and 2014 – 2020, respectively (Hu, unpublished data). For SNE, $[Ca^{2+}]$ was estimated for the river endmember by obtaining TA data from TCEQ from the Sabine and Neches rivers (spanning 1974 – 2013) and dividing TA by two as an estimate of riverine $[Ca^{2+}]$ (assuming TA was a result of weathering). The linear relationship between the river endmember (Sal = 0, $[Ca^{2+}]$ = 0.28 mmol kg^{-1}) and the ocean endmember (Sal= 35, $[Ca^{2+}]$ = 10.28 mmol kg^{-1}) was then used to estimate $[Ca^{2+}]$, and the data were corrected accordingly. It is worth noting that this Ω_{Ar} correction method may introduce some level of error (based on fluctuations in endmember $Ca^{2+}$and Ca^{2+}consumption dynamics within each estuary), but the corrected value should be more appropriate than direct seacarb calculations. It has also

been demonstrated that Ca^{2+}/S relationship can remain linear even when evaporation leads to hypersalinity (McCutcheon et al. 2019).

2.2.4 Regression analyses

Theil-Sen (TS) regression analysis with the Siegel modification (Siegel 1982) was chosen to generate a series of linear relationships between carbonate system parameters and time (decimal year) at each station; because of its non-parametric approach and robustness to outliers, TS regression is well-suited to explore trends in multi-laboratory agency data (Siegel 1982; Kaushal et al. 2013; Stets et al. 2014). All analyses were conducted in R, version 4.0.3, and the *mblm* package was used for regressions (R Core Team, 2020; Komsta, 2019). Rates of increase or decrease in parameters were reported only for those TS regressions that were significant based on alpha = 0.05. Trends are reported at individual stations rather than aggregating into bay units (as was done for investigations of pH and TA trends by Hu et al. (2015)) to fully picture spatial heterogeneity. Trends in pH are reported rather than trends in $[H^+]$; comparison of these trends should not be misleading since the region had similar average values in pH (Fassbender et al. 2021).

To confirm that the long-term trends in calculated parameters that were detected by TS regression were valid despite the relatively large propagated error associated with the calculated variables, simulation analyses were conducted to recalculate the slopes of TS regressions over 1000 simulations at each station for pCO_2, DIC, and Ω_{Ar}. For each simulation, resampled values for each data point were randomly selected within a normal curve using the calculated propagated error for each calculated parameter as the standard deviation for the curve. A 95% confidence interval of the 1000 new estimates of the TS regression slope was then calculated; if

the confidence interval included a value of zero, then the simulation suggested that there was not a long-term trend in the given parameter (see Discussion for the advantages of this approach).

2.2.5 Investigating spatial variability

Given the expectation of long-term trends in parameters (and the significant interaction between covariate decimal year and estuaries in analyses of covariance, ANCOVAs), differences between estuaries were investigated using a subset of "current" data. The "current" data consisted of data from (2010 – 2015) for all estuaries except for SNE. Since sampling concluded in 2008 in SNE and sampling frequency was low, data from 1998 – 2008 was used for SNE. Mean differences in carbonate system parameters between estuaries (using current data) were investigated with a single one-way analysis of variance (ANOVA).

In estuaries with sufficient sampling (TSJ, LCE, MAE, NE, LM) stations were categorized as either primary bay stations, i.e., stations in the bay that has direct connection to the GOM, or secondary bay stations, i.e., stations in bays that are separated from the GOM by the primary bays, for spatial comparisons within estuaries (Figure 1). Given that TSJ did not have any sampling in the primary bay areas from 2010 – 2015, the "current" subset was modified to 2000 – 2005 for only TSJ for primary/secondary comparisons. Differences in parameters between primary and secondary bays were not the same within all estuaries (based on significant interactions in two-way ANOVAs); thus, mean differences between primary and secondary bays were investigated within each estuary using t-tests.

2.3 Results

2.3.1 Long-term trends in carbonate system parameters

Many of the stations in the nwGOM estuaries experienced long-term trends in pH based on TS regression results (Fig. 2.2B, Table S2.1). Decreasing pH dominated in most estuaries;

decreasing trends were found in seven (of 10) TSJ stations, 11 (of 13) LCE stations, two (of two) GE stations, four (of five) MAE stations, 11 (of 13) NE stations, and one (of 10) LM stations, with rates of decrease ranging from -0.0002 – -0.0225 yr^{-1} (Table S2.1). Long-term increases in pH were also observed in the only SNE station, one TSJ station, two NE stations, and one LM station, with rates ranging from 0.0017 – 0.0063 yr^{-1} (Fig. 2.2B, Table S2.1). Similarly, temporal trends in TA were present at most stations, and most estuaries experienced long-term decreases. A decreasing TA trend was found at the only SNE station, six (of 10) TSJ stations, 12 (of 13) LCE stations, two (of two) GE stations, five (of five) MAE stations, 11(of 13) NE stations, and one (of 10) LM stations (Fig. 2.2C). Rates of TA decrease ranged from -1.4 – -30.3 μmol kg^{-1} yr^{-1} (Table S2.1). Long-term increases in TA were also observed at one TSJ station, two NE stations, and one LM station, with rates ranging from 1.9 – 16.7 μmol kg^{-1} yr^{-1} (Fig 2.2C, Table S2.1).

Temporal trends in pCO_2 were found at many stations, primarily dominated by long-term increases (Fig. 2.3A). Of the 54 stations, TS regression found 25 stations with long-term increases in pCO_2, including seven (of 10) TSJ stations, eight (of 13) LCE stations, one (of two) GE stations, two (of five) MAE stations, six (of 13) NE stations, and 1 (of 10) LM stations. Rates of pCO_2 increase ranged from 2 – 26 μatm yr^{-1} (Table S2.1). Long-term decreases in pCO_2 were also observed in only six of the 54 stations, including in the only SNE station, two MAE stations, two NE stations, and one LM station (Fig. 2.3A). Rates of pCO_2 decrease ranged from -2 – -10 μatm yr^{-1} (Fig. 2.4C, Table S2.1).

Temporal trends in DIC were found at many stations, primarily dominated by long-term decreases. The simple TS regression found 36 stations (out of 54) with long-term decreases in DIC, including the only SNE station, four (of 10) TSJ stations, 10 (of 13) LCE stations, two (of

two) GE stations, five (of five) MAE stations, 11 (of 13) NE stations, and three (of 10) LM stations. Rates of DIC decrease ranged from -0.9 – -26.1 μmol kg^{-1} yr^{-1}. Long-term increases were also observed, occurring at three (of the 54) stations: one TSJ station, one LCE station, and one LM station. Rates of DIC increase ranged from 4.7 – 15.0 μmol kg^{-1} yr^{-1} (Fig. 2.5D, Table S2.1).

Temporal trends in Ω_{Ar} were found at many stations, primarily dominated by long-term decreases. TS regression found 33 stations (of the 54 stations in the nwGOM estuaries) with long-term decreases in Ω_{Ar}, including seven (of 10) TSJ stations, 10 (of 13) LCE stations, two (of two) GE stations, three (of five) MAE stations, 10 (of 13) NE stations, and one (of 10) LM stations (Figs. 2.3C and 2.5E). Rates of Ω_{Ar} decrease ranged from -0.0050 – -0.1032 yr^{-1} (Fig. 2.5E and Table S2.1). Six stations (of 54) had long-term increases in Ω_{Ar}, with increasing Ω_{Ar} trends being most prominent in LM. Increases were found in four (of 10) stations in LM along with one TSJ station, and one NE station, with rates of increase ranging from 0.0073 – 0.0292 yr^{-1}. Long-term trends in β_{DIC} were primarily dominated by long-term decreases (25 out of 54) (Fig. 2.3D). The rate of β_{DIC} decrease ranged from -0.0010 – -0.0050 mmol kg^{-1} yr^{-1} (Fig. 2.5F, Table S2.1). Decreasing trends were found in the only SNE station, seven (of 10) TSJ stations, six (of 13) LCE stations, one (of two) GE stations, two (of five) MAE stations, seven (of 13) NE stations, and one (of 10) LM stations. Again, long-term increases were prominent in LM; increases were found in seven (of 10) stations in LM as well as one station in each of TSJ, LCE, MAE, and NE, with increases ranging from 0.0010 – 0.0020 mmol kg^{-1} yr^{-1}.

2.3.2 Spatial variability in carbonate system parameters

Carbonate chemistry in the region varied substantially between estuaries (Figure 2.4, Tables S2.1 and S2.2). SNE, the northernmost estuary, had a significantly different mean for

every parameter, including the lowest salinity, pH, TA, DIC, Ω_{Ar}, and β_{DIC}, and the highest pCO_2 (Figs. 2.4 and S2.2). Conversely, LM, the southernmost estuary, had the highest salinity, TA, DIC, Ω_{Ar}, and β_{DIC}, though only TA and β_{DIC} were significantly greater than all other estuaries (Figs. 2.4 and S2.2). TSJ also showed relatively unique carbonate chemistry, with relatively low TA, pCO_2, and DIC compared to the rest of the region (Fig. 2.4).

Some of the estuaries showed differences in carbonate chemistry parameters between primary and secondary bay stations (Fig. 2.4). LM was generally the exception to the rule for primary/secondary bay differences across all parameters (Fig. 2.4). With the exception of LME, salinity was lower on average in the secondary bays, although this difference was only significant in LCE ($p=0.0017$). pH was lower on average in the secondary bays (only significant in MAE, $p=0.0065$). pCO_2 was higher on average in the secondary bay, although this was only significant in MAE ($p = 0.0205$) and NE ($p = 0.0146$). Ω_{Ar} and β_{DIC} were lower on average in secondary bays, though Ω_{Ar} was only significantly different in MAE ($p= 0.0183$) and. β_{DIC} in MAE ($p= 0.0478$) and TSJ ($p= 0.0168$) DIC and TA did not vary greatly between primary and secondary bays, although differences were seen in TSJ.

2.4 Discussion

2.4.1 Propagated error in calculated carbonate system parameters and validation of long-term trends

While TCEQ SWQM data are not the same precision that would be expected in an analytical lab that is specialized in carbonate chemistry studies, the protocols have remained the same over time. Therefore, these data should be adequate to establish long-term trends, and a number of other studies in the literature have also made this assumption while using government-funded long-term water quality monitoring data (Raymond and Cole 2003; Raymond et al. 2008;

Waldbusser et al. 2011b; Stets et al. 2014, 2017; Hu et al. 2015; Barrera and Robbins 2017; Carstensen et al. 2018; Robbins and Lisle 2018; Van Dam and Wang 2019) or even citizen science data (Snyder et al. 2019) for interpreting carbonate chemistry trends.

Propagated error associated with calculated pCO_2, DIC, and Ω_{Ar} would be expected to be relatively high given the coarse analytical precision of the TCEQ data used in this analysis. Assuming analytical precision of pH as ±0.1, TA as ±115 µmol kg^{-1} (±5% of mean TA, 2300 µmol kg^{-1}), salinity as ±0.1, and temperature as ±0.1 ºC, the mean propagated error associated with calculated pCO_2 values was 184.9 ± 159.1 µatm, the mean propagated error associated with DIC values was 118.7 ± 5.4 µmol kg^{-1}, and the mean propagated error associated with Ω_{Ar} was 0.497 ± 0.264.

The simulation method used for validation of long-term trends confirmed the presence and signs of long-term trends in pCO_2, DIC, and Ω_{Ar} that were found from TS regression with only a few exceptions. The simulations were able to validate the existence and sign of 23 (of 25) of the increasing pCO_2 trends and four (of six) of the decreasing trends. The mean difference between significant slopes calculated by the single TS regression versus the simulation was -0.2 ± 1.0 µatm yr^{-1} (or 3.1% ± 19.3% of the TS slope estimates). The simulations were able to validate the existence and sign of 32 (of 36) of the increasing DIC trends and all three of the decreasing trends. The mean difference between significant slopes calculated by the single TS regression versus the simulation was -0.3 ± 1.1 µmol kg^{-1} yr^{-1} (or 4.8% ± 15.1% of the TS slope estimates). The simulations were able to validate the existence and sign of 29 (of 33) of the increasing trends in Ω_{Ar} and three (of six) of the decreasing trends in Ω_{Ar}. There was also one station in TSJ (13315) that did not have a significant trend based on the TS method but did have a significant, positive trend based on the simulation. The mean difference between significant

slopes calculated by the single TS regression versus the simulation was -0.0005 ± 0.0051 yr^{-1} (or 5.8% ± 21.7% of the TS slope estimates).

While there are some discrepancies between the two methods (single TS regression estimates and 95% confidence intervals of TS regressions of simulated data with incorporated propagated error), the overall picture of the presence and directions of long-term trends in carbonate system parameters within each of the estuaries remains unaltered (Figs. 2.3 and S2.2). This is the first time that the use of calculated carbonate system parameters in the estimation of long-term trends has been validated based on their associated propagated error. It is a promising finding for the utility of government-funded and citizen science-sponsored data, and it provides support for the continued sponsorship of such programs for understanding changes in coastal carbonate chemistry.

It is worth noting that DIC and pH are among the better combinations of parameters for carbonate system calculations. Since the TCEQ data did not include measures of DIC, TA and pH were used for speciation calculations; this simple use of titration TA has been shown to lead to overestimation of pCO_2 (Hunt et al. 2011) since organic alkalinity is not accounted for. Organic alkalinity has been assumed to be negligible in other studies when only TA and pH were available for speciation calculations (Prasad et al. 2013; Carstensen et al. 2018). Present day organic alkalinity in the region (MAE and NE, calculated by the difference in measured TA and TA calculated with DIC and pH) usually does not exceed 50 μmol kg^{-1}, or less than 2% of TA (Yao and Hu 2017; McCutcheon et al. 2019). It is assumed that there are not long-term trends in organic alkalinity but note that there is potential for trends in organic alkalinity to provide an additional source of error in our calculated parameters and long-term trends.

2.4.2 Spatial heterogeneity in carbonate system parameters and long-term trends

Around the world, several estuaries have now been shown to have long-term trends in pH and TA (Table 2.1), with a meta-analysis revealing equal likelihood of increasing or decreasing pH trends (Carstensen and Duarte 2019). The magnitude of annual change in pH and TA that is reported is on the same order of magnitude as trends that have been reported in other estuaries (Table 1). Only one other study to date has reported long-term trends in calculated carbonate system parameters; in Danish Fjords, Carstensen et al. (2018) reported mostly long-term increases in pCO_2 and DIC (Table 1). While such increasing DIC would generally be expected in environments with increasing pCO_2, the widespread decreasing trends that were found likely directly result from the long-term decreases in TA in the region. Carstensen et al. (2018) did not report values of annual change in Ω (although they did note increasing Ω and decreasing Ω surrounding a regime shift in one estuary), making this the first study to report long-term trends in both estuarine Ω and β_{DIC}. The large spatial variation in carbonate chemistry within estuaries is often due to control exerted by net ecosystem metabolism (NEM). Heterogeneity in NEM becomes apparent at distances of less than 2 km in the nwGOM estuaries (Russell and Montagna 2007). More freshwater-influenced regions of estuaries are generally more net heterotrophic than the rest of the estuary due to allochthonous carbon input (Caffrey 2004) and river water itself is generally supersaturated with CO_2 (Butman and Raymond 2011; Joesoef et al. 2015); thus, the elevated pCO_2 and depressed pH, Ω_{Ar}, and β_{DIC} found in the secondary bays relative to the primary bays (Fig. 2.4) are spatial relationships that could be noted along the freshwater gradient within many estuaries.

2.4.3 Implications of long-term trends

Trends in pCO_2 have implications for air-water CO_2 flux (Landschützer et al. 2013). Given that air-water CO_2 flux is a function of the gradient between atmospheric and surface water pCO_2, long-term trends in pCO_2 of surface water that differ from long-term trends of atmospheric CO_2 indicate changes in the water's magnitude of a carbon sink (absorbs atmospheric CO_2) or carbon source (outgasses CO_2 to the atmosphere) (Landschützer et al. 2013). For comparison to pCO_2 trends in estuaries, the average annual change in atmospheric pCO_2 between 1974 and 2015 was 1.72 µatm yr^{-1} (https://www.esrl.noaa.gov/gmd/ccgg/trends/data.html). Given that the majority of the stations throughout the nwGOM estuaries have experienced increasing pCO_2 exceeding the atmospheric rate (Table S2.1) and given that estuaries tended to have pCO_2 higher than that of the atmosphere (Table S2.1), it can safely be conclude that the nwGOM estuaries have increased in their level of CO_2 outgassing over the observed decades. The strongest long-term increases in pCO_2 were found in TSJ (Figs. 2.3A and 2.4C), indicating that it has become a stronger source of CO_2 over past decades. Rates of increase in pCO_2 were also generally higher across all nwGOM estuaries than surface ocean pCO_2 trends (1.88 µatm yr^{-1}; Doney 2010), indicating that advection of estuarine waters into the coastal GOM may also increase coastal pCO_2 trends.

CO_2 flux estimates from recent years in the nwGOM estuaries have been shown to vary between estuaries, with MAE and NE acting as mild CO_2 sources and GE and LCE acting as moderate CO_2 sources on an annual basis (Yao et al. 2020). Wet/dry cycles play a substantial role in the interannual variability of CO_2 fluxes in the region (Yao et al. 2020). As pCO_2 trends have varied between increasing and decreasing in NE and MAE, the flux there may not have changed drastically over the past decades. However, pCO_2 is clearly increasing in LCE,

indicating that it likely had lower CO_2 fluxes decades ago. Yao et al. (2020) did not consider the two northernmost (SNE and TSJ) nor the southernmost (LM) estuaries. Due to SNE and LM experiencing the extremes of substantial precipitation and evaporation gradients, their carbonate system characteristics differ greatly from the other estuaries in the nwGOM, as did the long-term trends that they have experienced (Fig. 2.5, Table S2.1). It is important to understand long-term trends such as these when fluxes are applied to regional or global carbon budgets.

Trends in Ω_{Ar} have implications for biological calcification as well as calcium carbonate preservation and burial (Fabry et al. 2008; Waldbusser et al. 2015). The nwGOM estuaries is inhabited by Eastern Oysters, ecologically and economically important species that require suitable carbonate chemistry to build and maintain their shells (Buzan et al. 2009; Pollack et al. 2011; Beseres Pollack et al. 2013). With the exception of SNE, nwGOM estuaries have generally remained supersaturated with respect to aragonite (Table S2.2), but even slight decreases in Ω_{Ar} while still maintaining supersaturation have been shown to negatively affect calcifying organisms (Gattuso 1998). Trends in Ω_{Ar} in the nwGOM estuaries were generally decreasing, except for LM (Fig. 2.4). Despite that Ω_{Ar} still remains well above saturation (except for SNE) and carbonate chemistry is likely a secondary stressor to changes in salinity in the region, this declining trend may have already reduced biological calcification rates over past decades and if the trend continues, it may threaten the shell budget and subsequently threaten sustained oyster populations into the future (Powell and Klinck 2007; Waldbusser et al. 2011a). It is also worth noting that the estuary that has experienced the greatest rate of decrease in Ω_{Ar} (TSJ, Figure 2.5E) is also the estuary with the heaviest reliance on commercial oyster harvests.

As noted by Hu et al. (2015), those stations with decreasing pH had a much higher rate of decrease than that in the open ocean, which is around 0.0017 yr^{-1} (González-Dávila et al. 2007;

Byrne et al. 2010) (Table S2.1). This indicates that estuarine waters may be more at risk to impacts associated with acidification and that coastal waters in the GOM may be subject to further acidification as estuarine water is flushed to the adjacent coastal ocean. Trends in buffer factors have implications for fluctuations in other carbonate system parameters, and β_{DIC} is particularly indicative of changes in pH. The long-term decreases that have been observed in β_{DIC} in the nwGOM estuaries over the past several decades indicate that the system has become less well buffered, and the pH response has become increasingly sensitive to DIC additions. Therefore, short-term processes like the stratification and development of hypoxia that can occur in the region (Applebaum et al. 2005; McCutcheon et al. 2019) or long-term processes like decreasing freshwater inflow or increasing atmospheric CO_2 all have the potential to cause greater fluctuations and disruption to the carbonate system now than the same processes would have decades ago. This long-term decrease in buffer capacity and increase in potential for change has been described in ocean environments previously (Shaw et al. 2013), but it has never explicitly been noted in estuarine environments. Despite this decrease in β_{DIC}, β_{DIC} is generally high in nwGOM estuaries, often exceeding the values in nwGOM open water, ~0.26 – 0.29 mmol kg^{-1} (Fig. 2.6E) when buffer capacity is generally lower in estuarine waters.

2.5 Conclusions

This study used the TCEQ SWQM's data record to examine long-term trends and spatial relationships in the carbonate system in the estuaries of the nwGOM. This dataset provides much more spatially and temporally extensive data than any current datasets collected by academic laboratories, and unlike many other regional monitoring programs, TCEQ has routinely monitored both pH and TA, making this one of the longest running estuarine datasets in the world that allows the calculation of the complete carbonate system. Carbonate system

parameters—pCO_2, DIC, Ω_{Ar}, and β_{DIC}—were calculated for each observation at the 54 stations where monitoring occurred for 20+ years. The mean carbonate system parameters varied between estuaries, with salinity, pH, TA, DIC, Ω_{Ar}, and β_{DIC} generally increasing from north to south. Smaller differences in means could also be observed within estuaries between primary and secondary bays.

Long-term trends in calculated parameters were investigated at each station using Theil-Sen regression. The northernmost and southernmost estuaries in the region often varied greatly from the other estuaries in their long-term trends. The central five estuaries (except for select stations near direct river input) have generally experienced long-term increases in pCO_2 and decreases in DIC, Ω_{Ar}, and β_{DIC} over past decades, and the magnitude of change generally increased from north to south. At all stations with increasing pCO_2, the rate of increase was greater than in the atmosphere, indicating that the estuaries have become an increasing source of CO_2 to the atmosphere. The decrease in Ω_{Ar}, while not yet nearing undersaturation, already has the potential to negatively affect calcifying organisms. The decreasing β_{DIC} indicates that the estuaries have been experiencing greater decrease in pH relative to a given addition of DIC over time.

Given that propagated error associated with calculated carbonate system parameters can be relatively large, propagated error was calculated and incorporated into simulations to validate the long-term trends. Simulation analyses generally found the same sign and magnitude of long-term trends, with only a few stations as exceptions. This was only the second study to investigate long-term trends in calculated estuarine carbonate system parameters and the first to validate those trends based on propagated errors.

References

Applebaum S., Montagna P.A., Ritter C. 2005. Status and trends of dissolved oxygen in Corpus Christi Bay, Texas, USA. *Environmental Monitoring and Assessment* 107: 297–311.

Barrera K.E., Robbins L.L. 2017. Historical patterns of acidification and increasing CO_2 flux associated with Florida springs. *Limnology and Oceanography* 62: 2404–2417.

Bauer J.E., Cai W.-J., Raymond P. A., Bianchi, T.S., Hopkinson, C.S., Regnier, P. A. G. 2013. The changing carbon cycle of the coastal ocean. *Nature* 504: 61–70.

Beseres Pollack J., Yoskowitz D., Kim H.C., Montagna P.A. 2013. Role and value of nitrogen regulation provided by oysters (*Crassostrea virginica*) in the Mission-Aransas Estuary, Texas, USA. *PLoS One* 8: 6–13.

Butman D., Raymond P.A. 2011. Significant efflux of carbon dioxide from streams and rivers in the United States. *Nature Geoscience* 4: 839–842.

Buzan D., Lee W., Culbertson J., Kuhn, N., Robinson, L. 2009. Positive relationship between freshwater inflow and oyster abundance in Galveston Bay, Texas. *Estuaries and Coasts* 32: 206–212.

Byrne R.H., Mecking S., Feely R.A., Liu X. 2010. Direct observations of basin-wide acidification of the North Pacific Ocean. *Geophysical Research Letters* 37: 1–5.

Caffrey J.M. 2004. Factors controlling net ecosystem metabolism in U.S. estuaries. *Estuaries* 27: 90–101.

Cai W.-J. 2011. Estuarine and coastal ocean carbon paradox: CO_2 sinks or sites of terrestrial carbon incineration? *Annual Review of Marine Science* 3: 123–45.

Cai W.-J., Pomeroy L.R., Moran M.A., Wang Y. 1999. Oxygen and carbon dioxide mass balance for the estuarine-intertidal marsh complex of five rivers in the southeastern U.S. *Limnology and Oceanography* 44: 639–649.

Cai W.J., Wang Y., Krest J., Moore W.S. 2003. The geochemistry of dissolved inorganic carbon in a surficial groundwater aquifer in North Inlet, South Carolina, and the carbon fluxes to the coastal ocean. *Geochimica et Cosmochimica Acta* 67: 631–637.

Carstensen J., Chierici M., Gustafsson B.G., Gustafsson E. 2018. Long-term and seasonal trends in estuarine and coastal carbonate systems. *Global Biogeochemical Cycles* 32: 1271–1288.

Carstensen J., Duarte C.M. 2019. Drivers of pH variability in coastal ecosystems. *Environmental Science and Technology* 53: 4020–4029.

Challener R.C., Robbins L.L., Mcclintock J.B. 2016. Variability of the carbonate chemistry in a shallow, seagrass-dominated ecosystem: Implications for ocean acidification experiments. *Marine and Freshwater Research* 67: 163–172.

de Putron S.J., McCorkle D.C., Cohen A.L., Dillon A.B. 2011. The impact of seawater saturation state and bicarbonate ion concentration on calcification by new recruits of two Atlantic corals. *Coral Reefs* 30: 321–328.

Doney S.C. 2010. The growing human footprint on the planet. *Science* 328: 1512–1516.

Dürr H.H., Laruelle G.G., van Kempen C.M., Slomp, C.P., Meybeck, M., Middelkoop, H. 2011. Worldwide typology of nearshore coastal systems: Defining the estuarine filter of river inputs to the oceans. *Estuaries and Coasts* 34: 441–458.

Egleston E.S., Sabine C.L., Morel F.M. 2010. Revelle revisited: Buffer factors that quantify the

response of ocean chemistry to changes in DIC and alkalinity. *Global Biogeochem Cycles* 24: GB1002.

Fabry V.J., Seibel B.A., Feely R.A., Orr J.C. 2008. Impacts of ocean acidification on marine fauna and ecosystem processes. *ICES Journal of Marine Science* 65: 414–432.

Fassbender, A., Orr, J., & Dickson, A. 2021. Technical note: Interpreting pH changes. *Biogeosciences*, 18: 1407–1415.

Feely R.A., Alin S.R., Newton J., Sabine, C.L., Warner, M., Devol, A., Krembs, C., Maloy, C. 2010. The combined effects of ocean acidification, mixing, and respiration on pH and carbonate saturation in an urbanized estuary. *Estuarine and Coastal Shelf Science* 88: 442–449.

Frankignoulle M., Borges A.V. 2001. Direct and indirect pCO_2 measurements in a wide range of pCO_2 and salinity values (The Scheldt Estuary). *Aquatic Geochemistry* 7: 267–273.

Frankignoulle M., Canon C., Gattuso J-P. 1994. Marine calcification as a source of carbon dioxide: Positive feedback of increasing atmospheric CO_2. *Limnology and Oceanography* 39: 458–462.

Gattuso J. 1998. Effect of calcium carbonate saturation of seawater on coral calcification. *Global and Planetary Change* 18: 37–46.

Gattuso J., Epitalon J., Lavigne H. and Orr J. 2021. seacarb: Seawater Carbonate Chemistry. R package version 3.2.15. https://CRAN.R-project.org/package=seacarb

González-Dávila M., Santana-Casiano J.M., González-Dávila E.F. 2007. Interannual variability of the upper ocean carbon cycle in the northeast Atlantic Ocean. *Geophysical Research*

Letters 34: L07608.

Hofmann G.E., Smith J.E., Johnson K.S., Send, U., Levin, L. A., Micheli, F., Paytan, A., Price, N.N., Peterson, B., Takeshita, Y., Matson, P.G., Crook, E.D., Kroeker, K.J., Gambi, M.C., Rivest, E.B., Frieder, C. A, Yu, P.C., Martz, T.R. 2011. High-frequency dynamics of ocean pH: a multi-ecosystem comparison. *PLoS One* 6: e28983.

Hu X., Beseres Pollack J., McCutcheon M.R., Montagna, P. a., Ouyang, Z. 2015. Long-term alkalinity decrease and acidification of estuaries in Northwestern Gulf of Mexico. *Environmental Science and Technology* 49: 3401–3409.

Hunt C.W., Salisbury J.E., Vandemark D. 2011. Contribution of non-carbonate anions to total alkalinity and overestimation of pCO_2 in New England and New Brunswick rivers. *Biogeosciences* 8: 3069–3076.

Joesoef A., Huang W.J., Gao Y., Cai W.J. 2015. Air-water fluxes and sources of carbon dioxide in the Delaware Estuary: Spatial and seasonal variability. *Biogeosciences* 12: 6085–6101.

Kaushal S.S., Likens G.E., Utz R.M., Pace, M.L., Grese, M., Yepsen, M., 2013. Increased river alkalinization in the eastern U.S. *Environmental Science and Technology* 47: 10302–10311.

Landschützer P., Gruber N., Bakker D.C.E., Schuster, U., Nakaoka, S., Payne, M.R., Sasse, T.P., Zeng, J. 2013. A neural network-based estimate of the seasonal to inter-annual variability of the Atlantic Ocean carbon sink. *Biogeosciences* 10: 7793–7815.

Lejart M., Clavier J., Chauvaud L., Hily C. 2011. Respiration and calcification of *Crassostrea gigas*: Contribution of an intertidal invasive species to coastal ecosystem CO_2 fluxes. *Estuaries and Coasts* 35: 622–632.

Lukasz K. 2019. *mblm*: Median-Based Linear Models. R package version 0.12.1. https://CRAN. R-project.org/package=mblm

McCutcheon M.R., Staryk C.J., Hu X. 2019. Characteristics of the carbonate system in a semiarid estuary that experiences summertime hypoxia. *Estuaries and Coasts* 42: 1509-1523.

Millero F.J. 2010. Carbonate constant for estuarine waters. *Marine and Freshwater Research* 61: 139–142.

Mongin M., Baird M. 2014. The interacting effects of photosynthesis, calcification and water circulation on carbon chemistry variability on a coral reef flat : A modelling study. *Ecological Modelling* 284: 19–34.

Montagna P.A., Ward G., Vaughan B. 2011a. The importance of freshwater inflows to Texas estuaries. In: Water Policy in Texas: Responding to the Rise of Scarcity. pp 107–127

Montagna P.A., Brenner J., Gibeaut J., Morehead S. 2011b. Chapter 4: Coastal Impacts. In: Jurgen Schmandt, Gerald R. North and JC (ed) The Impact of Global Warming on Texas. University of Texas Press, pp 96–123.

Najjar R.G., Herrmann M., Cintrón S.M., Valle, D., Friedman, J.R., Friedrichs, M.A.M., Harris, L.A. 2019. Alkalinity in Tidal Tributaries of the Chesapeake Bay. *Journal of Geophysical Research : Oceans* 125: e2019JC015597.

Perez F.F., Fraga F. 1987. Association constant of fluoride and hydrogen ions in seawater. *Marine Chemistry* 21: 161–168

Pollack J.B., Kim H.C., Morgan E.K., Montagna P.A. 2011. Role of flood disturbance in natural

oyster (*Crassostrea virginica*) population maintenance in an estuary in South Texas, USA. *Estuaries and Coasts* 34: 187–197.

Powell E.N., Klinck J.M. 2007. Is oyster shell a sustainable estuarine resource? *Journal of Shellfish Research* 26: 181–194.

Prasad M.B.K., Kaushal S.S., Murtugudde R. 2013. Long-term pCO_2 dynamics in rivers in the Chesapeake Bay watershed. *Applied Geochemistry* 31: 209–215.

R Core Team 2020. R: A language and environment for statistical computing. R Foundation for Statistical Computing, Vienna, Austria. URL https://www.R-project.org/.

Raymond P.A., Bauer J.E., Cole J.J. 2000. Atmospheric CO_2 evasion, dissolved inorganic carbon production, and net heterotrophy in the York River estuary. *Limnology and Oceanography* 45: 1707–1717.

Raymond P.A., Cole J.J. 2003. Increase in the export of alkalinity from North America's largest river. *Science* 301: 88–91.

Raymond P.A., Oh N.-H., Turner R.E., Broussard W. 2008. Anthropogenically enhanced fluxes of water and carbon from the Mississippi River. *Nature* 451: 449–452.

Robbins LL, Lisle JT 2018. Regional Acidification Trends in Florida Shellfish Estuaries: a 20+ Year Look at pH, Oxygen, Temperature, and Salinity. *Estuaries and Coasts* 41: 1268–1281.

Russell M.J., Montagna P.A. 2007. Spatial and temporal variability and drivers of net ecosystem metabolism in western Gulf of Mexico estuaries. *Estuaries and Coasts* 30: 137–153

Shaw E.C., McNeil B.I., Tilbrook B., Matear, R., Bates, M.L. 2013. Anthropogenic changes to seawater buffer capacity combined with natural reef metabolism induce extreme future

coral reef CO_2 conditions. *Global Change Biology* 19: 1632–41.

Siegel A.F. 1982. Robust regression using repeated medians. *Biometrika* 69: 242–244

Snyder J.T., Whitney M.M., Dam H.G., Jacobs, M.W., Baumann, H. 2019. Citizen science observations reveal rapid , multi-decadal ecosystem changes in eastern Long Island Sound. *Marine Environmental Research* 146: 80–88.

Stets E.G., Butman D., McDonald C.P., Stackpoole, S.M., DeGrandpre, M.D., Striegl, R.G. 2017. Carbonate buffering and metabolic controls on carbon dioxide in rivers. *Global Biogeochemical Cycles* 31: 663–677.

Stets E.G., Kelly V.J., Crawford C.G. 2014. Long-term trends in alkalinity in large rivers of the conterminous US in relation to acidification, agriculture, and hydrologic modification. *Science of the Total Environment* 488–489: 280–289.

Uppström L.R. 1974. The boron/chlorinity ratio of deep-sea water from the Pacific Ocean. *Deep-Sea Research* 21: 161–162.

Van Dam B.R., Wang H. 2019. Decadal-scale acidification trends in adjacent North Carolina estuaries: Competing role of anthropogenic CO_2 and riverine alkalinity loads. *Frontiers in Marine Science* 6: 136.

Waldbusser G.G., Hales B., Langdon C.J., Haley, B.A., Schrader, P., Brunner, E.L., Gray, M.W., Miller, C.A., Gimenez, I. 2015. Saturation-state sensitivity of marine bivalve larvae to ocean acidification. *Nature Climate Change* 5: 273–280.

Waldbusser G.G., Steenson R.A., Green M.A. 2011a. Oyster shell eissolution rates in estuarine waters: Effects of pH and shell legacy. *Journal of Shellfish Research* 30: 659–669.

Waldbusser G.G., Voigt E.P., Bergschneider H., Green, M.A., Newell, R.I.E. 2011b. Biocalcification in the Eastern Oyster (*Crassostrea virginica*) in relation to long-term trends in Chesapeake Bay pH. *Estuaries and Coasts* 34: 221–231.

Wallace R.B., Baumann H., Grear J.S., Aller, R.C., Gobler, C.J, 2014. Coastal ocean acidification: The other eutrophication problem. *Estuarine, Coastal, and Shelf Science* 148: 1–13.

Yao H., Hu X. 2017. Responses of carbonate system and CO_2 flux to extended drought and intense flooding in a semiarid subtropical estuary. *Limnology and Oceanography* 62: S112–S130.

Yao H., Mccutcheon M.R., Staryk C.J., Hu X. 2020. Hydrologic controls on CO_2 chemistry and flux in subtropical lagoonal estuaries of the northwestern Gulf of Mexico. *Limnology and Oceanography* 65: 1380–1398.

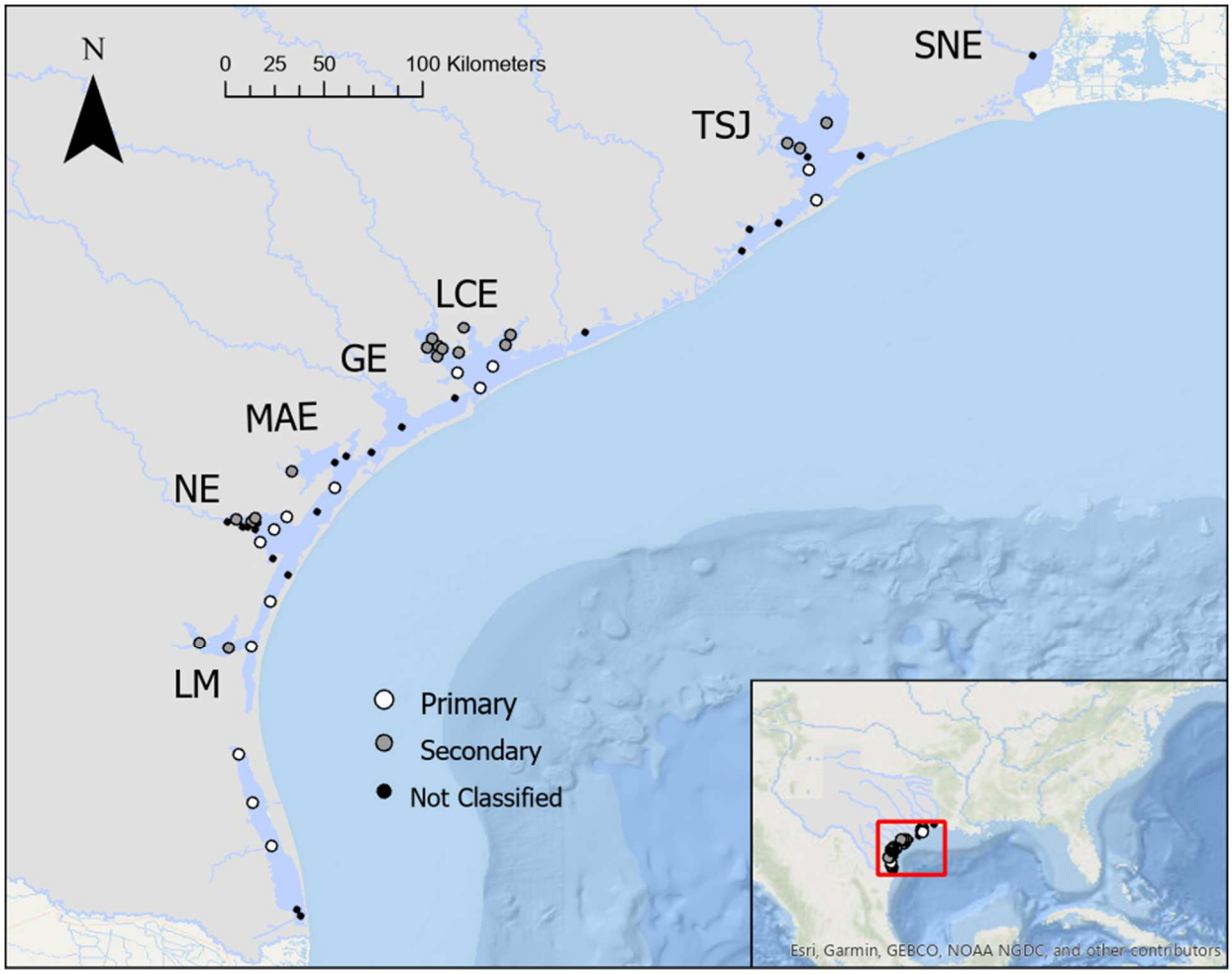

Figure 2.1. A map of study locations. Texas Commission on Environmental Quality Surface Water Quality Monitoring stations that were used in the analysis (greater than 20 years of sampling for temperature, salinity, pH, and total alkalinity) are shown in each of the seven estuaries along the Texas coast. Station numbers can be found in Figure S2.1.

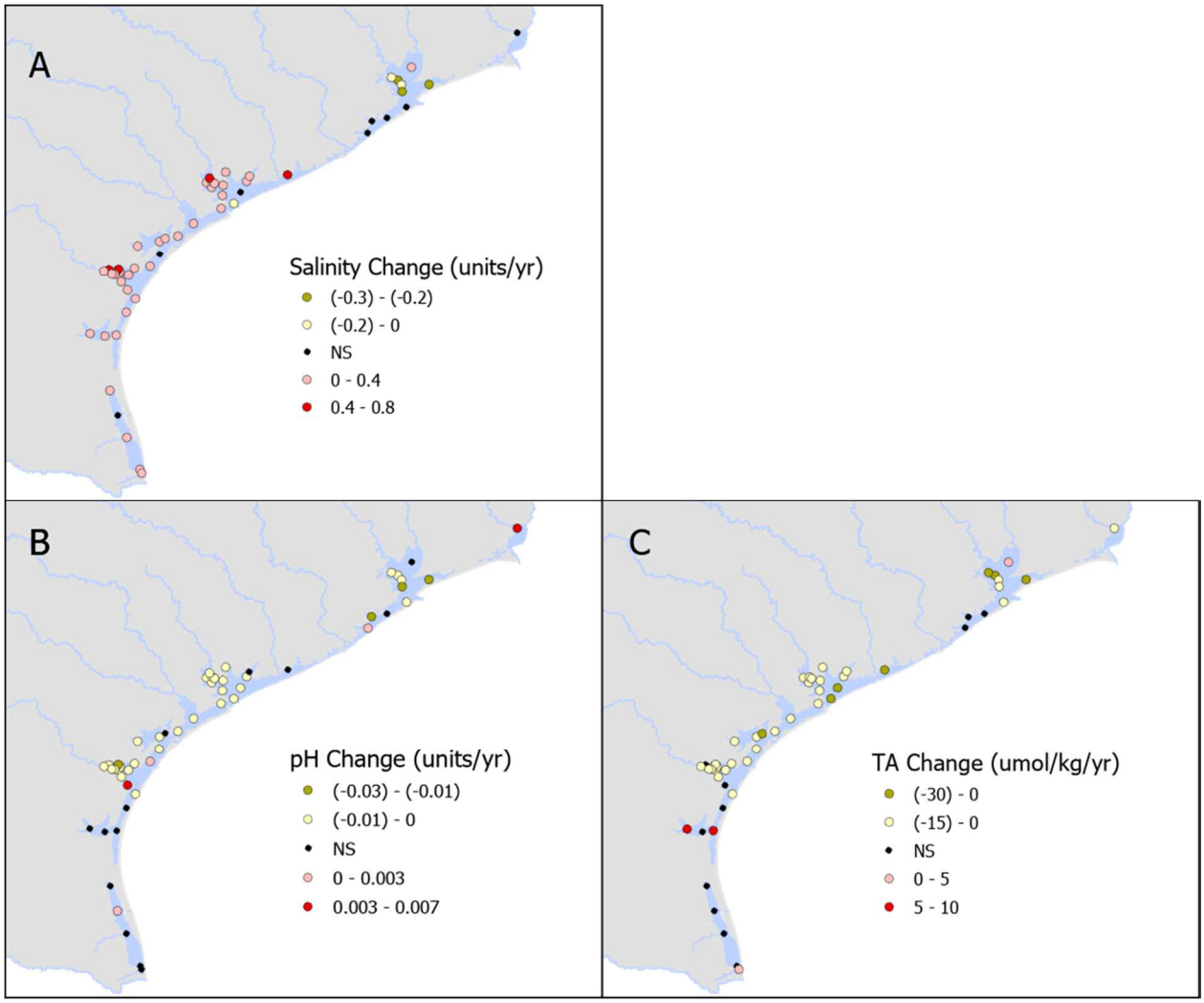

Figure 2.2. Annual rate of change in the measured parameters- salinity (A), pH (B), and total alkalinity (C)

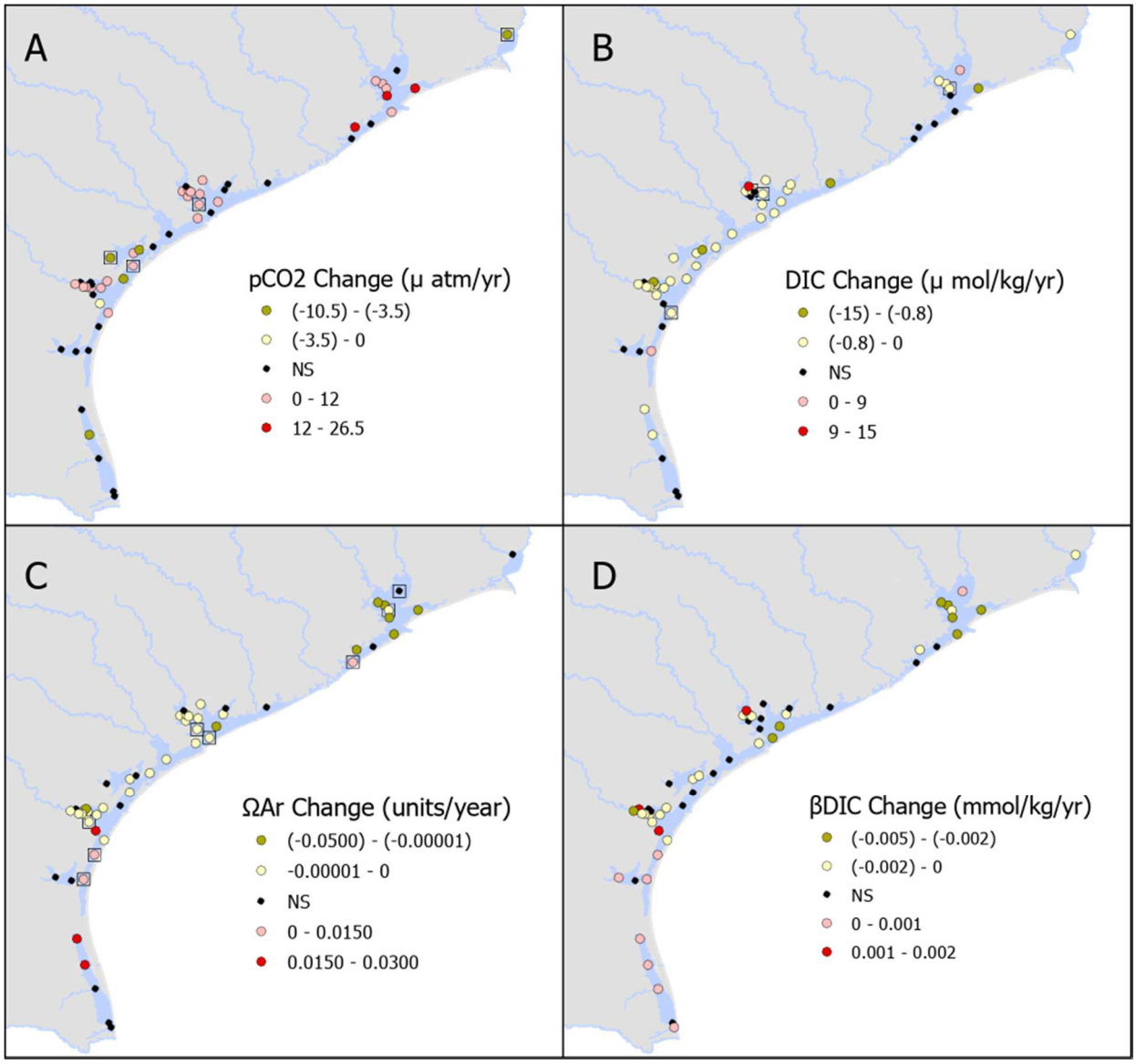

Figure 2.3. Annual rate of change in calculated carbonate system parameters – pCO_2 (A), dissolved inorganic carbon (B), Ω_{Ar} (C), and β_{DIC} (D). Black squares surrounding individual stations in (A), (B), and (C) indicate locations where long-term trends detected by TS regression were not validated (significant trend of the same sign) by the simulation analyses.

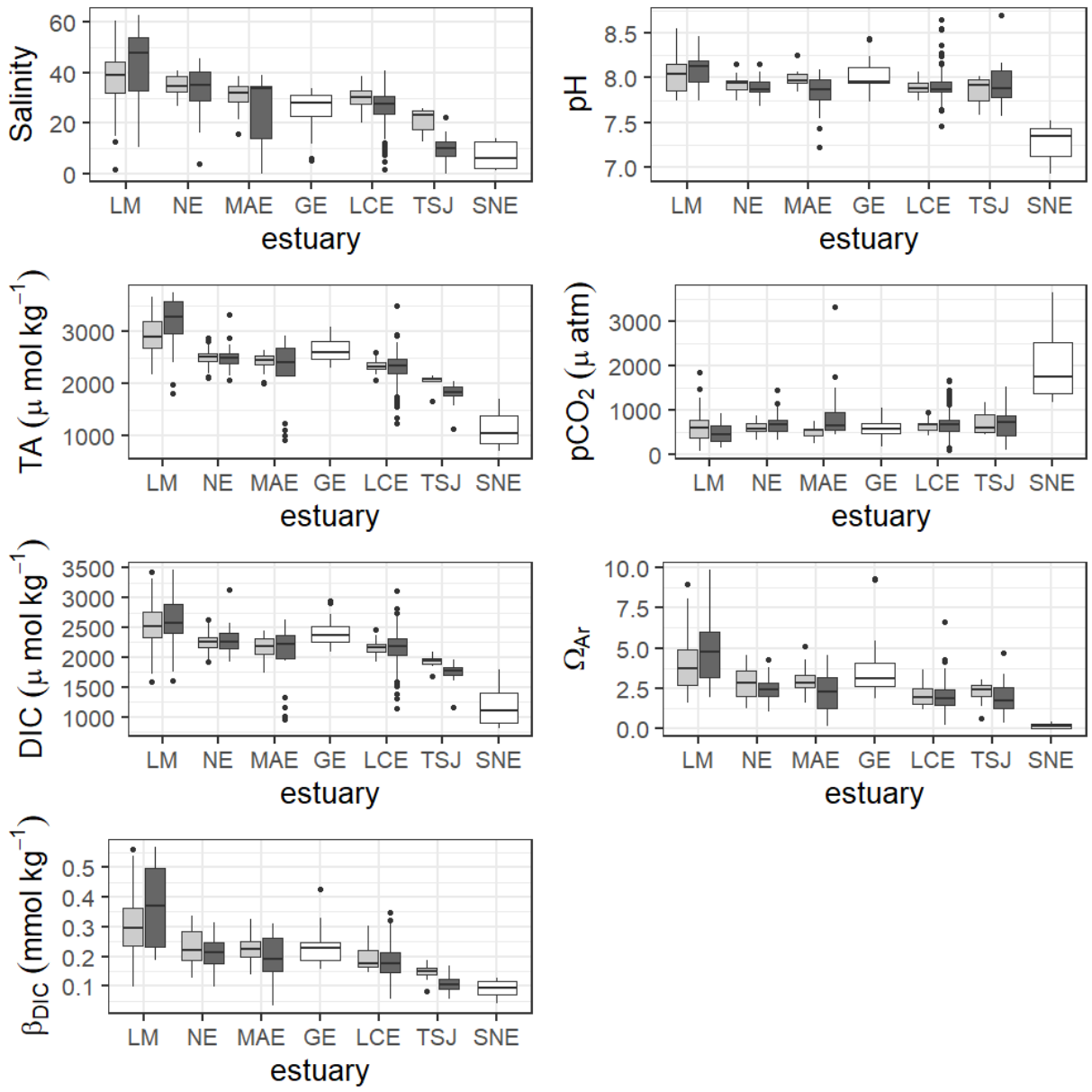

Figure 2.4. Boxplots showing the distribution of parameters within primary (light gray) and secondary (dark gray) bays within estuaries using the most recent six years of data. Estuaries that could not be split into primary and secondary are shown in white.

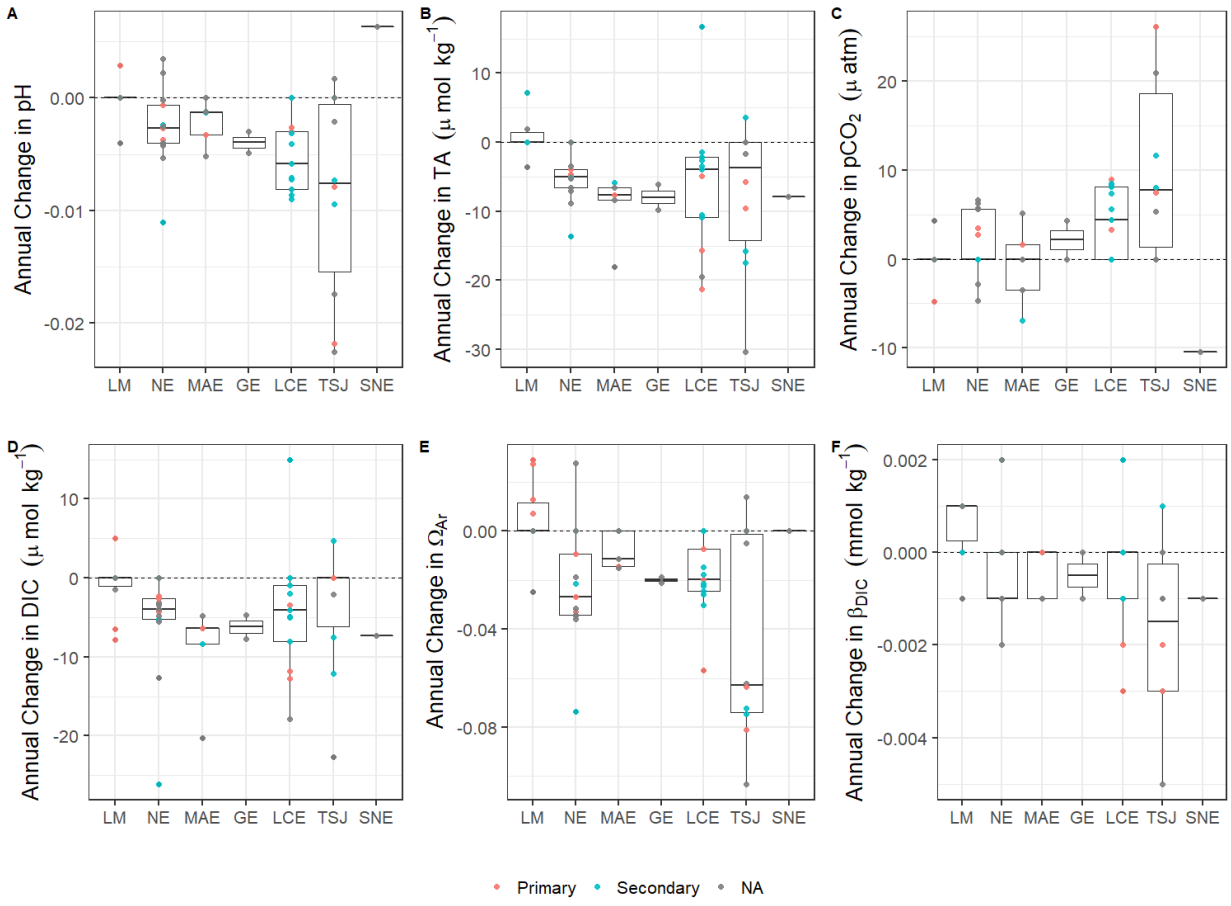

Figure 2.5. Boxplots of the annual rate of change of carbonate system parameters at stations within each estuary. Estuaries are listed from southern-most (LM) to northern-most (SNE). Point data showing the rate of change at each station are colored to represent the station classification as within a primary bay (orange), secondary bay (blue). Data with not primary/secondary classification is shown in gray.

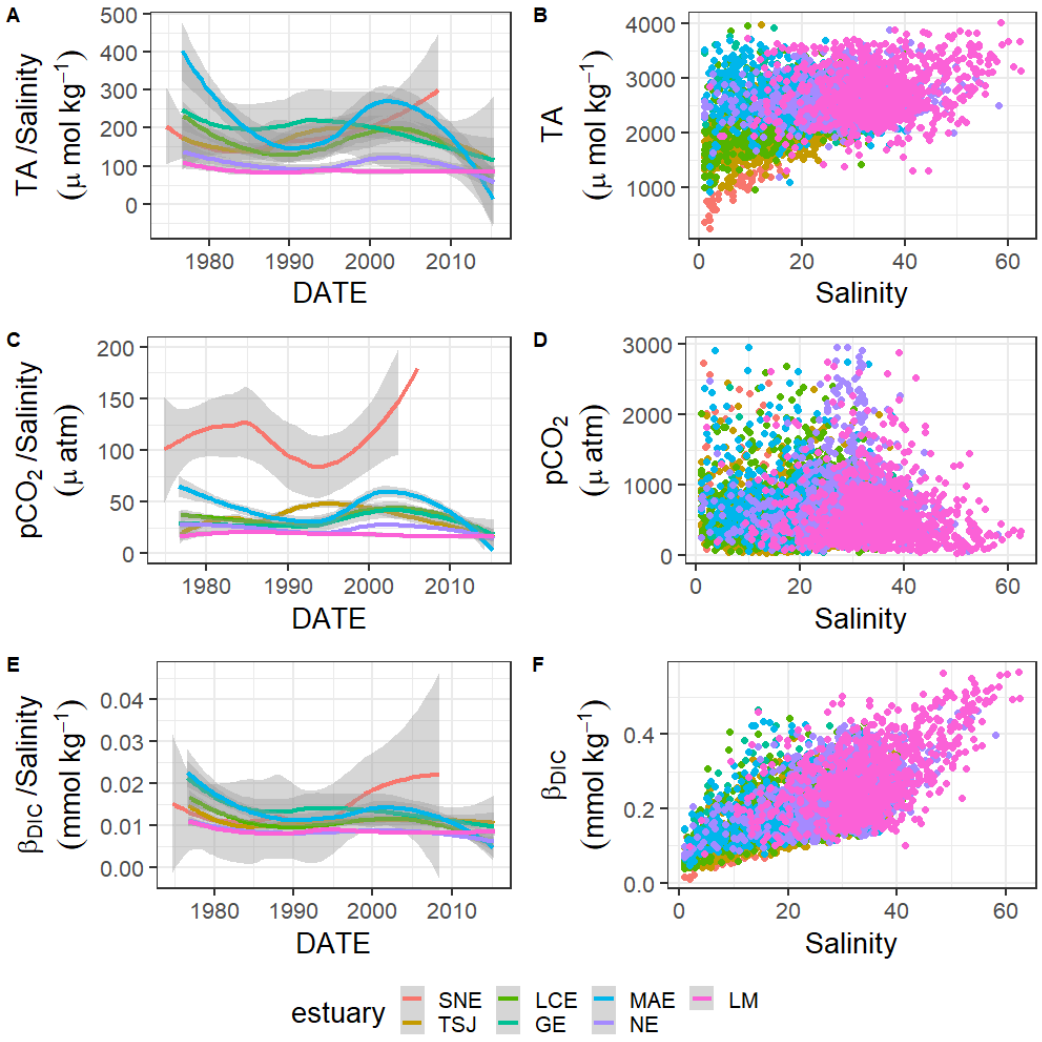

Figure 2.6. Relationships between salinity and carbonate system parameters—TA (A, B), pCO_2 (C, D), and β_{DIC} (E, F)—in each estuary. B, D, and F are showing direct relationships with salinity, and A, C, and E are showing loess models of the change in ratios between carbonate system parameters and salinity over time.

Table 2.1. Long-term trends in carbonate chemistry parameters that have been previously reported in estuaries around the world.

Estuary	**Years of trend**	**pH (units yr^{-1})**	**TA (µmol kg^{-1} yr^{-1})**	***p*CO$_2$ (µatm yr^{-1})**	**DIC (µmol kg^{-1})**	**Source**
Ringkøbing Fjord, Denmark	’80-’95	0.0214	22.6	-33.8[e]	15.1 [e]	Carstensen et al. 2018
Ringkøbing Fjord, Denmark	’96-’16	-0.0088	-3.1	12.4 [e]	-6.0 [e]	Carstensen et al. 2018
Roskilde Fjord, Denmark	’72-’16	-0.0031	19.0	7.81 [e]	7.5 [e]	Carstensen et al. 2018
Skive Fjord, Denmark	’80-’10	-0.0061	18.8	8.06 [e]	6.2 [e]	Carstensen et al. 2018
Baltic Sea	’95 – ‘14		3.4			Müller et al. 2016
Gulf of Bothnia	’95 – ‘14		7			Müller et al. 2016
West Australian estuaries	’95 – ‘16	< -0.00018 - >0.00018				Carstensen and Duarte 2019
Long Island Sound, Thames	’74 – ‘16	-0.004				Snyder et al. 2019
Chesapeake, Chester	’85 – ‘08	0.018[a]				Waldbusser et al. 2011
Chesapeake, Chester	’86 – ‘05		4.9[b]			Najjar et al. 2020
Chesapeake, Choptank	’85 – ‘08	0 [a]				Waldbusser et al. 2011
Chesapeake, Patuxent	’85 – ‘08	0.010 [a]				Waldbusser et al. 2011
Chesapeake, Rappahannock	’85 – ‘08	0.011 [a]				Waldbusser et al. 2011
Chesapeake, James	’85 – ‘08	0.007 [a]				Waldbusser et al. 2011

Chesapeake, Tangier	’85 – ‘08	0.005 [a]			Waldbusser et al. 2011
Chesapeake, Potomac	’84 – ’12		10.9 – 20.8[b]		Najjar et al. 2020
Chesapeake, Potomac	’85 – ‘06			-	Prasad et al. 2013
Chesapeake, Anacostia	’84 – ‘12		5.6 – 11.6[b]		Najjar et al. 2020
Chesapeake, Anacostia	’85 – ‘06			-	Prasad et al. 2013
Neuse River Estuary, NC	’05 – ‘17	0[c]			Van Dam and Wang 2019
Neuse River Estuary, NC	’05 – ‘17	-0.02[d]			Van Dam and Wang 2019
New River Estuary, NC	’05 – ‘17	0[c,d]			Van Dam and Wang 2019
St. Joseph, FL (GOM)	’85-’08	-0.0006			Robbins and Lisle 2018
Wakulla, FL (GOM)	’82-’08	0			Robbins and Lisle 2018
St Johns North, FL (Atl)	’82-’04	0			Robbins and Lisle 2018
Cedar Key, FL (GOM)	’85-’08	-0.0003			Robbins and Lisle 2018
Citrus County, FL (GOM)	’84-’08	-0.0003			Robbins and Lisle 2018
Volusia, FL (Atl)	’81-’04	-0.0004			Robbins and Lisle 2018
Tampa Bay, FL (GOM)	’83-’08	-0.0004			Robbins and Lisle 2018
South Banana River, FL (Atl)	’92-’04	-0.0007			Robbins and Lisle 2018
Indian River, FL (Atl)	’78-’04	-0.0003			Robbins and Lisle 2018
Ten Thousand Islands, FL (GOM)	’83-’08	-0.0022			Robbins and Lisle 2018

Sabine-Neches Estuary, TX	’69 –‘10	0.0081	7.0	Hu et al. 2015
Trinity San-Jacinto Estuary, TX	’69 –‘10	-0.0068 – 0 [e]	-4.9 – 2.6 [e]	Hu et al. 2015
Lavaca-Colorado Estuary, TX	’69 –‘10	-0.0056 – 0 [e]	-19.3 – (-3.6) [e]	Hu et al. 2015
Guadalupe Estuary, TX	’69 –‘10	-0.0041 [e]	-17.0 [e]	Hu et al. 2015
Mission-Aransas Estuary, TX	’69 –‘10	-0.0026 – 0 [e]	-12.2 – (-7.9) [e]	Hu et al. 2015
Nueces Estuary, TX	’69 –‘10	-0.0063 – 0 [e]	-8.4 – 0 [e]	Hu et al. 2015
Laguna Madre Estuary, TX	’69 –‘10	0	-7.6 – 0	Hu et al. 2015

[a] summertime annual trend is provided (the study also reported springtime trends)

[b] trends reported within each estuary are the range (min – max) of rates of change reported for stations/bays within each estuary.

[c] surface water trend is reported (the study reported surface and bottom)

[d] bottom water trend is reported (the study reported surface and bottom)

[e] parameter values used in regression for trend were calculated rather than measured

Supplementary Materials

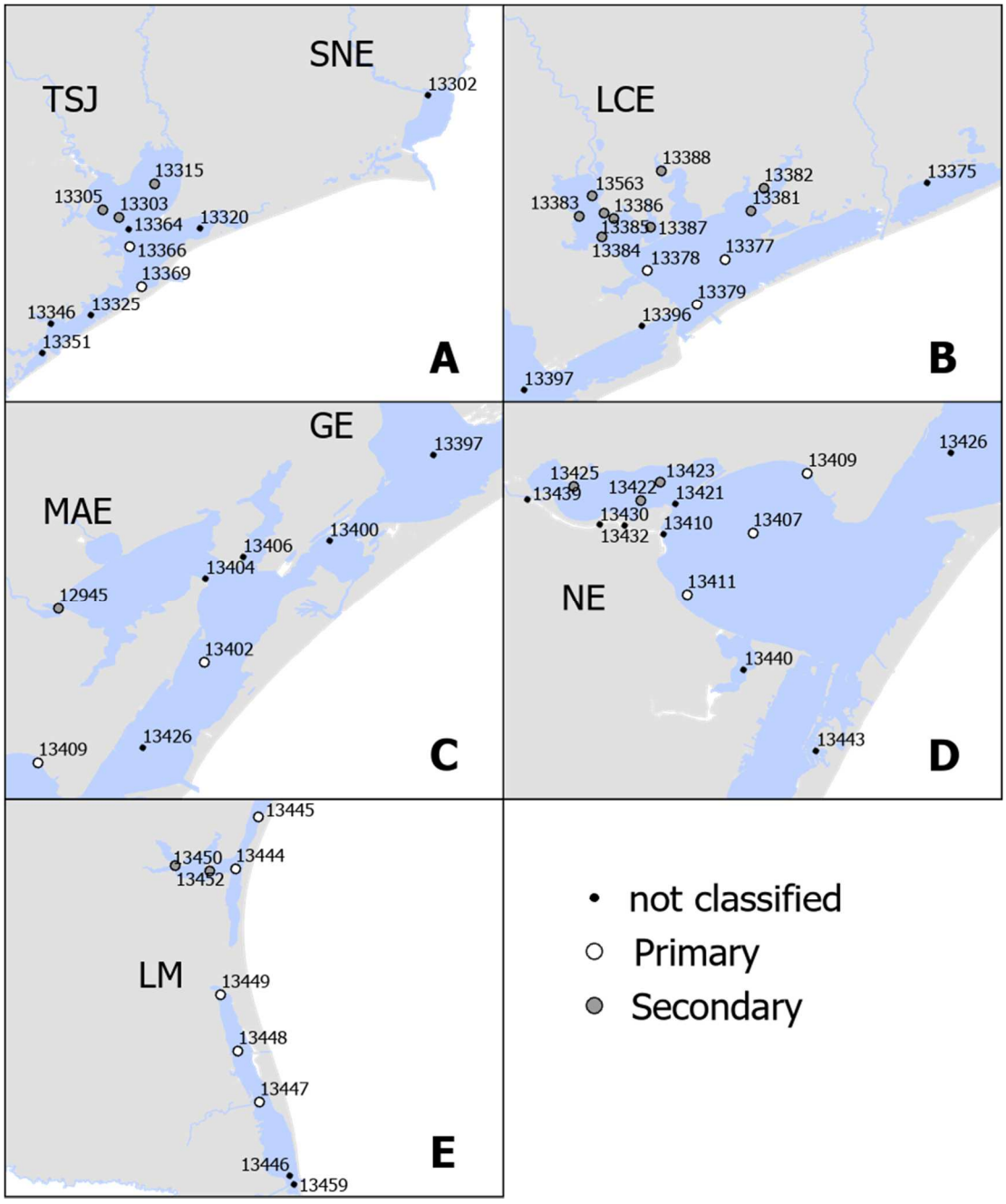

Figure S2.1. Location of numbered TCEQ stations within the estuaries of the nwGOM. Map subsets A-E are ordered from north to south.

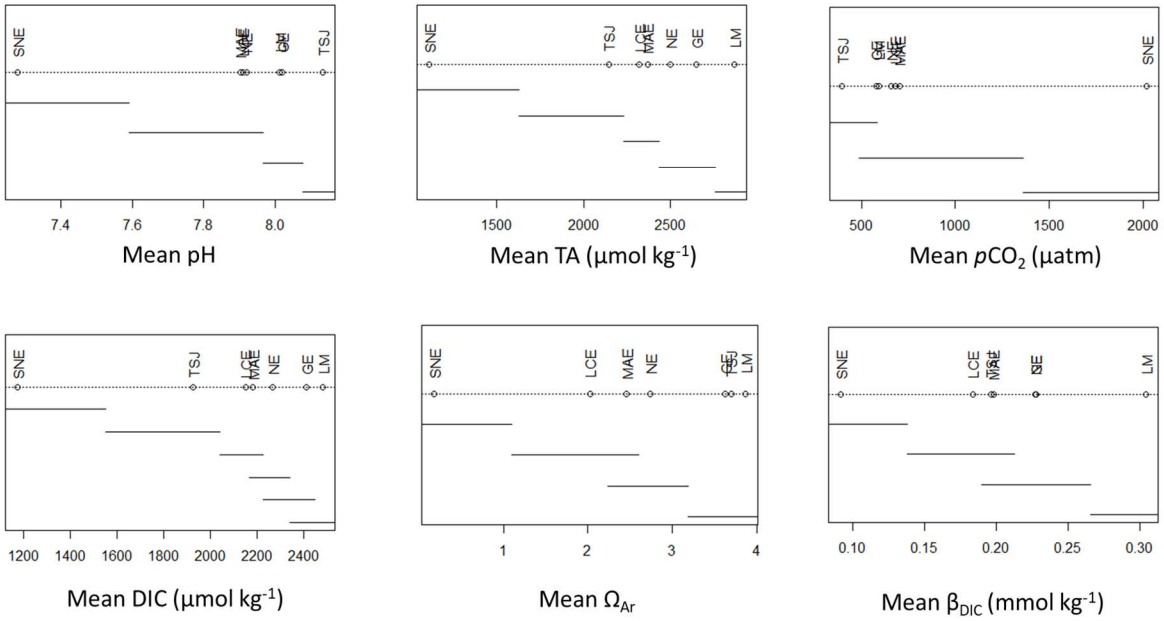

Figure S2.2. Mean values of measured and calculated carbonate system parameters within each estuary (2010 – 2015 data only, except for SNE – see methods). Means of estuaries connected by a line are not significantly different based on the results of post hoc multiple comparisons (Tukey, α=0.05).

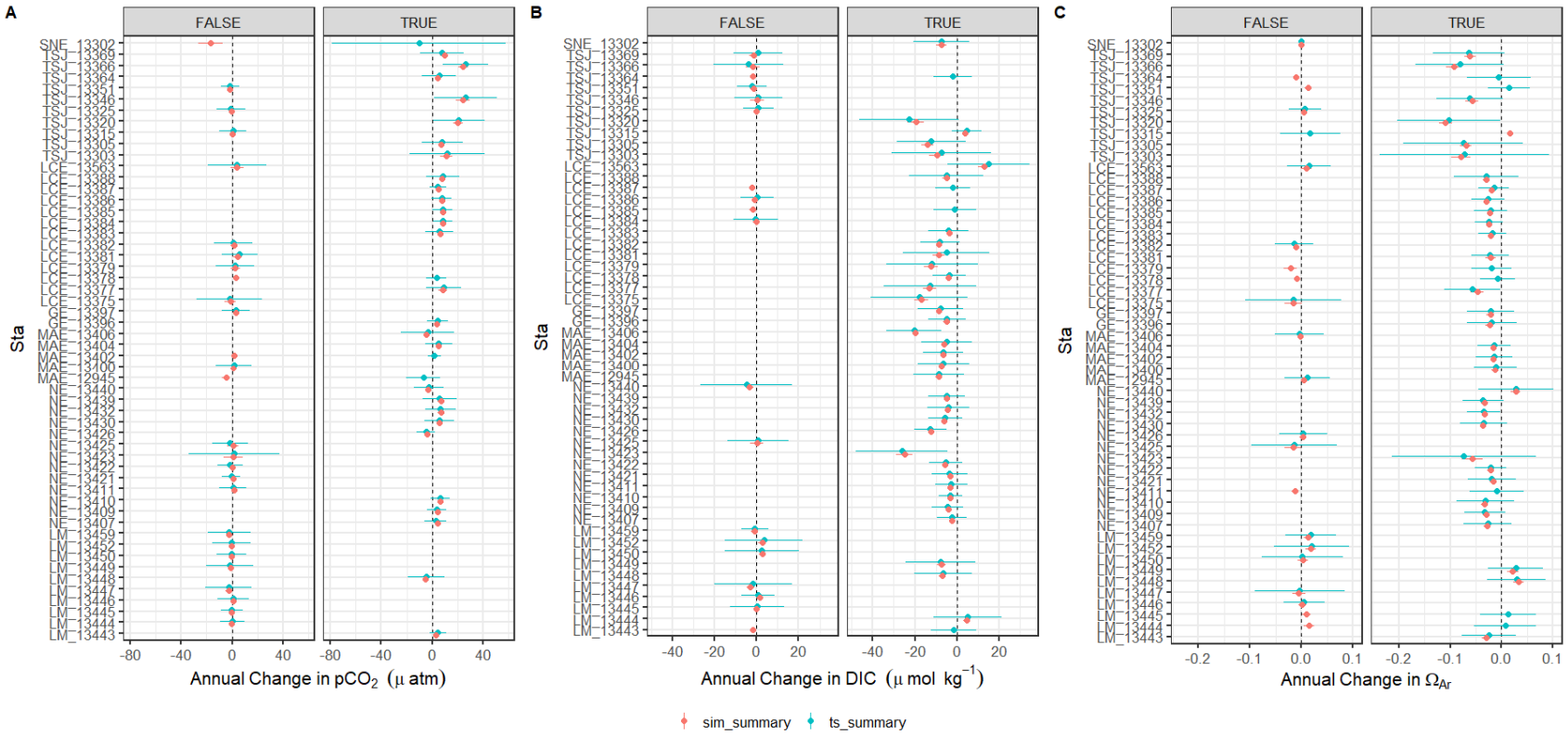

Figure S2.3. Comparison of single Theil-Sen regressions (blue) and TS regressions from simulations accounting for the propagated error (red) associated with pCO_2 (A), DIC (B), and Ω_{Ar} (C). The FALSE column displays those stations where the parameter did not have a significant long-term trend, while the TRUE column represents those stations that did have a significant long-term trend. The bounds of each data point indicate the median absolute difference (MAD) of slopes associated with the single TS regression or the 95% confidence interval in the slopes from 1000 simulations.

Table S2.1. Annual trends in carbonate chemistry parameters based on Theil-Sen regression analyses. NS is reported when the regression was not significant based on alpha = 0.05. Model significance is denoted by asterisks (* <0.05, **<0.01, *** <0.0001). Stations are grouped into estuaries, and estuaries are listed from north to south.

Estuary	Sta	Data Range (yrs)	Temp (°C yr^{-1})	Salinity (units yr^{-1})	pH (yr^{-1})	TA (µmol kg^{-1} yr^{-1})	pCO_2 (µatm yr^{-1})	DIC (µmol kg^{-1} yr^{-1})	Ω_{Ar}	β_{DIC} (mmol kg^{-1} yr^{-1})
SNE	13302	34	NS	NS	0.0063 *	-7.9 *	-10.4 *	-7.3 **	NS	-0.001 *
TSJ	13303	20	NS	-0.24 ***	-0.0073 **	-15.8 ***	11.7 **	-7.5 ***	-0.0721 ***	-0.003 ***
	13305	38	0.18 **	-0.03 *	-0.0094 ***	-17.4 ***	8.0 **	-12.1 ***	-0.0746 ***	-0.003 ***
	13315	21	0.10 *	0.04 *	NS	3.6 **	NS	4.7 ***	NS	0.001 **
	13320	39	NS	-0.29 ***	-0.0225 ***	-30.3 ***	20.9 ***	-22.7 ***	-0.1032 ***	-0.005 ***
	13325	21	NS	NS	NS	NS	NS	NS	NS	NS
	13346	27	NS	NS	-0.0174 ***	NS	26.1 ***	NS	-0.0621 ***	-0.001 **
	13351	39	0.10 *	NS	0.0017 *	NS	NS	NS	0.0141 *	NS
	13364	20	NS	-0.08 **	-0.0021 **	-1.6 **	5.3 ***	-2.1 **	-0.0050 *	-0.001 **
	13366	27	NS	-0.26 ***	-0.0218 ***	-9.6 ***	26.1 ***	NS	-0.0811 ***	-0.003 ***
	13369	39	NS	NS	-0.0079 ***	-5.7 ***	7.5 **	NS	-0.0634 ***	-0.002 ***
LCE	13375	36	NS	0.49 ***	NS	-19.5 ***	NS	-17.9 ***	NS	NS
	13377	27	0.11 *	NS	-0.0081 ***	-21.3 ***	9.0 **	-12.7 ***	-0.0569 ***	-0.003 ***
	13378	39	0.05 *	0.17 ***	-0.0026 ***	-4.9 ***	3.3 *	-3.4 ***	-0.0071 **	NS

	13379	39	NS	-0.17 **	-0.0030 *	-15.7 ***	NS	-11.8 ***	-0.0197 **	-0.002 ***
	13381	39	0.13 **	0.17 **	-0.0041 **	-10.9 **	NS	-5.0 **	-0.0225 **	-0.001 **
	13382	39	NS	0.13 ***	NS	-10.5 ***	NS	-8.0 ***	NS	NS
	13383	39	NS	0.23 ***	-0.0071 ***	-3.9 **	5.6 ***	-4.1 **	-0.0176 ***	-0.001 *
	13384	23	0.07 *	0.19 ***	-0.0072 ***	-1.4 *	8.2 ***	NS	-0.0243 ***	0.000 **
	13385	27	NS	0.13 ***	-0.0081 ***	-2.1 **	8.1 ***	-0.9 *	-0.0214 ***	-0.001 **
	13386	38	NS	0.18 ***	-0.0090 ***	-2.1 **	7.4 ***	NS	-0.0259 ***	-0.001 **
	13387	27	NS	0.18 ***	-0.0058 ***	-2.6 **	4.4 ***	-2.0 **	-0.0147 ***	NS
	13388	27	0.07 **	0.05 *	-0.0086 ***	-3.4 *	8.5 ***	-4.9 *	-0.0301 ***	NS
	13563	39	NS	0.73 ***	-0.0031 *	16.7 **	NS	15.0 **	NS	0.002 **
GE	13396	36	0.08 **	0.10 ***	-0.0049 ***	-6.1 ***	4.3 **	-4.7 ***	-0.0188 ***	-0.001 ***
	13397	39	0.11 **	0.20 ***	-0.0030 **	-9.8 ***	NS	-7.7 ***	-0.0211 **	NS
MAE	12945	38	NS	0.33 ***	-0.0013 *	-5.9 ***	-6.9 **	-8.4 ***	NS	NS
	13400	39	NS	0.18 ***	-0.0012 **	-6.6 ***	NS	-6.4 ***	-0.0011 **	NS
	13402	39	NS	NS	-0.0033 ***	-7.6 ***	1.6 **	-6.4 ***	-0.0145 ***	0.000 **
	13404	39	NS	0.16 ***	-0.0052 ***	-8.4 ***	5.2 **	-4.8 ***	-0.0149 ***	-0.001 *
	13406	34	NS	0.09 ***	NS	-18.0 ***	-3.5 *	-20.3 ***	NS	-0.001 *
NE	13407	39	NS	0.10 ***	-0.0027 ***	-3.9 ***	2.7 ***	-2.3 ***	-0.0267 ***	-0.001 ***
	13409	39	0.09 *	0.11 ***	-0.0037 ***	-5.0 ***	3.5 ***	-4.3 ***	-0.0327 ***	-0.001 **

	13410	39	NS	0.10 ***	-0.0053 ***	-4.6 ***	6.3 ***	-3.1 ***	-0.0317 ***	-0.001 ***
	13411	39	NS	0.11***	-0.0006 *	-4.7 ***	NS	-2.6 ***	-0.0093 *	-0.001 *
	13421	39	NS	0.18 ***	-0.0002 *	-3.4 **	NS	-3.4 ***	-0.0189 **	NS
	13422	39	NS	0.20 ***	-0.0024 **	-5.1 ***	NS	-5.2 ***	-0.0214 ***	NS
	13423	39	NS	0.60 ***	-0.0110 *	-13.6 **	NS	-26.1 ***	-0.0735 *	NS
	13425	39	NS	0.77***	-0.0040 **	NS	NS	NS	NS	0.002 **
	13426	39	NS	0.09 ***	0.0022 **	-8.8 ***	-4.7 ***	-12.6 ***	NS	NS
	13430	20	NS	0.11 ***	-0.0042 ***	-6.6 ***	5.6 **	-5.5 ***	-0.0345 ***	-0.001 ***
	13432	23	NS	0.11 ***	-0.0040 ***	-7.0 ***	6.6 ***	-4.0 ***	-0.0343 ***	-0.001 ***
	13439	34	NS	0.09 ***	-0.0025 ***	-5.3 ***	5.7 **	-4.8 ***	-0.0358 ***	-0.002 ***
	13440	39	-0.13 **	0.17 *	0.0035 ***	NS	-2.8 **	NS	0.0279 **	0.002 ***
LM	13443	38	NS	0.12 ***	-0.0040 **	-3.6 ***	4.3 **	-1.4	-0.0249 ***	-0.001 **
	13444	38	NS	0.19 ***	NS	7.2 **	NS	5.0 *	0.0073 **	0.001 ***
	13445	39	0.06 *	0.17 ***	NS	NS	NS	NS	0.0128 **	0.001 **
	13446	38	-0.09 **	0.10 ***	NS	NS	NS	NS	NS	NS
	13447	38	NS	0.23 ***	NS	NS	NS	NS	NS	0.001 *
	13448	37	0.13 **	NS	0.0029 **	NS	-4.8 **	-6.5 **	0.0292 ***	0.001 ***
	13449	36	0.15 ***	0.08 *	NS	NS	NS	-7.8 **	0.0275 *	0.001 **
	13450	37	NS	0.10 *	NS	NS	NS	NS	NS	NS
	13452	35	NS	0.18 **	NS	7.2 **	NS	NS	NS	0.001 *
	13459	37	NS	0.09 ***	NS	1.9 **	NS	NS	NS	0.001 *

Table S2.2. Mean carbonate system characteristics (across all stations and all sampling, 1974 – 2015) in the estuaries of the nwGOM. Estuaries are listed from northeast to southwest. Estuaries that had multiple stations within the primary and secondary bays have separate means reported for primary (P) and secondary (S) stations, while means for the entire estuary (E) are reported for estuaries without ample stations.

Estuary	**Estuary Section**	**Salinity**	**pH**	**TA ($\mu mol\ kg^{-1}$)**	**pCO_2 (μatm)**	**DIC ($\mu mol\ kg^{-1}$)**	**Ω_{Ar}**	**β_{DIC} ($mmol\ kg^{-1}$)**
SNE	E	6.7 ± 4.4	7.28 ± 0.37	973 ± 322	2377 ± 2266	1043 ± 317	0.2 ± 0.2	0.10 ± 0.07
TSJ	P	20.2 ± 6.4	7.98 ± 0.25	2050 ± 241	580 ± 341	1899 ± 225	2.7 ± 1.6	0.16 ± 0.05
	S	13.0 ± 6.8	8.10 ± 0.30	1924 ± 311	505 ± 413	1787 ± 258	3.1± 2.0	0.14 ± 0.06
LCE	P	25.0 ± 6.6	8.01 ± 0.23	2335 ± 278	577 ± 380	2131 ± 267	2.5 ± 1.2	0.20 ± 0.06
	S	19.7 ± 8.7	7.99 ± 0.27	2269 ± 364	676 ± 548	2110 ± 331	2.4 ± 1.4	0.17 ± 0.06
GE	E	22.0 ± 8.6	8.05 ± 0.25	2563 ± 378	641 ± 525	2428 ± 372	3.8 ± 2.2	0.22 ± 0.06
MAE	P	24.4 ± 8.4	8.04 ± 0.23	2523 ± 290	584 ± 456	2291 ± 281	3.2 ± 1.6	0.22 ± 0.06
	S	16.0 ± 11.6	7.93 ± 0.25	2556 ± 502	961 ± 788	2438 ± 487	2.3 ± 1.4	0.16 ± 0.06
NE	P	31.2 ± 5.4	7.99 ± 0.20	2537 ± 255	608 ± 405	2279 ± 236	3.2 ± 1.4	0.24 ± 0.06
	S	26.4 ± 10.3	7.93 ± 0.25	2556 ± 293	789 ± 538	2364 ± 277	2.2 ± 0.2	0.21 ± 0.07
LM	P	33.7 ± 9.3	8.05 ± 0.26	2792 ± 459	626 ± 672	2437 ± 494	4.0 ± 1.9	0.29 ± 0.09
	S	37.5 ± 12.3	8.04 ± 0.27	2840 ± 593	594 ± 483	2437 ± 516	4.2 ± 2.2	0.31 ± 0.12

CHAPTER III: TEMPORAL VARIABILITY AND DRIVING FACTORS OF THE CARBONATE SYSTEM IN THE ARANSAS SHIP CHANNEL, TX: A TIME-SERIES STUDY

Abstract

The coastal ocean experiences substantial heterogeneity in water chemistry, including carbonate chemistry parameters such as pH and partial pressure of CO_2 (pCO_2), because of the diversity of co-occurring biogeochemical processes. To better understand coastal and estuarine acidification and air-sea CO_2 fluxes, it is important to study baseline variability and driving factors of carbonate chemistry. Using both discrete bottle sample collection (2014-2020) and hourly sensor measurements (2016-2017), temporal variability was explored, from diel to interannual scales, in the carbonate system (specifically pH and pCO_2) at the Aransas Ship Channel located in northwestern Gulf of Mexico. Using other co-located environmental sensors, the driving factors of that variability were also explored. Both sampling methods demonstrated significant seasonal variability at the location, with highest pH (lowest pCO_2) in the winter and lowest pH (highest pCO_2) in the summer. Significant diel variability was also evident from sensor data, but the time of day with elevated pCO_2/depressed pH was not consistent across the entire monitoring period, sometimes reversing from what would be expected from a biological signal. Though seasonal and diel fluctuations were smaller than many other areas previously studied, carbonate chemistry parameters were among the most important environmental parameters to distinguish between time of day and between seasons. It is evident that

temperature, biological activity, freshwater inflow, and tide level (despite the small tidal range) are all important controls on the system, with different controls dominating at different time scales. The results indicate that the controlling factors of the carbonate system may not be exerted equally on both pH and pCO_2 on diel timescales, causing separation of their diel or tidal relationships during certain seasons. Despite known temporal variability on shorter timescales, discrete sampling was generally representative of the average carbonate system and average air-sea CO_2 flux on a seasonal and annual basis based on comparison with sensor data.

3.1 Introduction

Coastal waters and estuaries, the dynamic environments where the coast and freshwater inflows meet the ocean, are economically and ecologically important because they are biological hotspots, but they are also heavily influenced by anthropogenic activity. Because of the diversity of co-occurring biogeochemical processes, coastal waters (especially estuaries) experience substantial spatial and temporal heterogeneity in water chemistry, including carbonate chemistry parameters such as pH and partial pressure of CO_2 (pCO_2) (Hofmann et al. 2011; Waldbusser and Salisbury, 2014). Carbonate chemistry, or the speciation of inorganic carbon in seawater, is important because an addition of CO_2 acidifies seawater, whether it is a result of uptake from the atmosphere (generally acknowledged as ocean acidification, or OA) or it is produced by biogeochemical processes in the water (that may intensify or alleviate the effects of OA). Acidification can negatively affect marine organisms, especially those that construct calcium carbonate shells and skeletons (Barton et al. 2015; Bednaršek et al. 2012; Ekstrom et al. 2015; Gazeau et al. 2007; Gobler and Talmage, 2014). Additionally, despite the small surface area of coastal waters relative to the global ocean, coastal waters are recognized as important contributors in global carbon cycling (Borges, 2005; Cai, 2011; Laruelle et al. 2018).

While open ocean environments are relatively well studied and understood regarding carbonate chemistry, acidification, and air-sea CO_2 fluxes, large uncertainties remain in coastal environments. Estuaries are especially challenging to fully understand because of the heterogeneity between and within estuaries that is driven by diverse processes operating on different time scales such as river discharge, nutrient and organic matter loading, stratification, and coastal upwelling (Jiang et al. 2013; Mathis et al. 2012). The traditional sampling method for carbonate system characterization involving discrete water sample collection and laboratory analysis is known to lead to biases in average pCO_2 and CO_2 flux calculations due to daytime sampling that neglects to capture diel variability (Li et al. 2018). Mean diel ranges in pH can exceed 0.1 unit in many coastal environments, and especially high diel ranges (even exceeding 1 pH unit) have been reported in biologically productive areas or areas with higher mean pCO_2 (Challener et al. 2016; Cyronak et al. 2018; Schulz and Riebesell, 2013; Semesi et al. 2009; Yates et al. 2007). These diel ranges can far surpass the magnitude of the changes in open ocean surface waters that have occurred since the start of the industrial revolution and rival spatial variability in productive systems, indicating their importance for a full understanding of the carbonate system.

Despite the need for high-frequency measurements, sensor deployments have been limited in estuarine environments (especially compared to their extensive use in the open ocean) because of the challenges associated with varying conditions, biofouling, and sensor drift (Sastri et al. 2019). Carbonate chemistry monitoring in the Gulf of Mexico (GOM), has been relatively minimal compared to the United States east and west coasts. The GOM estuaries currently have less exposure to concerning levels of acidification than other estuaries because of their high temperatures (causing water to hold less CO_2 and support high productivity year-round) and

often suitable river chemistries (i.e., relatively high buffer capacity) (McCutcheon et al. 2019; Yao et al. 2020). However, respiration-induced acidification is present in both the open GOM (e. g., subsurface water influenced by the Mississippi River Plume and outer shelf region near the Flower Garden Banks National Marine Sanctuary) and GOM estuaries, and most estuaries in the northwestern GOM have also experienced long-term acidification (Cai et al. 2011; Hu et al. 2018, 2015; Kealoha et al. 2020; McCutcheon et al. 2019; Robbins and Lisle, 2018). This known acidification as well as the relatively high CO_2 efflux from the estuaries of the northwest GOM illustrates the necessity to study the baseline variability and driving factors of carbonate chemistry in the region. In this study, temporal variability in the carbonate system in Aransas Ship Channel—a tidal inlet where the lagoonal estuaries meet the coastal waters in a semi-arid region of the northwestern GOM—was explored using both discrete bottle sample collection and hourly sensor measurements, and the driving factors of that variability were explored using data from other co-located environmental sensors.

3.2 Materials and Methods

3.2.1 Location

Autonomous sensor monitoring and discrete water sample collections for laboratory analysis of carbonate system parameters were performed in the Aransas Ship Channel (ASC, located at 27˚50'17"N, 97˚3'1"W). ASC is one of the few permanent tidal inlets that intersect a string of barrier islands and connect the GOM coastal waters with the lagoonal estuaries in the northwest GOM (Fig. 1). ASC provides the direct connection between the northwestern GOM and the Mission-Aransas Estuary (Copano and Aransas Bays) to the north and Nueces Estuary (Nueces and Corpus Christi Bays) to the south (Fig. 3.1). The region is microtidal, with a relatively small tidal range, ranging from ~ 0.6 m tides on the open coast to less than 0.3 m in

upper estuaries (Montagna et al. 2011). Mission-Aransas Estuary (MAE) is fed by two small rivers, the Mission (1787 km^2 drainage basin) and Aransas (640 km^2 drainage basin) Rivers (http://waterdata.usgs.gov/), which both experience low base flows punctuated by periodic high flows during storm events. MAE has an average residence time of one year (Solis and Powell, 1999), so there is a substantial lag between time of rainfall and riverine delivery to ASC in the lower estuary. A significant portion of riverine water flowing into Aransas Bay originates from the larger rivers further northeast on the Texas coast via the Intracoastal Waterway (i.e., Guadalupe River (26,625 km^2 drainage basin) feeds San Antonio Bay, which has a much shorter residence time of nearly 50 days) (Solis and Powell, 1999; USGS, 2001).

3.2.2 Continuous Monitoring

Autonomous sensor monitoring (referred to throughout as continuous monitoring) of pH and pCO_2 was conducted from Nov. 8, 2016 to Aug. 23, 2017 at the University of Texas Marine Science Institute's research pier in ASC. The sensor deployment was shorter than intended because the pier was destroyed in the aftermath of Hurricane Harvey in 2017. The pH data were collected using an SAtlantic® SeaFET pH sensor (on total pH scale) and pCO_2 data were collected using a Sunburst® SAMI-CO_2. Temperature and salinity data were measured by a YSI® 600OMS V2 sonde. Hourly data (single hourly measurements, measured on the hour) collected by all sensors (pH, pCO_2, salinity, and temperature) were saved in the onboard data loggers and downloaded during service trips to the field site. Sensor failures or pump failures occurred for short periods of time throughout the deployment. Measurements were recorded on 262 individual days, with 176 of those days having the full set of 24 (hourly) measurements.

Ideally, *in-situ* sensors should be deployed under the sea surface. However, to reduce the maintenance cost and effort for sensors deployed in warm water that experiences intense

biofouling, the sensors were set up to measure pH and pCO_2 from an *ex situ* position using *in situ* seawater. Water was pumped from ~1 m below the sea surface into the bottom spigot of a 100-Qt cooler that housed the SAMI-CO2 and SeaFET sensors. To allow water outflow, a 1" hole was drilled at the opposite side of the spigot near the top of the cooler rim, allowing water to flow back to the sea surface. The pump was programmed to turn on 20 minutes before each hour, pumping more than enough water to fully flush the cooler, and sensors recorded measurements on the hour. The YSI sonde was deployed directly into ASC inside a 2" PVC pipe at ~1 m below the sea surface.

Visits to the field site were conducted every two weeks to service all sensors and clean the cooler. Additionally, duplicate, discrete water samples were collected on the hour during service trips for quality assurance of sensor data and to check that surface water and cooler chemistries aligned. (See supplemental materials for additional information about discrete quality assurance samples, removal of suspicious sensor data, and a direct comparison of discrete quality assurance samples to sensor data). Based on discrete quality assurance samples, there was an average offset of 0.05 ± 0.10 between the cooler pH measured spectrophotometrically in the laboratory and measured by the SeaFet. The direction and magnitude of offset between the sensor and laboratory pH did not display a clear trend over time, thus the average difference was used to establish a correction of -0.05 across the entire sensor pH dataset. The difference between the sensor pCO_2 and calculated pCO_2 was not used for a correction since there is error associated with the calculation of pCO_2 from discrete samples and the spectrophotometric measurements of the SAMI-CO2 should not experience drift.

3.2.3 Discrete sample collection and analysis

Long-term monitoring via discrete water sample collection was conducted at ASC from May 2, 2014 to February 25, 2020 (in addition to the quality assurance discrete sample collections). Sampling was conducted every two weeks during the summer months and monthly during the winter months from a small vessel at a location < 20 m from the sensor deployment. Water sample collection followed standard protocol for ocean carbonate chemistry studies (Dickson et al. 2007). Ground glass borosilicate bottles (250 mL) were filled with surface water and preserved with 100 µL saturated mercury chloride ($HgCl_2$). Apiezon® grease was applied to the bottle stopper, which was then secured to the bottle using a rubber band and a nylon hose clamp.

These samples were used for laboratory dissolved inorganic carbon (DIC) and pH measurements. DIC was measured by injecting 0.5 mL of sample into 1 ml 10% H_3PO_4 (balanced by 0.5 M NaCl) with a high-precision Kloehn syringe pump. The CO_2 gas produced through sample acidification was then stripped using high-purity nitrogen gas and carried into a Li-Cor infrared gas detector. DIC analyses had a precision of 0.1%. Certified Reference Material (CRM) was used to ensure the accuracy of the analysis (Dickson et al. 2003). For samples with salinity>20, pH was measured using a spectrophotometric method at 25 ± 0.1°C (Carter et al. 2003) and the Douglas and Byrne (2017) equation. Analytical precision of the spectrophotometric method for pH measurement was ±0.0004 pH units. A calibrated Orion Ross glass pH electrode was used to measure pH at 25 ± 0.1°C for samples with salinity<20, and analytical precision was ±0.01 pH units. All pH values obtained using the potentiometric method were converted to total scale at *in situ* temperature (Millero, 2001). Salinity of the discrete samples was measured using a benchtop salinometer calibrated by MilliQ water and a known

salinity CRM. For discrete samples, pCO_2 was calculated in CO2Sys for Excel using laboratory-measured salinity, DIC, pH, and *in situ* temperature for calculations (Xu et al. 2017). Carbonate speciation calculations were done using Millero (2010) carbonic acid dissociation constants (K_1 and K_2), Dickson (1990) bisulfate dissociation constant, and Uppström (1974) borate concentration.

3.2.4 Calculation of CO_2 fluxes

Equation 3.1 was used for air-water CO_2 flux calculations (Wanninkhof, 1992; Wanninkhof et al. 2009). Positive flux values indicate CO_2 emission from the water into the atmosphere (the estuary acting as a source of CO_2), and negative flux values indicate CO_2 uptake by the water (the estuary acting as a sink for CO_2).

$$F = k\, K_0\, (pCO_{2,w} - pCO_{2,a}) \qquad (3.1)$$

where k is the gas transfer velocity (in m d^{-1}), K_0 (in mol l^{-1} atm^{-1}) is the solubility constant of CO_2 (Weiss, 1974), and $pCO_{2,w}$ and $pCO_{2,a}$ are the partial pressure of CO_2 (in µatm) in the water and air, respectively.

We used the wind speed parameterization for gas transfer velocity (*k*) from Jiang et al. (2008) converted from cm h^{-1} to m d^{-1}, which is thought to be the best estuarine parameterization at this time (Crosswell et al. 2017), as it is a composite of *k* over several estuaries. The calculation of *k* requires a windspeed at 10 m above the surface, so windspeeds measured at 3 m above the surface were converted using the power law wind profile (Hsu, 1994; Yao and Hu, 2017). To assess uncertainty, other parameterizations with direct applications to estuaries in the literature were also used to calculate CO_2 flux (Raymond and Cole, 2001; Ho et al. 2006). It is noted that parameterization of *k* based on solely windspeed is flawed because several additional

parameters can contribute to turbulence including turbidity, bottom-driven turbulence, water-side thermal convection, tidal currents, and fetch (Wanninkhof 1992; Abril et al. 2009; Ho et al. 2014; Andersson et al. 2017), however it is currently the best option for this system given the limited investigations of CO_2 flux and contributing factors in estuaries.

Hourly averaged windspeed data for use in CO_2 flux calculations were retrieved from the NOAA-controlled Texas Coastal Ocean Observation Network (TCOON; https://tidesandcurrents.noaa.gov/tcoon.html). Windspeed data from the nearest TCOON station (Port Aransas Station – located directly in ASC, < 2 km inshore from our monitoring location) was prioritized when data were available. During periods of missing windspeed data at the Port Aransas Station, wind speed data from TCOON's Aransas Pass Station (< 2 km offshore from monitoring location) were next used, and for all subsequent gaps, data from TCOON's Nueces Bay Station (~ 40 km away) were used (Fig. 1). Additional information on windspeed data used can be found in supplementary materials. For continuous monitoring data, each hourly measurement of pCO_2 was paired with the corresponding hourly averaged windspeed for flux calculations. For discrete sample data, the pCO_2 calculated for each sampled day was paired with the corresponding daily averaged windspeed (calculated from the retrieved hourly averaged windspeeds) for flux calculations.

Monthly mean atmospheric xCO_2 data (later converted to pCO_2) for flux calculations were obtained from NOAA's flask sampling network of the Global Monitoring Division of the Earth System Research Laboratory at the Key Biscayne (FL, USA) station (https://www.esrl.noaa.gov/gmd/dv/data/index.php?site=KEY&parameter_name=Carbon%2BDioxide). Data from Key Biscayne were not available for the entire period of our discrete sample collection, so monthly global average values were used

(ftp://aftp.cmdl.noaa.gov/products/trends/co2/co2_mm_mlo.txt) to fill in missing values (16 months from January 2019 – February 2020). This substitution of global average values is justified because the monthly means between Key Biscayne and global xCO_2 over the initial 56 months of our discrete sampling only differed by 1.2 ± 1.5 µatm (i.e, 0.3% ± 0.4%). Each pCO_2 observation (whether using continuous or discrete data) was paired with the corresponding monthly averaged windspeed for flux calculations.

3.2.5 Additional data retrieval and data processing to investigate carbonate system variability and controls

All reported annual mean values are seasonally weighted to account for disproportional sampling between seasons. However, reported annual standard deviation is associated with the un-weighted, arithmetic mean (Table S3.1). Temporal variability was investigated in the form of seasonal and diel variability (Tables S3.1 and S3.2). For seasonal analysis, December to February was considered winter, March to May was considered spring, June to August was considered summer, and September to November was considered fall. It is important to note that the Fall season had much fewer continuous sensor observations than other seasons because of the timing of sensor deployment. For diel comparisons, daytime and nighttime variables were defined as 09:00-15:00 local standard time and 21:00-03:00 local standard time, respectively, based on the 6-hour periods with highest and lowest photosynthetically active radiation (PAR; data from co-located sensor, obtained from the Mission-Aransas National Estuarine Research Reserve (MANERR) at https://missionaransas.org/science/download-data). Diel ranges in parameters were calculated (daily maximum minus daily minimum) and only reported for days with the full 24 hours of hourly measurements (176 out of 262 measured days) to ensure that data gaps did not influence the diel ranges (Table S3.2).

Controls on pCO_2 from thermal and non-thermal (i.e., combination of physical and biological processes) were investigated following Takahashi et al. (2002) over annual, seasonal, and daily time scales using both continuous and discrete data. Over any given time period, this method uses the ratio of the ranges of temperature-normalized pCO_2 ($pCO_{2,nt}$, Eq. 3.2) and the mean annual pCO_2 perturbed by the difference between mean and observed temperature ($pCO_{2,t}$, Eq. 3.3) to calculate the relative influence of non-thermal and thermal effects on pCO_2 (T/B, Eq. 3.4). When calculating annual T/B values with discrete data, only complete years (sampling from January to December) were included (2014 and 2020 were omitted). When calculating daily T/B values with continuous data, only complete days (24 hourly measurements) were included.

$$pCO_{2,nt} = pCO_{2,obs} \times \exp[\delta \times (T_{mean} - T_{obs})] \quad (3.2)$$

$$pCO_{2,t} = pCO_{2,mean} \times \exp[\delta \times (T_{obs} - T_{mean})] \quad (3.3)$$

Where the value for δ (0.0411 $°C^{-1}$), which represents average [$\partial\, ln\, pCO_2$ / ∂ Temperature] from field observations, was taken directly from Yao and Hu (2017), T_{obs} is the observed temperature, and T_{mean} is the mean temperature over the investigated time period.

$$T/B = \frac{\max(pCO_{2,thermal}) - \min(pCO_{2,thermal})}{\max(pCO_{2,non-thermal}) - \min(pCO_{2,non-thermal})} \quad (3.4)$$

Where a T/B greater than one indicates that temperature's control on pCO_2 is greater than the control from non-thermal factors and a T/B less than one indicates that non-thermal factors' control on pCO_2 is greater than the control from temperature.

Tidal control on parameters was investigated using our continuous monitoring data and tide level data obtained from NOAA's Aransas Pass Station (same Aransas Pass Station used for windspeed data, < 2 km offshore from monitoring location, Fig. 3.1) at

https://tidesandcurrents.noaa.gov/waterlevels.html?id=8775241&name=Aransas,%20Aransas%20Pass&state=TX. Hourly measurements of water level were merged with our sensor data by date and hour. Given that there were gaps in available water level measurements (and no measurements prior to December 20, 2016), the usable dataset was reduced from 6088 observations to 5121 observations and fall was omitted from analyses. To examine differences between parameters during high tide and low tide, high tide was defined as tide level greater than the third quartile tide level value and low tide as a tide level less than the first quartile tide level value.

Other factors that may exert control on the carbonate system were investigated through parameter relationships. In addition to previously discussed tide and windspeed data, dissolved oxygen (DO), PAR, turbidity, and chlorophyll fluorescence data from MANERR-deployed environmental sensors that were co-located at our monitoring location were obtained (https://missionaransas.org/science/download-data). Given that MANERR data are all measured in the bottom water (>5 m) while our sensors were measuring surface waters, the observations with significant water column stratification (defined as a salinity difference > 3 between surface water and bottom water) were excluded from analyses. Omitting stratified water reduced our continuous dataset from 6088 to 5524 observations (removing 260 winter, 133 spring, 51 summer, and 120 fall observations), and omitting observations where there were no MANERR data to determine stratification further reduced the dataset to 4112 observations. Similarly, removing instances of stratification reduced discrete sample data from 104 to 89 surface water observations.

3.2.6 Statistical analyses

All statistical analyses were performed in R, version 4.0.3 (R Core Team, 2020). To investigate differences between daytime and nighttime parameter values (temperature, salinity, pH, pCO_2, and CO_2 flux) using continuous monitoring data across the full sampling period and within each season, paired *t*-tests were used, pairing each respective day's daytime and nighttime values (Table S3.2). Loess models (locally weighted polynomial regression) were also used to identify changes in diel patterns over the course of our monitoring period (performed in splines package in R; R Core Team, 2020).

Two-way ANOVAs were used to examine differences in parameter means between seasons and between monitoring methods (Table S3.3). Since there were significant interactions (between season and sampling type factors) in the two-way ANOVAs for each individual parameter (Table S3.3), differences between seasons were investigated within each monitoring method (one-way ANOVAs) and the differences between monitoring methods were investigated within each season (one-way ANOVAs). For the comparison of monitoring methods, both the full discrete sampling data as well as a subset of the discrete sampling data to overlap with the continuous monitoring period (referred to throughout as reduced discrete data or D_C in figures) were included along with the continuous data. To interpret differences between monitoring methods, a difference in means between the continuous monitoring and discrete monitoring datasets would only indicate that the 10-month period of continuous monitoring was not representative of the 5+ year period that discrete samples have been collected, but a difference in means between the continuous data and discrete sample data collected during the continuous monitoring period represents discrepancies between types of monitoring. Post-hoc multiple

comparisons (between seasons within sampling types and between sampling types within seasons) were conducted using the Westfall adjustment (Westfall, 1997).

Differences in parameters between high tide and low tide conditions were investigated using a two-way ANOVA to model parameters based on tide level and season. In models for each parameter, there was a significant interaction between tide level and season factors (based on α=0.05, results not shown), thus t-tests were used (within each season) to examine differences in parameters between high and low tide conditions. Note that fall was omitted from this analysis because tide data were only available at the location beginning December 20, 2016. Sample sizes were the same for each parameter (High tide – winter: 354, spring: 569, summer: 350; Low tide – winter: 543, spring: 318, summer: 415).

Additionally, to gain insight to carbonate system controls through correlations, Pearson correlation analyses were conducted to examine individual correlations of pH and pCO_2 (both continuous and discrete) with other environmental parameters (Table S3.4).

To better understand overall system variability over different time scales, linear discriminant analysis (LDA) was used, which is a multivariate statistic that allows dimensional reduction to determine the linear combination of environmental parameters (individual parameters reduced into linear discriminants, LDs) that allow the best differentiation between day and night as well as between seasons (performed using the MASS package in R; Venables and Pipley, 2020). The pCO_2, pH, temperature, salinity, tide level, wind speed, total PAR, DO, turbidity, and fluorescent chlorophyll were included in this analysis. All variables were centered and scaled to allow direct comparison of their contribution to the system variability. The magnitude (absolute value) of coefficients of the LDs (Table 3.1) represents the relative importance of each individual environmental parameter in the best discrimination between day

and night and between seasons, i.e., the greater the absolute value of the coefficient, the more information the associated parameter can provide about whether the sample came from day or night (or winter, spring, or summer). Only one LD could be created for the diel variability (since there are only two classes to discriminate between – day and night). Two LDs could be created for the seasonal variability (since there were three classes to discriminate between – fall was omitted because of the lack of tidal data), but only the coefficients for LD1 are reported since LD1 captured 95.64% of the seasonal variability.

3.3 Results

3.3.1 Seasonal variability

Both the continuous and discrete data showed substantial seasonal variability for all parameters (Fig. 3.2, Tables S3.1 and S3.2). All discrete sample results reported here are for the entire 5+ years of monitoring; the subset of discrete sample data that overlaps with the continuous monitoring period will be addressed only in the discussion for method comparisons (Section 4.1.1). Both continuous and discrete data demonstrated significant differences in temperature between each season, with the highest temperature in summer and the lowest in winter (Fig. 3.2, Tables S3.1 and S3.2). Mean salinity during sampling periods was highest in the summer and lowest in the fall (Table S3.1). Significant differences in seasonal salinity occurred between all seasons except spring and winter for continuous data, but only summer differed from other seasons based on discrete data (Tables S3.1 and S3.2).

Carbonate system parameters also varied seasonally (Fig. 3.2). For both continuous and discrete data, winter had the highest seasonal pH (8.19 ± 0.08 and 8.162 ± 0.065, respectively) and lowest seasonal pCO_2 (365 ± 44 µatm and 331 ± 39 µatm, respectively), while summer had the lowest seasonal pH (8.05 ± 0.06 and 7.975 ± 0.046, respectively) and highest seasonal pCO_2

(463 ± 48 µatm and 511 ± 108, respectively) (Fig. 3.2, Table S3.1). All seasonal differences in pH and pCO_2 were significant, except for the non-significant difference with discrete data between spring and fall for both parameters (Table S3.2).

Mean CO_2 flux differed by season (Fig. 3.3, Tables S3.1 and S3.2). Both continuous and discrete data records resulted in net negative CO_2 fluxes during fall and winter months, with winter being most negative. Both methods reported a net positive flux for summer, while spring fluxes were positive according to continuous data and negative according to the 5+ years of discrete data (Fig. 3.3, Table S3.1). Annual net CO_2 fluxes were near zero (Table S3.1).

Results of the LDA incorporated carbonate system parameters along with additional environmental parameters to get a full picture of system variability over seasonal timescales (Table 3.1). The most important parameter in system variability that allowed differentiation between seasons was temperature (Table 3.1, Seasonal LD1), as would be expected with the clear seasonal temperature fluctuations (Fig. S3.1-E). The second most important parameter for seasonal differentiation was chlorophyll, likely indicating clear seasonal phytoplankton blooms. The carbonate chemistry also played a critical role in seasonal differentiation, as pCO_2 was the third most important factor (Table 3.1).

3.3.2 Diel variability

The 10 months of in-situ continuous monitoring revealed that there was substantial diel variability in measured parameters (Fig. 3.4, Table S3.3). Temperature had a mean diel range of 1.3 ± 0.8°C (Table S3.3). Daytime and nighttime temperature differed significantly during the summer and fall months, with higher temperatures at night for both seasons (Table S3.3). Note that significant differences in day and night temperature within seasons do not indicate that the diel difference were observed on all days within the season, as large standard deviations in both

daytime and nighttime values result in considerable overlap. The mean diel range of salinity was 3.4 ± 2.7 (Table S3.3). Daytime and nighttime salinity differed significantly during the winter and fall months, with higher salinities at night for both seasons. The mean diel range of pH was 0.09 ± 0.05 (Table S3.3). Daytime and nighttime pH differed significantly during the winter, summer, and fall months; nighttime pH was significantly higher than that of the daytime during the summer and winter months, and daytime pH was significantly higher during the fall (Fig. 3.4, Table S3.3). The mean diel range of pCO_2 was 58 ± 33 µatm (Fig. 3.4, Table S3.3). Daytime and nighttime pCO_2 differed significantly during the winter and summer months; nighttime pCO_2 was significantly higher than that of the daytime during the summer and daytime pCO_2 was significantly higher during the winter (Fig. 3.4, Table S3.3). Despite day-night differences in pCO_2, there was no significant difference in daytime and nighttime DO during any season (paired t-tests, winter p = 0.1573, spring p = 0.4877, summer p = 0.794).

Loess models that investigated the evolution of day-night difference in parameters revealed that other environmental parameters, including salinity, temperature, and tide level, also had diel patterns the varied over the duration of our continuous monitoring (Fig. 3.5).

CO_2 flux also fluctuated on a daily scale, with a mean diel range of 34.1 ± 29.0 mmol m^{-2} d^{-1} (Table S3.3). However, there was not a significant difference in CO_2 flux calculated for daytime versus nighttime hours for the entire monitoring period or any individual season based on α=0.05 (paired t-test, Table S3.3).

Results of the LDA for differentiation between daytime and nighttime conditions revealed that the most important factor was PAR, as would be expected (Table 3.1, Diel LD1). Temperature was the second most important factor to differentiate between day and night. The carbonate chemistry also played a critical role in day/night differentiation, as pCO_2 was the third

most important parameter, providing more evidence for differentiation between day and night than other parameters that would be expected to vary on a diel timescale (e.g., chlorophyll and DO) (Table 3.1).

3.3.3 Controlling factors and correlates

The relative influence of thermal and non-thermal factors (T/B) in controlling pCO_2 varied over different time scales (Table 3.2). Based on continuous data, non-thermal processes generally exerted more control than thermal processes (T/B<1) within each season and over most (167/178) days (Table 3.2). For the entire 5+ years of discrete monitoring, non-thermal processes also exerted more control than temperature on pCO_2. However, discrete data demonstrated that there was substantial interannual variability in T/B, with annual T/B ranging from 0.48 to 1.17 and two of the five sampled years having T/B greater than one (i.e., more thermal influence). While the majority of individual seasons that were sampled experienced stronger non-thermal control on pCO_2 (T/B <1), the only season that never experienced stronger thermal control was summer, with summer T/B values ranging from 0.21 – 0.35 for the 6 sampled years (Table 3.4).

Tidal fluctuations seemed to have a significant effect on carbonate system parameters (Table 3). Both temperature and salinity were higher at low tide during the winter and summer months and higher at high tide during the spring. pCO_2 was higher during low tide during all seasons. pH was higher during high tide during the winter and summer, but this reversed during the spring, when pH was higher at low tide. CO_2 flux also varied with tidal fluctuations. CO_2 flux was higher (more positive or less negative) in the low tide condition for all seasons (though the difference was not significant in spring), i.e., the location was less of a CO_2 sink during low tide conditions in the winter and more of a CO_2 source during low tide conditions in the summer.

Mean water level varied between all seasons; mean spring (highest) water levels were on average 0.08 m higher than winter (lowest) water levels (ANOVA $p<0.0001$, fall was not considered because of a lack of water level data). The mean daily tidal range during our continuous monitoring period was 0.39 m ± 0.13 m, which did not significantly differ between seasons (ANOVA $p=0.739$). However, the day-night difference in tide level exhibited a strong seasonal pattern during the continuous monitoring period, with spring and summer having higher tide level during the daytime and winter having higher tide level during the nighttime (Fig. 3.5). This same seasonal pattern in day-night difference in tide level is exhibited from Dec 20, 2016 (when the tide data is first available) through the rest of our discrete monitoring period (Feb 25, 2020), indicating that tidal control on diel variability of carbonate system parameters was likely consistent throughout this 3+ year period.

There were significant correlations between carbonate system parameters (pH and pCO_2) and many of the other environmental parameters, including windspeed, DO, turbidity, and fluorescent chlorophyll (Table S3.4). Both the continuous and discrete sampling types indicate that pH has a significant negative relationship with both temperature and salinity and pCO_2 has a significant positive relationship with both temperature and salinity (Fig. 3.6). However, correlations with temperature were stronger for continuous data and correlations with salinity were stronger for discrete data (Table S3.4). The strongest correlations between continuous carbonate system data and all investigated environmental parameters were with DO (positive correlation with pH and negative correlation with pCO_2; Table S3.4). It is worth noting that there were no observations of hypoxia at our study site during our monitoring, with minimum DO levels of 3.9 mg L^{-1} and 4.0 mg L^{-1} for our continuous monitoring period and our discrete sampling period, respectively.

3.4 Discussion

3.4.1 Comparing continuous monitoring and discrete sampling: Representative sampling in a temporally variable environment

Discrete water sample collection and analysis is the most common method that has been employed to attempt to understand the carbonate system of estuaries. However, it is difficult to know if these samples are representative of the spatial and temporal variability in carbonate system parameters. While this time-series study cannot conclude whether our broader sampling efforts in the MAE are representative of the spatial variability in the estuary, it can investigate how representative our bimonthly to monthly sampling is of the more high-frequency temporal variability that ASC experiences.

There were several instances where seasonal parameter means significantly differed between the 10-month continuous monitoring period and the 5+ year discrete sampling period (Table 3, $C \neq D$ or $D_c \neq D$) including temperature in the summer and fall, salinity in the spring, pH in the summer and fall, and pCO_2 in winter, spring, and summer. While clear seasonal variability was demonstrated for most parameters (using both continuous and discrete data for the entire period), these differences between the 10-month continuous monitoring period and our 5+ year monitoring period illustrate that there is also interannual variability in the system. Therefore, short periods of monitoring are unable to fully capture current baseline conditions.

During the continuous monitoring period (2016-2017), no significant difference between sampling methods was found in the seasonal mean temperature, salinity, or pCO_2. The two sampling methods also resulted in the same mean pH for all seasons except for summer, when the sensor data recorded a higher mean pH than discrete samples (Tables 3.1 and 3.3). During this case, it can be concluded that discrete monitoring did not accurately represent the system

variability that was able to be captured by the sensor monitoring. Since summer daytime pH was less than nighttime pH, the discrete samples (daytime only sampling) would be expected to underestimate pH. However, given that most seasons did not show differences in pH or pCO_2 between sampling methods, the descriptive statistics associated with the discrete monitoring did a fair job of representing system means. This is evidence that long-term discrete monitoring efforts, which are much more widespread in estuarine systems than sensor deployments, can be generally representative of the system despite known temporal variability on shorter time scales.

Understanding the relationships of pH and pCO_2 with temperature and salinity is important in a system (Fig. 3.6). Based on the results of an Analysis of Covariance (ANCOVA), the relationship (slope) of pH with both temperature and salinity and of pCO_2 with salinity were not significantly different between types of monitoring (considering the sensor deployment period only), supporting the effectiveness of long-term discrete monitoring programs when sensors are unable to be deployed. However, ANCOVA did reveal the relationship of pCO_2 with temperature is significantly different (method:temp $p=0.0062$) between monitoring methods.

The high temporal resolution of sensor data is presumably better for estimating CO_2 flux at a given location than discrete sampling. Previous studies have pointed out that discrete sampling methods, which generally involve only daytime sampling, do not adequately capture the diel variability in the carbonate system and may therefore lead to underestimation of CO_2 fluxes. However, no significant difference (within any season) was found between CO_2 flux values calculated with sensor data versus discrete samples (Table S3.2, Fig. 3.3). Calculated CO_2 fluxes also did not significantly differ between day and night during any season, despite some differences in pCO_2 (Table S3.3), likely due to the large error associated with the calculation of CO_2 flux (Table 3.1, Fig. 3.5) which will be further discussed below. Therefore, the expected

underestimation of CO_2 flux based on diel variability of pCO_2 was not encountered at our study site, validating the use of discrete samples for quantification of CO_2 fluxes (until methods with less associated error are available). Even given less error in calculated flux, estimated fluxes would likely not differ between methods on an annual scale (as pCO_2 did not), but CO_2 fluxes may differ on a seasonal scale since the differences between daytime and nighttime pCO_2 were not consistent across seasons (Table S3.3, Fig. 3.4).

There are many factors contributing to error associated with CO_2 flux. There is still large error associated with estimates of estuarine CO_2 flux because turbulent mixing is difficult to model and turbulence is the main control on CO_2 gas transfer velocity, k, in shallow water environments. Thus, our wind speed parameterization of k is imperfect and likely the greatest source of error. Other notable sources of error include the data treatment. For example, I chose to seasonally weight the individual calculated flux values in the calculation of annual flux to account for differences in sampling frequency between seasons. From continuous data, the weighted average flux was 0.2 mmol m^{-2} d^{-1}, although choosing not to seasonally weight and simply look at the arithmetic mean of fluxes calculated directly from sampling dates would have resulted in an annual CO_2 flux of -0.7 mmol m^{-2} d^{-1} for the same period. Similarly, the weighted average flux from all 5+ years of discrete data was -0.9 mmol m^{-2} d^{-1}, but the arithmetic mean of fluxes would have resulted in an annual CO_2 flux of 0.2 mmol m^{-2} d^{-1} for the same period. Another source of error that could be associated with the calculation of flux from the discrete data is the way in which wind speed data are aggregated to be used in the windspeed parameterization. I decided to use daily averages of the windspeed for calculations. Using the windspeed measured for the closest time to our sampling time or the monthly averaged wind speed may have resulted in very different flux values.

3.4.2 Factors controlling temporal variability in carbonate system parameters

Our study site had a relatively small range of pH and pCO_2 on both diel and seasonal scales compared to other coastal regions (Challener et al. 2016; Yates et al. 2007). This small variability is likely tied to a combination of the subtropical setting (small temperature variability), the lower estuary position of our monitoring (further removed from the already small freshwater influence), little ocean upwelling influence, and the system's relatively high buffer capacity that results from the high alkalinity of the freshwater endmembers (Yao et al. 2020). Just as the extent of hypoxia-induced acidification was relatively low in Corpus Christi Bay because of the bay's high buffer capacity (McCutcheon et al. 2019), the extent of pH fluctuation resulting from all controlling factors at ASC would also be modulated by the region's high intrinsic buffer capacity.

We demonstrated that both temperature and non-thermal processes exert control on pCO_2, but non-thermal control generally surpasses thermal control in ASC over multiple time scales (Table 3.2, T/B<1). The magnitude of pCO_2 variation attributed to non-thermal processes varied greatly (i.e., $\Delta pCO_{2,nt}$ had large standard deviations, Table 3.2). For example, during the year of strongest non-thermal control (2016), $\Delta pCO_{2,nt}$ was 538 µatm versus $\Delta pCO_{2,nt}$ of 208 µatm in the year of weakest thermal control (2019). Conversely, the magnitude of pCO_2 variation attributed to temperature was consistent across time scales. For example, during the year of strongest thermal control (2015), $\Delta pCO_{2,t}$ was 276 µatm versus $\Delta pCO_{2,t}$ of 243 µatm in the year of weakest non-thermal control (2019). Spring and fall seasons, which experienced the greatest temperature swings (Table S3.1), had greater relative temperature control exerted on pCO_2 out of all seasons (Table 3.2). The difference in T/B between sampling methods is relatively small over the 10-month sensor deployment period, but it is worth noting that T/B did

not align over shorter seasonal time scales sampling methods (Table 3.2). Continuous monitoring demonstrated a greater magnitude of fluctuation resulting from both temperature and non-thermal processes (i.e., greater $\Delta pCO_{2,t}$ and $\Delta pCO_{2,nt}$), indicating that the extremes are generally not captured by the discrete, daytime sampling, and sensor data would provide a better understanding of system controls.

The greater influence of non-thermal controls that is reported here conflicts with Yao and Hu (2017), who found that ASC was primarily thermally controlled (T/B 1.53 – 1.79) from May 2014 to April 2015. Yao and Hu (2017) also found that locations in the upper estuary experienced lower T/B during flooding conditions than drought conditions. Although the opposite was found at ASC, it is likely that the high T/B calculated at ASC by Yao and Hu (2017) was still a result of the drought condition due to the long residence time of the estuary. Since 2015, there has not been another significant drought in the system, so it seems that non-thermal controls on pCO_2 are more important at this location under normal freshwater inflow conditions.

Significantly warmer water temperatures were observed during the nighttime in both summer and fall (Fig. 3.5), indicating that temperature could exert a slight control on the carbonate system over a diel time scale. More substantial temperature swings between seasons would result in more temperature control over a seasonal timescale. ASC seems to have less thermal control of the carbonate system than offshore GOM waters, as temperature had substantially higher explanatory value for pH and pCO_2 based on simple linear regressions in offshore GOM waters (R^2 = 0.81 and 0.78, respectively (Hu et al. 2018)) than at ASC (R^2 = 0.30 and 0.52, respectively, for sensor data and R^2 = 0.38 and 0.25, respectively, for discrete data).

Though annual average pCO_2 (and CO_2 flux) are higher in the upper MAE and lower offshore than at our study site, the same seasonal patterns that was observed here (i.e., elevated pCO_2 and positive CO_2 flux in the summer and depressed pCO_2 and negative CO_2 flux during the winter, Table S3.1, Fig. S3.1) has also been observed throughout the entire MAE and the open Gulf of Mexico (Hu et al. 2018; Yao and Hu, 2017). These seasonal patterns correspond with both the directional response of the system to temperature and net community metabolism response to changing temperature, i.e., elevated respiration in summer months (Caffrey, 2004). Despite that there were no observations of hypoxia, there was a strong relationship between the carbonate system parameters and DO (Table S3.4), suggesting that net ecosystem metabolism may exert an important control on the carbonate system on certain time scales. The lack of day-night difference in DO despite the significant day-night difference in both pH and pCO_2 suggests that net community metabolism is likely not a strong controlling factor on diel time scales. Biological control likely becomes more important over seasonal timescales.

While the tidal range in the northwestern GOM is relatively small (1.30 m over our 10-month continuous monitoring period), the tidal inlet location of our study site results in proportionally more “coastal water” during high tide and proportionally more “estuarine water” during low tide. The carbonate chemistry signal of these different water masses was seen in the differences between high tide and low tide conditions at ASC (i.e., high tide having lower pCO_2 because coastal waters are less heterotrophic than estuarine waters, Table 3.3). Consequently, the relative importance of thermal versus non-thermal controls may be modulated by tide level. Thermal and non-thermal pCO_2 terms were calculated separately during high tide and low tide periods and found that non-thermal control is more important during low tide conditions (within each season T/B is 0.10 ± 0.07 lower during the low tide than high tide). This is likely because

low tide has proportionally more "estuarine water" at the location and because there is less volume of water for the end products of biological processes to accumulate. The difference in T/B between high tide and low tide conditions was greatest in the spring, likely due to a combination of elevated spring-time productivity and larger tidal ranges in the spring.

The GOM is one of the few places in the world that experiences diurnal tides (Seim et al. 1987; Thurman, 1994), so theoretically, the fluctuations in pCO_2 associated with tides may align to either amplify or reduce/reverse the fluctuations that would result from diel variability in net community metabolism. Based on diel tidal fluctuations at this site (i.e., higher tides during the day in the spring and summer and higher tides at night during the winter, Fig. 3.5), tidal control should amplify the biological control signal (nighttime pCO_2 > daytime pCO_2) during spring and summer and reduce or reverse the biological control signal during the winter. This was supported by our pCO_2 data, which showed nighttime pCO_2 significantly greater than daytime pCO_2 in the summer, as expected from the biological signal (Table S3.3, Fig. 3.5). The full reversal of the biological signal in the winter (Table S3, nighttime pCO_2 < daytime pCO_2) indicated that tidal control exceeded biological control (i.e., the higher tides at nighttime in winter brought in enough low CO_2 water from offshore to fully offset the nighttime buildup of CO_2 from lack of photosynthesis during nighttime hours). The diel variability in pH did not mirror pCO_2 as would be expected. The loess models show that pCO_2 closely follows the directional response to both tide level and temperature, while pH does not (Fig. 3.5), indicating that controlling factors of the carbonate system may not be exerted equally on both pH and pCO_2 over different time scales.

Previous studies have indicated that freshwater inflow may exert a primary control on the carbonate system in the estuaries of the northwestern GOM (Hu et al. 2015; Yao et al. 2020; Yao and Hu, 2017). Carbonate system variability is much lower at ASC than it is in the more upper

reaches of MAE, likely due to the lesser influence of freshwater inflow and its associated changes in biological activity at ASC (Yao and Hu, 2017). Given the location of our sampling in the lower portion of the estuary and the long residence time in the system, river discharge was not directly addressed as a controlling factor, but the influence of freshwater inflow may be evident in the response of the system to changes in salinity. Fluctuating salinity at ASC may also result from direct precipitation, stratification, and tidal fluctuations; however, the low R^2 (0.02) associated with a simple linear regression between tide level and salinity ($p<0.0001$) indicates that salinity fluctuations are more indicative of non-tidal factors. Salinity data from both sensor and discrete monitoring were strongly correlated with both pH and pCO_2, with correlation coefficients nearing (continuous) or surpassing (discrete) that of the correlations with temperature (Fig. 3.6; Table S3.4). Periods of lower salinity had higher pH and lower pCO_2, likely due to enhanced freshwater influence and subsequent elevated primary productivity at the study site.

We investigated wind speed as a possible control on the carbonate system to gain insight into the effect of wind-driven CO_2 fluxes on the inventory of CO_2 in the water column (and subsequent impacts to the entire carbonate system). The Texas coast has relatively high wind speeds, with the mean wind speed observed during our continuous monitoring period being 5.8 m s^{-1}. While this results in relatively high calculated CO_2 fluxes (Fig. 3.3), the seasonal relationship between pCO_2 and windspeed does not support a change in inventory with higher winds. Since spring and summer both have a mean estuarine pCO_2 greater than atmospheric level (and positive CO_2 flux, Table S3.1) a negative relationship between windspeed and pCO_2 would be necessary to support this hypothesis, but winter, spring, and fall all experience increases in pCO_2 with increasing wind based on simple linear regression.

3.4.3 Carbonate chemistry as a component of overall system variability

Estuaries and coastal areas are dynamic systems with human influence, riverine influence, and influence from an array of biogeochemical processes, resulting in highly variable environmental conditions. Based on an LDA used to assess overall system variability using a suite of environmental parameters compiled at a single location, it can be concluded that carbonate chemistry parameters are among the most important of variants on both daily and seasonal time scales in this coastal setting. Of the two carbonate system components that were incorporated (pH and pCO_2), pCO_2 was the most critical in discriminating along diel or seasonal scales despite similar seasonal differences that were identified by ANOVA (Table S3.2) and more seasons with significant diel differences in pH (Table S3.3). pH seemed to be a larger component of overall system variability on a seasonal time scale (compared to the very small contribution seen on a diel scale, Table 3.1). Given that the seasonal and diel variability in carbonate chemistry at this location is relatively small compared to other coastal areas that are in the literature, the high contribution of carbonate chemistry to overall system variability that was detected is likely to be present at other coastal locations around the world.

3.5 Conclusions

We monitored carbonate chemistry parameters (pH and pCO_2) using both sensor deployments (10 months) and discrete sample collection (5+ years) at the Aransas Ship Channel, TX, to characterize temporal variability. Significant seasonal variability and diel variability in carbonate system parameters were both present at the location. Diel fluctuations were smaller than many other areas previously studied. The difference between daytime and nighttime values of carbonate system parameters varied between seasons, occasionally reversing the expected diel variability due to biological processes. Temperature, freshwater influence, biological activity,

and tide level (despite the small tidal range) all seem to exert important controls on the carbonate system at the location. Carbonate chemistry (particularly pCO_2) was among the most important environmental parameters to in overall system variability to distinguish between both diel and seasonal environmental conditions.

Despite known temporal variability on shorter timescales, discrete sampling was generally representative of the average carbonate system on a seasonal and annual basis based on comparison with our sensor data. Additionally, there was no difference in CO_2 flux between sampling types supporting the validity of discrete sample collection for carbonate system characterization.

This is one of the first studies that investigates high-temporal frequency data from deployed sensors that measure carbonate system parameters in an estuary-influenced environment. Long-term, effective deployments of these monitoring tools could greatly improve our understanding of estuarine systems. This study's detailed investigation of data from multiple, co-located environmental sensors was able to provide insight into potential driving forces of carbonate chemistry on diel and seasonal time scales; this provides strong support for the implementation of carbonate chemistry monitoring in conjunction with preexisting coastal environmental monitoring infrastructure, which has had little application in estuarine environments thus far. Strategically locating such sensors in areas that are subject to local OA drivers or support large biodiversity or commercially important species may be the most crucial in guiding future mitigation and adaptation strategies for natural systems and aquaculture facilities.

References

Barton, A., Waldbusser, G.G., Feely, R.A., Weisberg, S.B., Newton, J.A., Hales, B., Cudd, S., Eudeline, B., Langdon, C.J., Jefferds, I., King, T., Suhrbier, A., Mclaughlin, K. 2015. Impacts of coastal acidification on the Pacific Northwest shellfish industry and adaptation strategies implemented in response. *Oceanography* 28: 146–159.

Bednaršek, N., Tarling, G.A., Bakker, D.C.E., Fielding, S., Jones, E.M., Venables, H.J., Ward, P., Kuzirian, A., Lézé, B., Feely, R.A., Murphy, E.J. 2012. Extensive dissolution of live pteropods in the Southern Ocean. *Nature Geoscience* 5: 881–885.

Borges, A. V. 2005. Do we have enough pieces of the jigsaw to integrate CO_2 fluxes in the coastal ocean? *Estuaries* 28: 3–27.

Caffrey, J.M. 2004. Factors controlling net ecosystem metabolism in U.S. estuaries. *Estuaries* 27: 90–101.

Cai, W.-J. 2011. Estuarine and coastal ocean carbon paradox: CO_2 sinks or sites of terrestrial carbon incineration? *Annual Review of Marine Science* 3: 123–145.

Cai, W.-J., Hu, X., Huang, W.-J., Murrell, M.C., Lehrter, J.C., Lohrenz, S.E., Chou, W.-C., Zhai, W., Hollibaugh, J.T., Wang, Y., Zhao, P., Guo, X., Gundersen, K., Dai, M., Gong, G.-C. 2011. Acidification of subsurface coastal waters enhanced by eutrophication. *Nature Geoscience* 4: 766–770.

Challener, R.C., Robbins, L.L., Mcclintock, J.B. 2016. Variability of the carbonate chemistry in a shallow, seagrass-dominated ecosystem: Implications for ocean acidification experiments. *Marine and Freshwater Research* 67: 163–172.

Crosswell, J.R., Anderson, I.C., Stanhope, J.W., Van Dam, B., Brush, M.J., Ensign, S., Piehler, M.F., McKee, B., Bost, M., Paerl, H.W. 2017. Carbon budget of a shallow, lagoonal estuary: Transformations and source-sink dynamics along the river-estuary-ocean continuum. *Limnology and Oceanography* 62: S29–S45.

Cyronak, T., Andersson, A.J., D'Angelo, S., Bresnahan, P., Davidson, C., Griffin, A., Kindeberg, T., Pennise, J., Takeshita, Y., White, M. 2018. Short-term spatial and temporal carbonate chemistry variability in two contrasting seagrass meadows: Implications for pH buffering capacities. *Estuaries and Coasts* 41: 1282–1296.

Dickson, A.G. 1990. Standard potential of the reaction: AgCl(s) + 1 $2H_2$(g) = Ag(s) + HCl(aq), and and the standard acidity constant of the ion HSO_4- in synthetic sea water from 273.15 to 318.15 K. *Journal of Chemical Thermodynamics* 22: 113–127.

Ekstrom, J. a., Suatoni, L., Cooley, S.R., Pendleton, L.H., Waldbusser, G.G., Cinner, J.E., Ritter, J., Langdon, C., van Hooidonk, R., Gledhill, D., Wellman, K., Beck, M.W., Brander, L.M., Rittschof, D., Doherty, C., Edwards, P.E.T., Portela, R. 2015. Vulnerability and adaptation of US shellfisheries to ocean acidification. *Nature Climate Change* 5: 207–214.

Gattuso, J., Epitalon, J., Lavigne, H. and Orr, J. (2021). seacarb: Seawater Carbonate Chemistry. R package version 3.2.15. https://CRAN.R-project.org/package=seacarb

Gazeau, F., Quiblier, C., Jansen, J.M., Gattuso, J.-P., Middelburg, J.J., Heip, C.H.R. 2007. Impact of elevated CO_2 on shellfish calcification. *Geophysical Research Letters* 34: L07603.

Gobler, C.J., Talmage, S.C. 2014. Physiological response and resilience of early life-stage Eastern oysters (*Crassostrea virginica*) to past, present and future ocean acidification 2: 1–

15.

Ho, D.T., Law, C.S., Smith, M.J., Schlosser, P., Harvey, M., Hill, P. 2006. Measurements of air-sea gas exchange at high wind speeds in the Southern Ocean: Implications for global parameterizations 33: 1–6.

Hofmann, G.E., Smith, J.E., Johnson, K.S., Send, U., Levin, L. a, Micheli, F., Paytan, A., Price, N.N., Peterson, B., Takeshita, Y., Matson, P.G., Crook, E.D., Kroeker, K.J., Gambi, M.C., Rivest, E.B., Frieder, C. a, Yu, P.C., Martz, T.R. 2011. High-frequency dynamics of ocean pH: a multi-ecosystem comparison. *PLoS One* 6: e28983.

Hsu S. A. 1994. Determining the Power-Law Wind-Profile Exponent under Near-Neatral Stability Condidtions at Sea. *Journal of Applied Meteorology* 33: 757–765.

Hu, X., Beseres Pollack, J., McCutcheon, M.R., Montagna, P. A., Ouyang, Z. 2015. Long-term alkalinity decrease and acidification of estuaries in Northwestern Gulf of Mexico. *Environmental Science and Technology* 49: 3401–3409.

Hu, X., Nuttall, M.F., Wang, H., Yao, H., Staryk, C.J., McCutcheon, M.R., Eckert, R.J., Embesi, J.A., Johnston, M.A., Hickerson, E.L., Schmahl, G.P., Manzello, D., Enochs, I.C., DiMarco, S., Barbero, L. 2018. Seasonal variability of carbonate chemistry and decadal changes in waters of a marine sanctuary in the Northwestern Gulf of Mexico. *Marine Chemistry* 205: 16–28.

Jiang, L.-Q., Cai, W.-J., Wang, Y. 2008. A comparative study of carbon dioxide degassing in river- and marine-dominated estuaries. *Limnology and Oceanography* 53: 2603–2615.

Jiang, L.Q., Cai, W.J., Wang, Y., Bauer, J.E. 2013. Influence of terrestrial inputs on continental

shelf carbon dioxide. *Biogeosciences* 10: 839–849.

Kealoha, A.K., Shamberger, K.E.F., DiMarco, S.F., Thyng, K.M., Hetland, R.D., Manzello, D.P., Slowey, N.C., Enochs, I.C. 2020. Surface water CO_2 variability in the Gulf of Mexico (1996–2017). *Scientific Reports* 10: 1–13.

Laruelle, G.G., Cai, W.-J., Hu, X., Gruber, N., Mackenzie, F.T., Regnier, P. 2018. Continental shelves as a variable but increasing global sink for atmospheric carbon dioxide. *Nature Communications* 9: 454.

Li, D., Chen, J., Ni, X., Wang, K., Zeng, D., Wang, B., Jin, H., Huang, D., Cai, W.-J. 2018. Effects of biological production and vertical mixing on sea surface pCO_2 variations in the Changjiang River plume during early autumn: A buoy-based time series study. *Journal of Geophysical Research: Oceans* 123: 6156–6173.

Mathis, J.T., Pickart, R.S., Byrne, R.H., Mcneil, C.L., Moore, G.W.K., Juranek, L.W., Liu, X., Ma, J., Easley, R.A., Elliot, M.M., Cross, J.N., Reisdorph, S.C., Bahr, F., Morison, J., Lichendorf, T., Feely, R.A. 2012. Storm-induced upwelling of high pCO_2 waters onto the continental shelf of the western Arctic Ocean and implications for carbonate mineral saturation states 39: 4–9.

McCutcheon, M.R., Staryk, C.J., Hu, X. 2019. Characteristics of the carbonate system in a semiarid estuary that experiences summertime hypoxia. *Estuaries and Coasts* 42: 1509 - 1523

Millero, F.J. 2010. Carbonate constant for estuarine waters. *Marine and Freshwater Research* 61: 139–142.

Montagna, P. A., Brenner, J., Gibeaut, J., Morehead, S. 2011. Chapter 4: Coastal Impacts, in: Jurgen Schmandt, Gerald R. North, and J.C. (Ed.), The Impact of Global Warming on Texas. University of Texas Press, pp. 96–123.

R Core Team. 2020. R: A language and environment for statistical computing. R Foundation for Statistical Computing, Vienna, Austria. URL https://www.R-project.org/.

Raymond, P. A., Cole, J.J. 2001. Gas exchange in rivers and estuaries: Choosing a gas transfer velocity. *Estuaries* 24: 312.

Robbins, L.L., Lisle, J.T. 2018. Regional acidification trends in Florida shellfish estuaries: a 20+ year look at pH, oxygen, temperature, and salinity. *Estuaries and Coasts* 41: 1268–1281.

Sastri, A.R., Christian, J.R., Achterberg, E.P., Atamanchuk, D., Buck, J.J.H., Bresnahan, P., Duke, P.J., Evans, W., Gonski, S.F., Johnson, B., Juniper, S.K., Mihaly, S., Miller, L.A., Morley, M., Murphy, D., Nakaoka, S.I., Ono, T., Parker, G., Simpson, K., Tsunoda, T. 2019. Perspectives on in situ sensors for ocean acidification research. *Frontiers in Marine Science* 6: 1–6.

Schulz, K.G., Riebesell, U. 2013. Diurnal changes in seawater carbonate chemistry speciation at increasing atmospheric carbon dioxide. *Marine Biology* 160: 1889–1899.

Seim, H.E., Kjerfve, B., Sneed, J.E. 1987. Tides of Mississippi Sound and the adjacent continental shelf. *Estuarine, Coastal, and Shelf Science* 25: 143–156.

Semesi, I.S., Beer, S., Björk, M. 2009. Seagrass photosynthesis controls rates of calcification and photosynthesis of calcareous macroalgae in a tropical seagrass meadow. *Marine Ecology Progress Series* 382: 41–47.

Solis, R.S., Powell, G.L., 1999. Hydrography, Mixing Characteristics, and Residence Time of Gulf of Mexico Estuaries.

Takahashi, T., Sutherland, S.C., Sweeney, C., Poisson, A., Metzl, N., Tilbrook, B., Bates, N., Wanninkhof, R., Feely, R.A., Sabine, C., Olafsson, J., Nojiri, Y. 2002. Global sea-air CO_2 flux based on climatological surface ocean pCO_2, and seasonal biological and temperature effects. *Deep-Sea Research Part II: Topical Studies in Oceanography* 49: 1601–1622.

Thurman, H. V. 1994. Introductory Oceanography, seventh edition. pp. 252–276.

Uppström, L.R. 1974. The boron/chlorinity ratio of deep-sea water from the Pacific Ocean. *Deep-Sea Research* 21: 161–162.

USGS, 2001. Discharge Between San Antonio Bay and Aransas Bay, Southern Gulf Coast, Texas, May-September 1999.

Venables, W. N. & Ripley, B. D. 2002. Modern Applied Statistics with S. Fourth Edition. Spring er, New York. ISBN 0-387-95457-0

Waldbusser, G.G., Salisbury, J.E. 2014. Ocean acidification in the coastal zone from an organism's perspective: Multiple system parameters, frequency domains, and habitats. *Annual Review of Marine Science* 6: 221–247.

Wanninkhof, R. 1992. Relationship between wind speed and gas exchange. *Journal of Geophysical Research* 97: 7373–7382.

Wanninkhof, R., Asher, W.E., Ho, D.T., Sweeney, C., McGillis, W.R. 2009. Advances in quantifying air-sea gas exchange and environmental forcing. *Annual Review of Marine Science* 1: 213–244.

Weiss, R.F. 1974. Carbon dioxide in water and seawater: the solubility of a non-ideal gas. *Marine Chemistry* 2: 203–215.

Westfall, P.H. 1997. Multiple testing of general contrasts using logical constraints and correlations. *Journal of the American Statistical Association* 92: 299–306.

Xu, Y.-Y., D. Pierrot, and W.-J. Cai. 2017. Ocean carbonate system com- putation for anoxic waters using an updated CO2SYS program. *Marine Chemistry* 195: 90–93.

Yao, H., Hu, X. 2017. Responses of carbonate system and CO_2 flux to extended drought and intense flooding in a semiarid subtropical estuary. *Limnology and Oceanography* 62: S112–S130.

Yao, H., McCutcheon, M.R., Staryk, C.J., Hu, X. 2020. Hydrologic controls on CO_2 chemistry and flux in subtropical lagoonal estuaries of the northwestern Gulf of Mexico. *Limnology and Oceanography* 65: 1380–1398.

Yates, K.K., Dufore, C., Smiley, N., Jackson, C., Halley, R.B. 2007. Diurnal variation of oxygen and carbonate system parameters in Tampa Bay and Florida Bay. *Marine Chemistry* 104: 110–124.

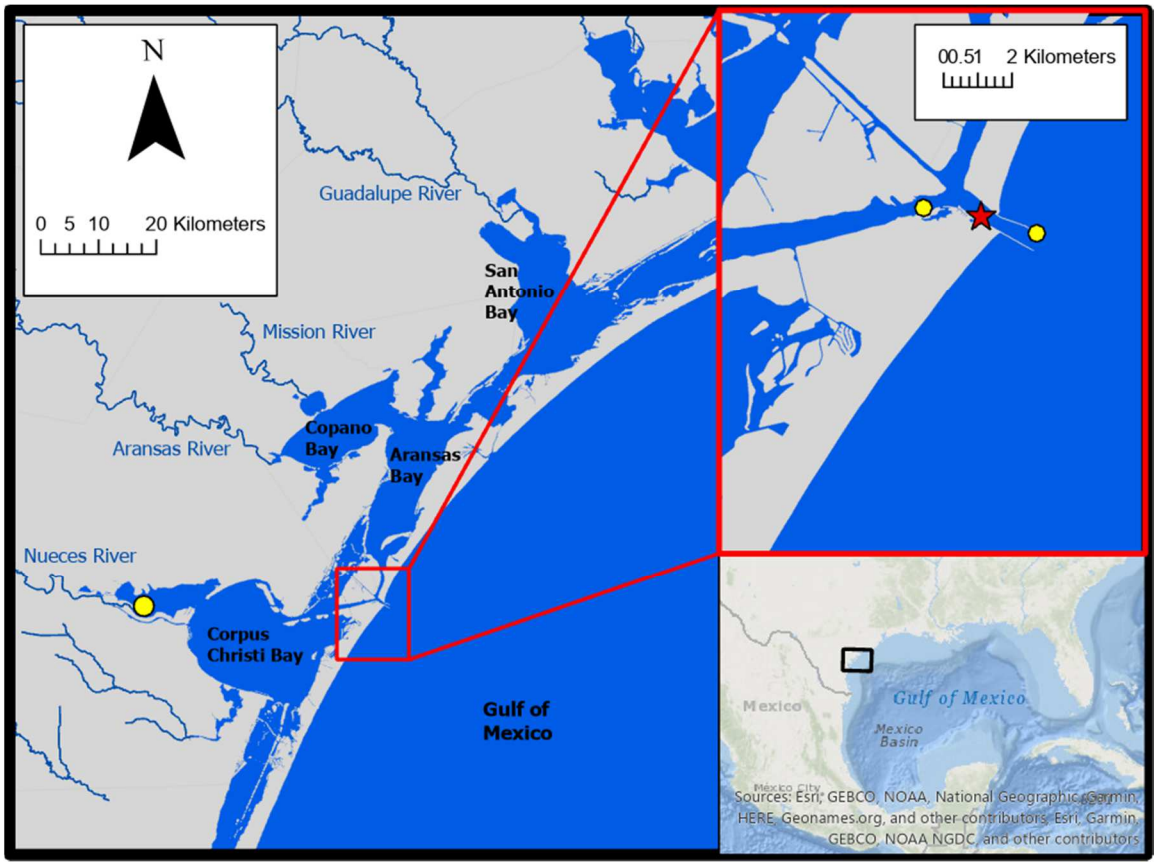

Figure 3.7. Study area. The location of monitoring in the Aransas Ship Channel (red star) and the locations of NOAA stations used for wind data (yellow circles) are shown.

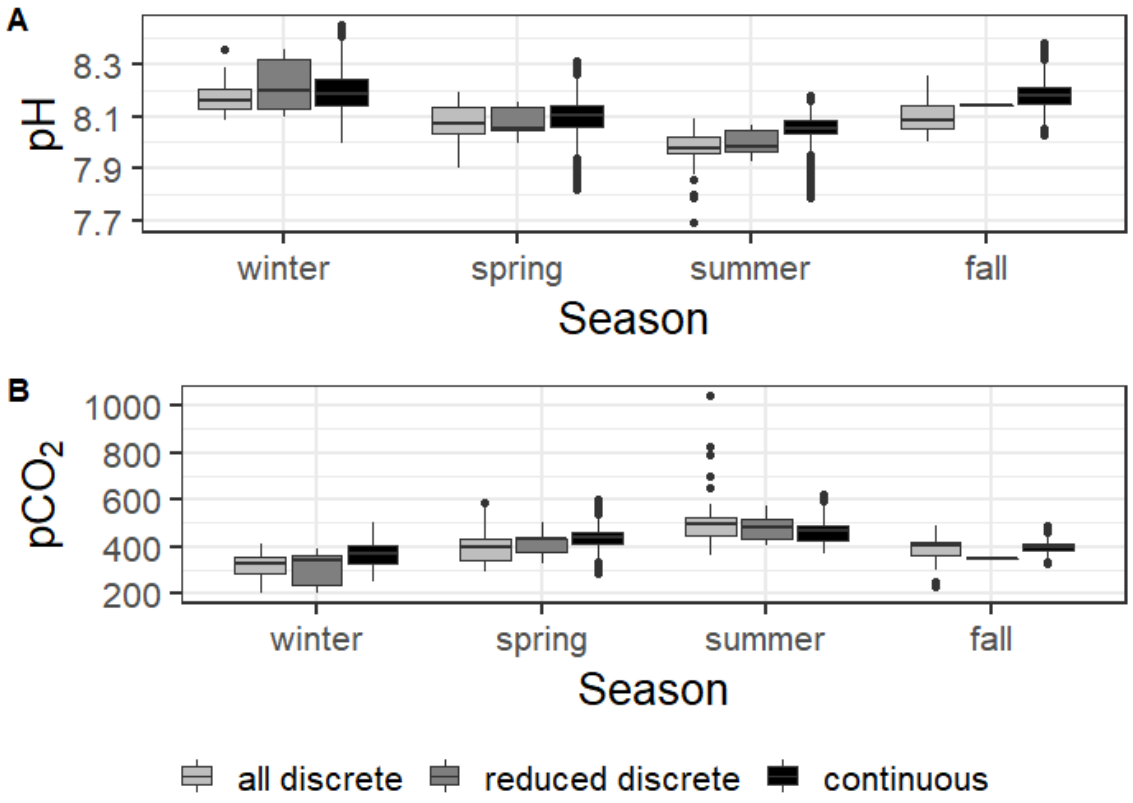

Figure 3.2. Boxplots of seasonal variability in pH and pCO_2 using all discrete data, reduced discrete data (to overlap with continuous monitoring, Nov. 8, 2016 – Aug 23, 2017), and continuous sensor data.

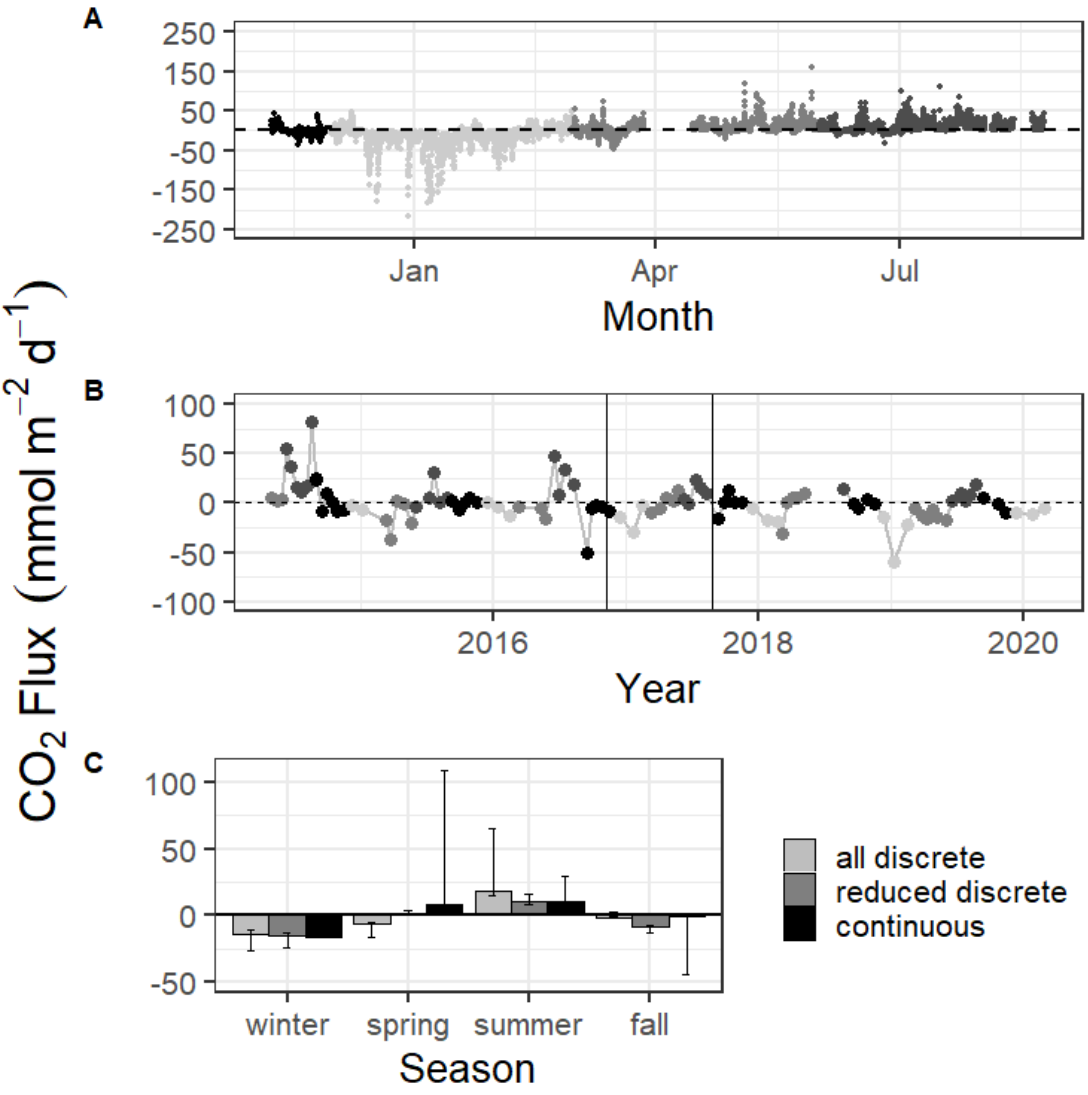

Figure 3.3. CO_2 flux calculated over the sampling periods from continuous (A) and discrete (B) data using the Jiang et al. (2008) wind speed parameterization. Gray scale in (A) and (B) denote different seasons. Vertical lines in (B) denote the time period of continuous monitoring. (C) shows the seasonal mean CO_2 flux calculated using the Jiang et al. (2008) gas transfer velocity parameterization and error bars representing mean CO_2 flux calculation using Ho (2006) and Raymond and Cole (2001) windspeed parameterizations.

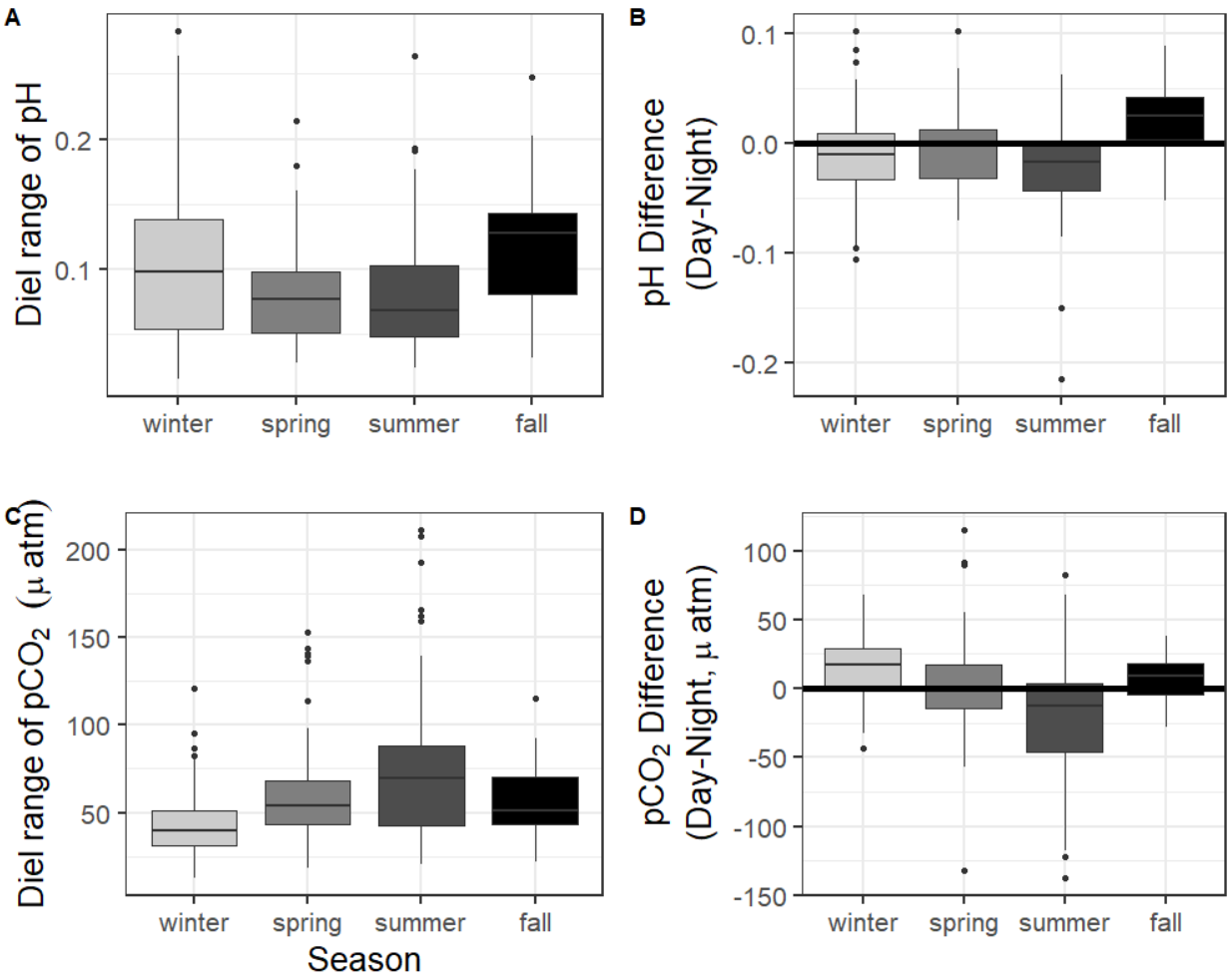

Figure 3.4. Boxplots of the diel range (maximum minus minimum) and difference in daily parameter mean daytime minus nighttime measurements for pH and pCO_2 from continuous sensor data.

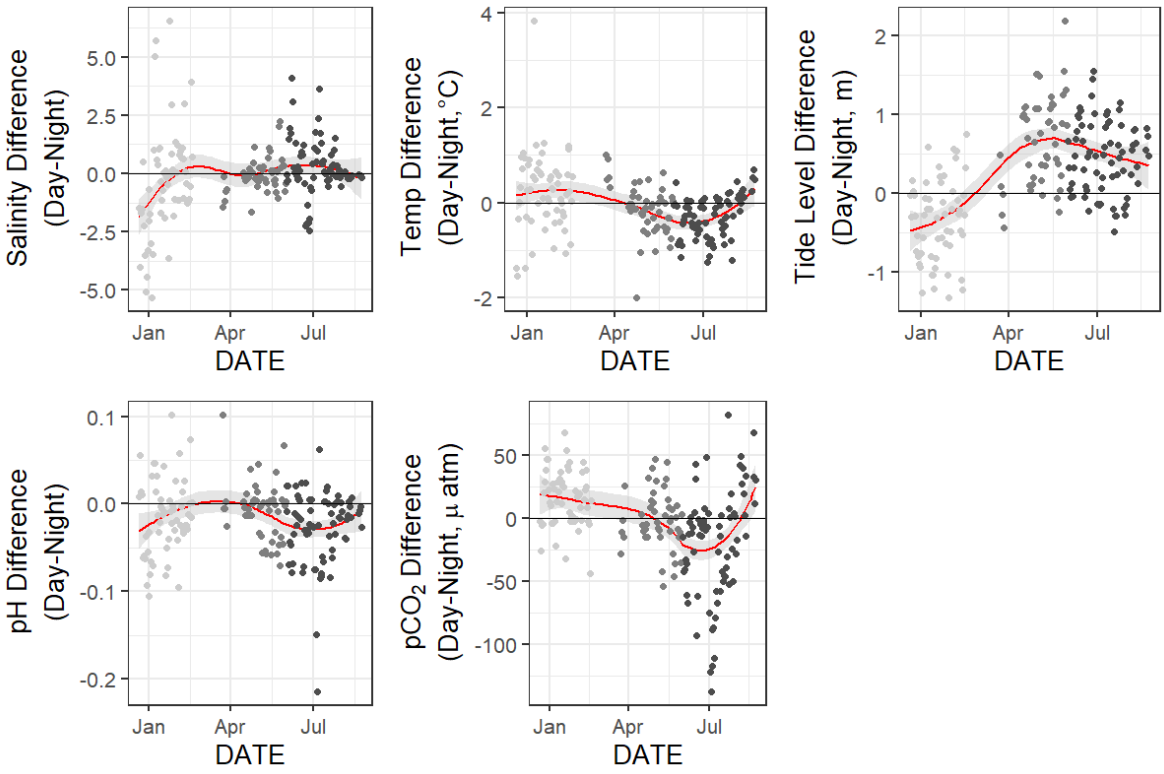

Figure 3.5. Loess models (red line) and their confidence intervals (gray bands) showing the difference in daily parameter mean daytime minus nighttime measurements. The gray scale of the data points represents the four seasons over which data were collected.

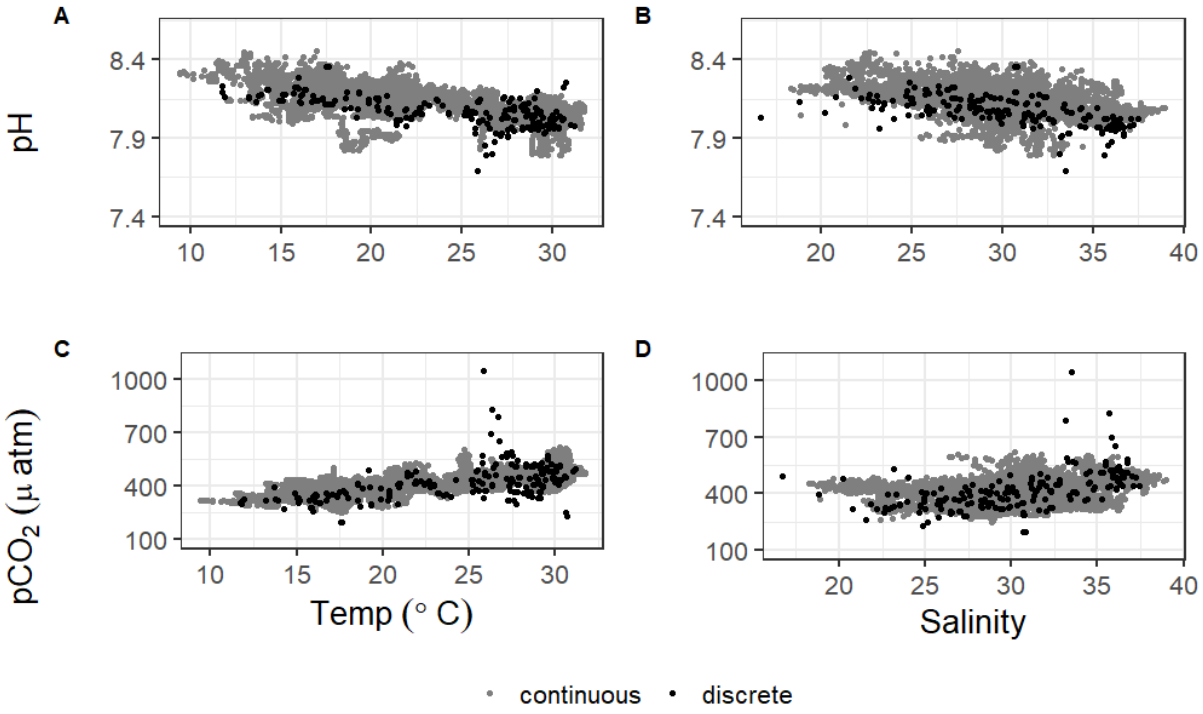

Figure 3.6. Correlations of pH and pCO_2 with temperature and salinity from continuous sensor data (gray) and all discrete data (black).

Table 3.1. Coefficients of linear discriminants (LD) from LDA using continuous sensor data and other environmental parameters. Discriminants for both diel and seasonal variability shown.

	Seasonal	**Diel**
	LD1	**LD1**
Temperature (°C)	-3.53	0.54
Salinity	0.04	0.15
pCO_2 (µatm)	-0.29	-0.16
pH	0.10	0.06
Tide Level (m)	-0.24	0.10
Wind speed (ms^{-1})	0.05	-0.00
Total PAR	-0.07	-2.29
DO ($mg\ L^{-1}$)	0.09	-0.08
Turbidity	0.15	-0.06
Fluor. Chlorophyll	-0.40	0.14

Table 3.2. Thermal versus non-thermal control on pCO_2 over different time scales using both continuous sensor data (C) and discrete sample data (D). If more than one segment of time is being considered (n>1), ΔpCO_2 values are the mean ± standard deviation of all segments, T/B range is the minimum and maximum T/B, and the number out of n with T/B>1 is recorded.

Time Period / Scale	**Sampling type**	**n**	**$\Delta pCO_{2,t}$ (µatm)**	**$\Delta pCO_{2,nt}$ (µatm)**	**T/B**	**Number out of n with T/B >1**
Full Monitoring Period (May 2, 2014- Feb. 25, 2020)	D	1	301.9	537.8	0.56	
Annual	D	5	259.3 ± 16.0	319.1 ± 130.9	0.48 – 1.17	2/5
Continuous Monitoring Period (Nov 2016 – August 2017)	C	1	355.0	360.7	0.98	
	D	1	236.3	229.9	1.03	
Winter	C	1	168.2	328.4	0.51	
	D	6	42.2 ± 23.4	101.7 ± 78.7	0.20 – 4.90	1/6
Spring	C	1	171.4	246.9	0.69	
	D	6	142.3 ± 53.7	147.8 ± 67.3	0.59 – 2.42	2/6
Summer	C	1	100.2	179.9	0.56	
	D	6	46.9 ± 26.6	176.9 ± 108.3	0.21 – 0.35	0/6
Fall	C	1	105.9	181.6	0.58	
	D	6	179.8 ± 59.5	176.6 ± 78.1	0.59 – 3.06	2/6
Daily	C	178	21.8 ± 11.8	63.8 ± 30.3	0.05 – 1.68	11/178

Table 3.3. Mean and standard deviation of temperature, salinity, pH, pCO_2, and calculated CO_2 flux (from continuous sensor measurements) during high and low tide conditions.

Parameter	Season	High Tide Mean	Low Tide Mean	Difference between tide levels, t-test p-value
Temperature (°C)	Winter	16.7 ± 1.7	17.6 ± 2.0	**<0.0001**
	Spring	24.4 ± 2.7	23.6 ± 2.7	**<0.0001**
	Summer	29.3 ± 0.5	30.1 ± 0.7	**<0.0001**
Salinity	Winter	30.2 ± 2.5	31.3 ± 2.9	**<0.0001**
	Spring	30.4 ± 1.9	30.0 ± 2.7	**0.0071**
	Summer	30.5 ± 2.4	34.5 ± 3.0	**<0.0001**
pH	Winter	8.20 ± 0.08	8.15 ± 0.06	**<0.0001**
	Spring	8.07 ± 0.09	8.10 ± 0.07	**<0.0001**
	Summer	8.08 ± 0.04	8.04 ± 0.06	**<0.0001**
pCO_2 (µatm)	Winter	331 ± 40	378 ± 42	**<0.0001**
	Spring	435 ± 33	443 ± 50	**0.0154**
	Summer	419 ± 30	482 ± 48	**<0.0001**
CO_2 Flux (mmol m^{-2} d^{-1})	Winter	-33.0 ± 38.1	-11.7 ± 21.8	**<0.0001**
	Spring	7.4 ± 14.0	8.7 ± 14.8	**0.2248**
	Summer	1.8 ± 6.3	16.0 ± 14.5	**<0.0001**

Supplementary Materials

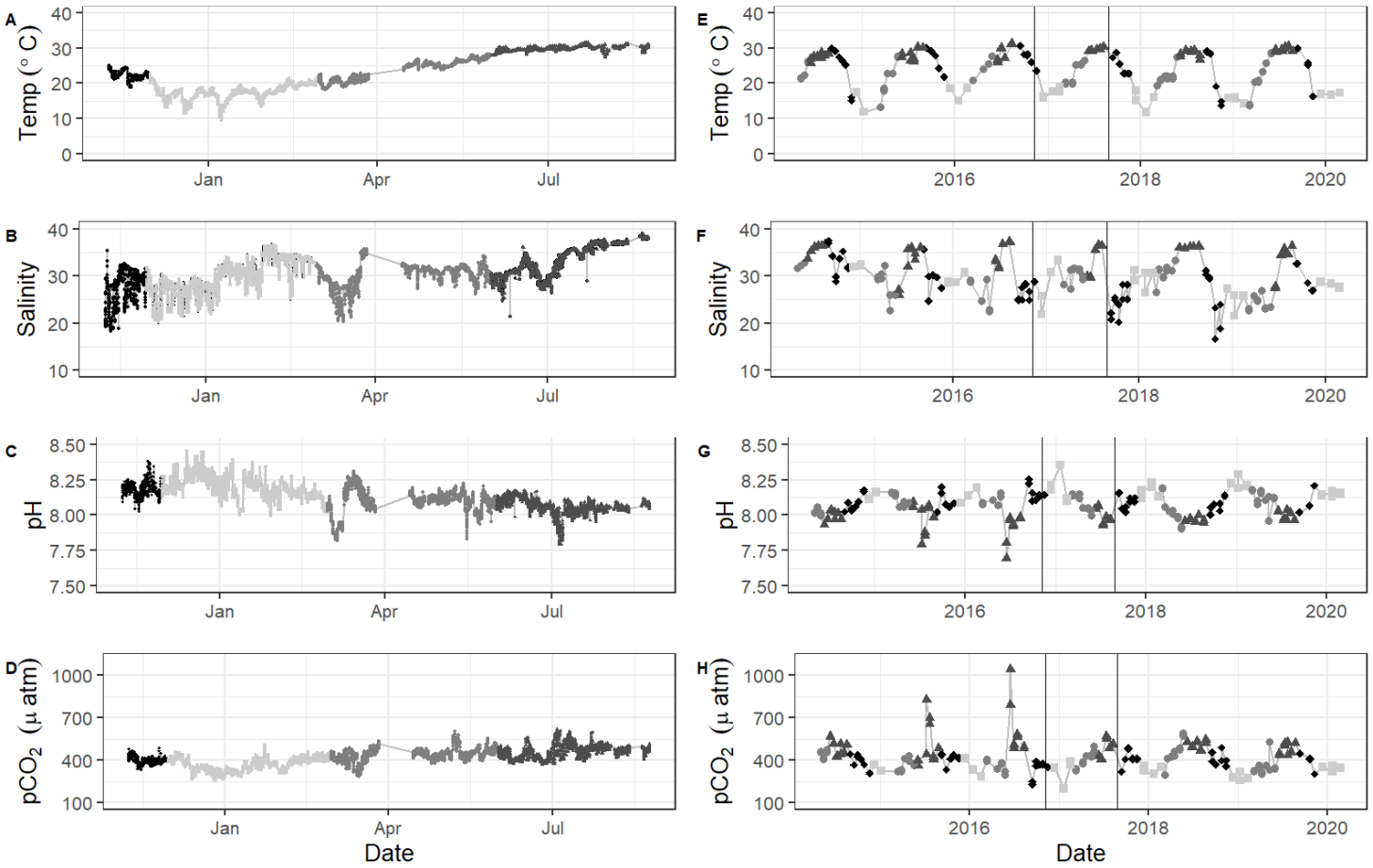

Figure S3.1. Time series data from continuous monitoring (A-D, Nov 8, 2016 to Aug 3, 2017) and discrete sample analysis (E-H, May 2, 2014- Feb. 25, 2020) at the Aransas Ship Channel. Gray scale (and shape) in the datapoints represents divisions between the four seasons. Vertical lines in (E-H) denote the time period of continuous monitoring.

Table S3.1. Mean and standard deviation of annual and seasonal parameters from continuous monitoring and discrete sampling. CO_2 fluxes and their standard deviations were calculated using the Jiang et al. (2008) wind speed parameterization for gas transfer velocity (in bold). Additional flux values reported in brackets use Ho et al. (2006) and Raymond and Cole (2001) parameterizations.

Parameter		**Continuous Monitoring**	**Discrete Sampling**	
	Time Period	Nov. 8 2016 – Aug 23, 2017	Nov. 8 2016 – Aug 23, 2017	May 2, 2014- Feb. 25, 2020
Temperature (°C)	**Annual**	23.1 ± 5.3	23.5 ± 5.0	24.1 ± 5.3
	Winter	17.3 ± 2.1	17.3 ± 1.1	16.2 ± 2.0
	Spring	23.8 ± 2.8	23.4 ± 2.9	22.6 ± 3.7
	Summer	29.7 ± 0.8	29.6 ± 0.5	28.7 ± 1.4
	Fall	22.5 ± 2.1	23.6 ± 0.1	25.5 ± 4.5
Salinity	**Annual**	30.8 ± 3.7	30.4 ± 3.5	30.1 ± 4.4
	Winter	30.0 ± 3.7	29.3 ± 4.6	28.9 ± 2.9
	Spring	30.2 ± 2.6	30.0 ± 1.7	28.7 ± 3.4
	Summer	33.3 ± 3.2	33.6 ± 3.2	34.6 ± 2.8
	Fall	27.6 ± 3.7	28.8 ± 0.1	28.4 ± 4.5
pH	**Annual**	8.12 ± 0.10	8.092 ± 0.078	8.079 ± 0.092
	Winter	8.19 ± 0.08	8.157 ± 0.041	8.162 ± 0.065
	Spring	8.09 ± 0.09	8.078 ± 0.056	8.077 ± 0.066
	Summer	8.05 ± 0.06	7.999 ± 0.051	7.975 ± 0.046
	Fall	8.18 ± 0.05	8.136 ± 0.001	8.100 ± 0.071
***p*CO_2 (µatm)**	**Annual**	416 ± 60	400 ± 71	406 ± 100
	Winter	365 ± 44	349 ± 31	331 ± 39
	Spring	436 ± 45	413 ± 54	396 ± 67
	Summer	463 ± 48	480 ± 59	511 ± 108
	Fall	400 ± 25	357 ± 2	386 ± 62
CO_2 Flux (mmol m^{-2} d^{-1})	**Annual**	**0.2 ± 23.7** [0.1, -87.6]	**-1.5 ± 9.2** [-2.6, -4.5]	**-0.8 ± 18.7** [-0.7, 5.3]

Winter	**-16.9 ± 29.2**	**-9.9 ± 5.2**	**-13.0 ± 13.5**
	[-14.6, -444.0]	[-8.3, -16.2]	[-10.6, -25.6]
Spring	**7.6 ± 15.0**	**1.0 ± 7.1**	**-6.5 ± 12.2**
	[6.5, 109.0]	[1.0, 3.3]	[-5.5, -18.0]
Summer	**10.8 ± 13.3**	**10.5 ± 7.8**	**18.3 ± 19.6**
	[9.1, 28.9]	[8.6, 16.3]	[15.3, 65.5]
Fall	**-0.9 ± 7.7**	**-7.5**	**-2.3 ± 13.7**
	[-0.7, -44.0]	[-6.2, -11.4]	[-1.9, -0.9]

Table S3.2. Tests examining differences in mean carbonate system parameters between seasons and between types of sampling. Statistic p-values are listed, with significant results based on α=0.05 bolded, and the F statistic is in parentheses. Comparisons with significantly different means in post-hoc analyses are listed as unequal beneath the one-way ANOVA results (All≠ indicates that every individual comparison between levels had significantly different means. W = winter, Sp = spring, Su = summer, F = fall; C = continuous sensor data, D = discrete sample data over the entire discrete monitoring period, D_C = Discrete sample data during only the period of continuous monitoring).

Parameter	**Two-way ANOVA**			**One-way ANOVA and post-hoc multiple comparison results for differences between types of sampling**				**One-way ANOVA and post-hoc multiple comparison results for difference between seasons**		
	Interaction	Season	Sampling type	winter	spring	summer	fall	Continuous	Discrete (Continuous Period)	Discrete (Entire Period)
Temp (°C)	**<0.0001** (15.8)	**<0.0001** (12369.7)	0.7346 (0.3)	0.0710 (2.6)	0.1052 (2.3)	**<0.0001** (19.6) D≠C	**<0.0001** (61.4) D≠C	**<0.0001** (12559) All≠	**<0.0001** (22.8) W≠Su; W≠Sp; W≠F; Su≠Sp; Su≠F	**<0.0001** (58.2) All≠
Salinity	**0.0141** (2.7)	**<0.0001** (598.7)	0.6509 (0.4)	0.1716 (1.8)	**0.0013** (6.7) D≠C	0.1921 (1.7)	0.7007 (0.4)	**<0.0001** (580.0) W≠Su; W≠F; Su≠Sp; Su≠F; Sp≠F	0.2516 (1.6)	**<0.0001** (17.5) W≠Su; Su≠Sp; Su≠F
pH	**0.0013** (3.7)	**<0.0001** (1412.3)	**<0.0001** (24.0)	0.4026 (0.9)	0.9238 (0.1)	**<0.0001** (24.1 D≠C **C≠D_C**	**<0.0001** (33.2) D≠C	**<0.0001** (1381.2) All≠	**0.0152** (5.7) W≠Su	**<0.0001** (35.3) W≠Su; W≠Sp; W≠F; Su≠Sp; Su≠F
***p*CO_2 (µatm)**	**<0.0001** (10.4)	**<0.0001** (1747.3)	**0.0147** (4.2)	**0.0018** (6.4)	**<0.0001** (17.4)	**0.0002** (8.4)	0.0398 (3.2)	**<0.0001** (1737.6)	**0.0407** (4.0)	**<0.0001** (8.4)

				D≠C	D≠C	D≠C	**All=**	All≠	W≠Su	W≠Su; W≠Sp; W≠F; Su≠Sp; Su≠F
CO_2 Flux (mmol m^{-2} d^{-1})	**0.0144** (2.6)	**<0.0001** (738.1)	0.6739 (0.4)	0.9140 (0.1)	**<0.0001** (11.8)	**0.0214** (3.9)	0.5849 (0.5)	**<0.0001** (725.9)	**0.0299** (4.5)	**<0.0001** (19.2)
					D≠C	D≠C		All≠	W≠Su	W≠Su; W≠F; Su≠Sp; Su≠F

Table S3.3. Diel variability in system parameters from continuous sensor data. Reported p-values are from a paired-*t* test; all significant results based on α=0.05 are bolded. Reported fluxes use the Jiang et al. (2008) gas transfer velocity parameterization.

Parameter	Time Period	Daytime Mean	Nighttime Mean	Day versus Night p-value	Mean Diel Range	Minimum Diel Range	Maximum Diel Range
Temperature (°C)	**Full Sampling Period**	23.0 ± 5.3	23.2 ± 5.4	**<0.0001**	1.3 ± 0.8	0.30	3.93
	Winter	17.2 ± 2.1	17.4 ± 2.1	0.2055	1.5 ± 0.8	0.3	3.8
	Spring	23.7 ± 2.7	23.8 ± 2.9	0.5579	1.2 ± 0.6	0.3	3.0
	Summer	29.6 ± 0.7	29.9 ± 0.8	**<0.0001**	1.0 ± 0.6	0.3	3.8
	Fall	22.0 ± 1.19	23.0 ± 1.0	**<0.0001**	1.8 ± 0.9	0.8	3.9
Salinity	**Full Sampling Period**	30.5 ± 4.1	31.0 ± 3.3	**0.0004**	3.4 ± 2.7	0.250	15.870
	Winter	29.6 ± 4.2	30.4 ± 3.1	**0.0051**	3.8 ± 2.2	0.25	9.48
	Spring	30.1 ± 2.6	30.2 ± 2.6	0.5604	2.5 ± 2	0.4	8.17
	Summer	33.4 ± 3.2	33.1 ± 3.3	0.0550	2.0 ± 1.7	0.3	9.73
	Fall	25.9 ± 3.9	29.0 ± 3.2	**<0.0001**	7.7 ± 3.6	1.2	15.87
pH	**Full Sampling Period**	8.12 ± 0.10	8.13 ± 0.09	**<0.0001**	0.09 ± 0.05	0.02	0.28
	Winter	8.18 ± 0.08	8.20 ± 0.07	**0.0108**	0.10 ± 0.05	0.02	0.28
	Spring	8.09 ± 0.09	8.10 ± 0.08	0.3286	0.08 ± 0.03	0.03	0.18
	Summer	8.04 ± 0.06	8.07 ± 0.05	**<0.0001**	0.08 ± 0.04	0.03	0.19
	Fall	8.20 ± 0.05	8.17 ± 0.05	**0.0038**	0.12 ± 0.04	0.03	0.20
***p*CO_2 (µatm)**	**Full Sampling Period**	417 ± 54	416 ± 65	0.7065	58 ± 33	12.6	211.3
	Winter	374 ± 44	358 ± 43	**<0.0001**	43 ± 21	12.6	121.1
	Spring	438 ± 42	437 ± 48	0.7237	61 ± 31	20.5	152.8
	Summer	452 ± 44	471 ± 51	**0.0003**	74 ± 42	23.6	211.3
	Fall	406 ± 24	399 ± 27	0.0545	56 ± 18	22	92.2

CO_2 Flux (mmol m^{-2} d^{-1})	**Full Sampling Period**	0.0 ± 6.3	-1.3 ± 5.9	0.3028	34.1 ± 29.0	2.7	189.0
	Winter	-14.9 ± 8.4	-19.1 ± 7.7	0.0676	46.6 ± 38.9	2.7	189.0
	Spring	7.6 ± 5.2	7.0 ± 5.2	0.6680	27.5 ± 18.5	4.9	115.0
	Summer	9.4 ± 5.6	11.7 ± 5.2	0.1167	32.3 ± 22.9	4.5	111.0
	Fall	0.1 ± 3.8	-0.3 ± 3.5	0.7449	17.0 ± 10.2	3.9	40.1

Table S3.4. Pearson correlation coefficients between carbonate system parameters and other environmental parameters for both continuous sensor data and discrete sample data. Parameter pairs with a significant correlation based on α=0.05 have a correlation coefficient reported. Asterisks are used to indicate the level of significance of the correlation, * $p<0.05$, ** $p<0.01$, *** $p<0.0001$. The correlation coefficient is listed as 0 if the relationship was not significant. N/A is listed when the analysis was omitted because the environmental parameter did not have observations corresponding to the date and time of at least half of our discrete sample measurements (45 observations).

	pH		***p*CO$_2$**		***p*CO$_2$, nonthermal**	
	Continuous	**Discrete**	**Continuous**	**Discrete**	**Continuous**	**Discrete**
Temperature (°C)	-0.55 ***	-0.59 ***	0.75 ***	0.53 ***	-0.73 ***	-0.45 ***
Salinity	-0.47 ***	-0.74 ***	0.53 ***	0.69 ***	-0.28 ***	0.35 **
Wind Speed (m s^{-1})	-0.04 **	N/A	0.15 ***	N/A	0	N/A
Dissolved Oxygen (mg L^{-1})	0.55 ***	0	-0.81 ***	0	0.45 ***	0
Tide Level (m)	0	0	-0.15 ***	0	-0.15 ***	-0.55 **
Turbidity	-0.08 ***	N/A	-0.14 ***	N/A	-0.28 ***	N/A
Fluor. Chlorophyll	0.12 ***	N/A	-0.22 ***	N/A	0.34 ***	N/A

Additional information on CO_2 flux calculations and windspeed data

Atmospheric xCO_2 data that were incorporated into calculations were monthly averages. This method is justified for flux calculations (even for pairing with the hourly continuous data), as the one example of frequent (i.e., every three hour) sampling of atmospheric xCO_2 in the Gulf of Mexico (off Louisiana coast) shows very little diel or even monthly fluctuation in atmospheric xCO_2 (https://www.pmel.noaa.gov/co2/story/Coastal+LA). This small variability on short time scales is likely due to the predominantly southeast winds that blow onshore. These southeast winds are also prevalent at ASC, so diel fluctuations in atmospheric xCO_2 (associated with the biological cycles of terrestrial plants or anthropogenic influence) are likely negligible.

NOAA/TCOON's Port Aransas (<2 km inshore from monitoring location) and Aransas Pass (<2 km offshore from monitoring location) stations did not begin recording windspeed data until Aug 5, 2016. Therefore, flux calculations for our discrete monitoring data spanning from May 2, 2014 to Aug 5, 2016 used windspeed data from the Nueces Bay Station (~40 km from our monitoring location). During the continuous monitoring period (Nov 8, 2015 – Aug 3, 2017), about 55 days (<20% of observations) lacked windspeed data from Port Aransas or Aransas Pass stations and used data from Nueces Bay station. Following the continuous monitoring period (Aug 23, 2017 – Feb 25, 2020), only about nine days of wind data had to be retrieved from the Nueces Bay station.

For those days during the 5+ year monitoring period that data were available at both the Port Aransas Station and the Nueces Bay station, the Nueces Bay Station did have higher windspeeds by an average of ~2.33 m/s, which could result in overestimation of the magnitude of CO_2 fluxes. Given this station windspeed offset (along with the many other factors that complicate the calculation of fluxes through windspeed parameterization), the actual values of

CO_2 flux should not be taken at face value. Missing data at the Port Aransas and Aransas Pass stations generally spanned full days (not individual hours of missing data), so both calculations of CO_2 flux with the continuous data and the discrete data would be pulling from the same station on the same day, which validates the comparison of methods as flux calculated by both sampling methods would receive the same bias.

Sensor data correction including removal of suspicious data

While the *ex-situ* position of the cooler was beneficial for easy maintenance of the deployed sensors, there was an issue of periodic pump failure due to a manufacture flaw that was later discovered, which would result in the cooler not appropriately representing the *in-situ* environment (Figure S3.2). Pump failure resulted in notable increases in pCO_2 and decreases in pH due to the buildup of respirational products (Fig. S3.2). Sensor data during known periods of pump failure were omitted from analysis (Fig. S3.2). Other suspect data based on the multiple data correlation comparisons were also removed as they were assumed to represent sensor malfunction (Fig. S3.3).

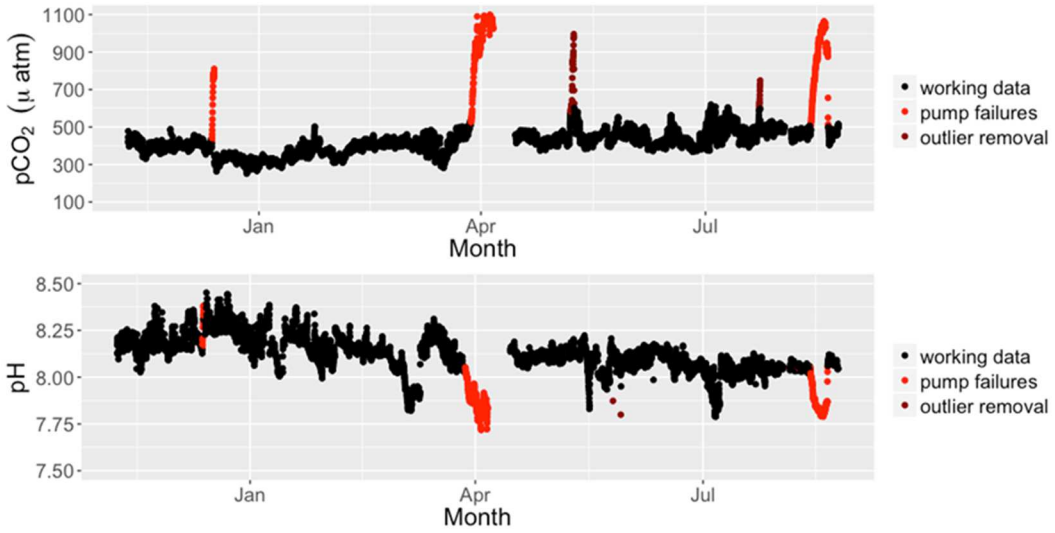

Figure S3.2. All recorded pCO_2 and pH data. Data points flagged for removal prior to analysis are shown in red.

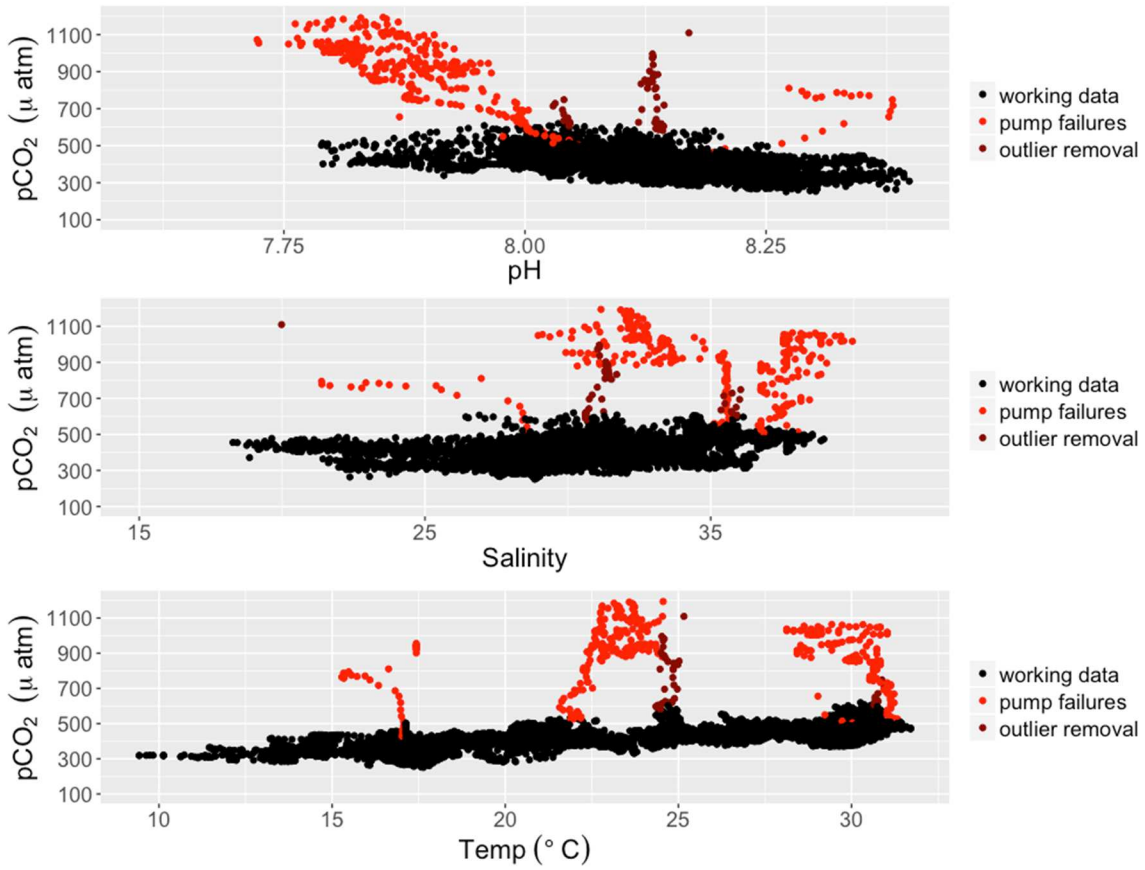

Figure S3.3. Relationships between sensor-measured carbonate system parameters and temperature and salinity. Data points flagged for removal prior to analysis are shown in red.

Direct agreement of measurement methods and quantified uncertainties associated with parameters

Discrete, quality assurance (QA) samples were collected during each sensor maintenance trip from both the channel near the pump inlet and from the cooler that housed the sensors. The same laboratory methods used for discrete sample analysis (Section 3.3) also apply for these discrete, quality control samples. Water temperature and salinity were also measured in both locations using a handheld YSI data sonde.

The offset between the sensor and laboratory pH was used to establish a correction to sensor pH. The mean difference between the SeaFET pH measurements and the QC samples (continuous – discrete) was 0.05 ± 0.08. Since there was not a clear pattern over time in the difference between sensor and laboratory-measured pH (Fig. S3.4), the average offset was used for a correction to all sensor data.

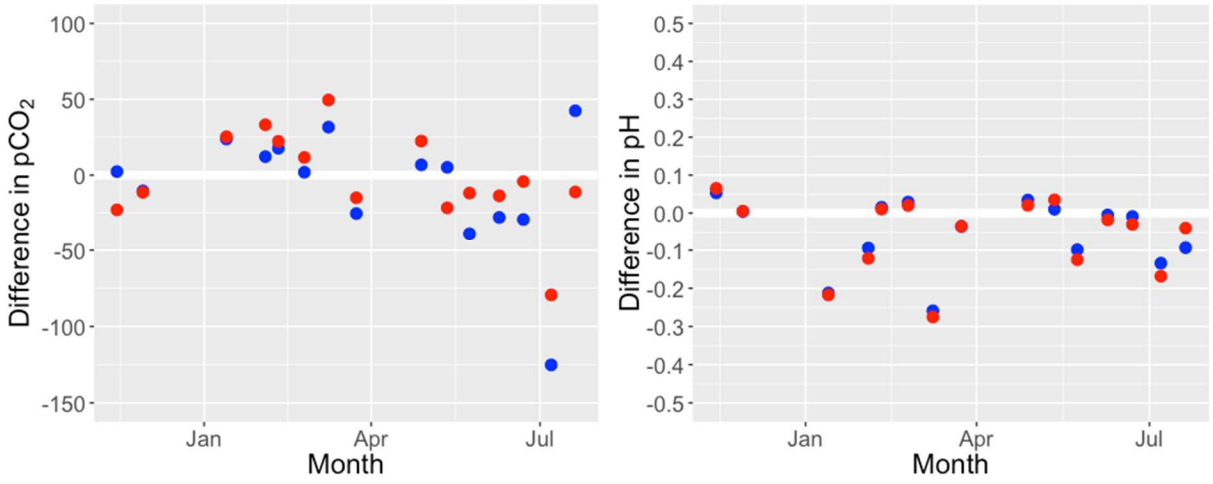

Figure S3.4. Differences in pCO_2 and pH between in situ sensors and lab-analyzed bottle samples from the cooler (blue) and the ship channel (red)

Direct comparisons were made between measurements from sensors and laboratory-analyzed bottle samples (both QA samples and long-term discrete monitoring samples, Table S3.5). The mean difference between the SAMICO2 pCO_2 measurements and the QC samples (continuous – discrete) was -18 ± 44 (Table S3.5) when discrete sample pCO_2 was calculated using Millero (2010) constants. Several different constants were used to calculate pCO_2 to check this offset; all were similar in mean and standard deviation, but the offset could be slightly reduced using Millero (2002) constants. Mean offsets and their associated standard deviations were larger when comparing sensor data to samples taken during our long-term discrete

monitoring effort (Table S3.5). This is not surprising given that the discrete sample collection did not occur at the exact time of the sensor measurement or the exact location of the cooler pump inlet.

Given that the analytical accuracy of the SeaFET instrument is 0.05 pH units (Table S3.6), the average offset between sensor and laboratory values of quality control samples demonstrates fair agreement (Table S3.5). Given that calculated uncertainty associated with calculated discrete pCO_2 was 7 ± 2, there was not great agreement between SAMICO2 pCO_2 and laboratory-calculated pCO_2 for QA samples. Greater sensor-laboratory agreement has been achieved for open ocean settings, but this larger standard deviation is likely a result of the temporal variability in the more complex estuarine environment where these instruments have been much less widely deployed to date.

Table S3.5. Mean ± standard deviation of the difference between discrete and continuous values. Reported pH differences are after the sensor pH correction.

	Difference between sampling methods	
	Sensor – QC samples * (n=12)	Sensor – discrete samples ** (n=13)
Salinity	-0.16 ± 1.44	0.50 ± 1.69
pH	0.00 ± 0.08	0.01 ± 0.12
pCO_2 (µatm)	-18 ± 44	25 ± 63

* Difference between sensor measurements and laboratory measurements of QA bottle samples taken at exact time of sensor measurement and directly from the sensor cooler

** Difference between sensor measurements and laboratory measurements of discrete samples for our 5+ year monitoring. These discrete samples were taken from a nearby station (within 100 m), and they were not taken directly on the hour, so sampling time was rounded to the nearest hour to pair with sensor data.

Propagated error associated with calculated carbonate system parameters was calculated using the *seacarb* package in R (Gattuso et al. 2021) using analytical errors associated with the measurements of the input pair, *in-situ* temperature and salinity, total boron, and the key dissociation constants (Table S3.6). Error associated with calculated parameters from discrete bottle samples was relatively small and likely a result of uncertainties in constants (Orr et al. 2018), but error associated with parameters calculated from sensor data was relatively large (Table S3.6). This large error is likely a result of both the relatively low analytical precision associated with the pH sensor and the poor mathematical combination of variables for speciation calculations. This high error is the reason that the discussion of any other calculated carbonate system parameters were omitted from the chapter. The high error suggests that it will be important that autonomous sensors that can measure alternative parameters and allow for lower propagated error are developed and broadly used to gain a full understanding of carbonate chemistry on high-frequency timescales.

Table S3.6. Analytical error for directly measured parameters and propagated error for calculated parameters (mean ± standard deviation).

	Error (Analytical or Propagated)	
	Discrete Sampling (n = 104)	**Continuous Monitoring (n = 6088)**
Temperature (°C)	0.1	0.1
Salinity	0.01	0.1
pH	0.0004	0.05
pCO_2 (µatm)	7 ± 2	1.0
DIC (µmol kg^{-1})	2.5	327.4 ± 63.2
TA (µmol kg^{-1})	7.4 ± 0.9	400.7 ± 81.0
Ω_{Ar}	0.19 ± 0.03	1.08 ± 0.31

CHAPTER IV: CHARACTERISTICS OF THE CARBONATE SYSTEM IN A SEMIARID ESTUARY THAT EXPERIENCES SUMMERTIME HYPOXIA

Reprinted by permission from Copyright Clearance Center: Springer Nature; *Estuaries and Coasts*; Characteristics of the Carbonate System in a Semiarid Estuary that Experiences Summertime Hypoxia, M. R. McCutcheon, C. J. Staryk, X. Hu; Vol. 42, pp. 1509 – 1523. Copyright (2019).

Abstract

In oceanic environments, two sources of CO_2 have been found to contribute to acidification of stratified water bodies, i.e., CO_2 invasion due to anthropogenic atmospheric CO_2 increase and respiration-produced CO_2 from organic matter remineralization. Acidification caused by these CO_2 sources has been observed frequently in numerous environments spanning from open continental shelves to enclosed estuaries. Here, observations on carbonate system dynamics are reported for a relatively well- buffered lagoonal estuary, Corpus Christi Bay (CCB), in a semiarid subtropical region that is influenced by summertime hypoxia as well as strong evaporation and seagrass vegetation in the vicinity. While the relationship between dissolved oxygen (DO) and pH in the bottom waters of CCB was positive as in other coastal and estuarine environments prone to hypoxia, the slope was significantly less than in other systems. The high buffering capacity in CCB was attributed to the presence of abundant seagrass meadows adjacent to CCB and strong evaporation-produced density flow that delivers low CO2 waters to the bottom of CCB. Thus, despite the occurrence of hypoxia, neither bottom water carbonate saturation state with respect to aragonite (Ω_{arag}) nor CO_2 partial pressure (pCO_2) reached critical levels, i.e., undersaturation (i.e., $\Omega_{arag}<1$) or hypercapnia ($pCO_2>1000$ μatm), respectively.

4.1 Introduction

Acidification of the global oceans is widely attributed to the invasion of atmospheric CO_2 due to anthropogenic activities (fossil fuel burning, deforestation, and cement production). As CO_2 invades ocean waters, the resulting carbonic acid dissociates, proton concentration increases (i.e., pH decreases), and carbonate ion ($[CO_3^{2-}]$) concentration decreases as $[CO_3^{2-}]$ buffers the added acid (Feely et al. 2004). These changes in seawater chemistry are considered a global threat because many species, especially calcareous organisms, are negatively affected. Many calcareous organisms in the coastal oceans are ecosystem engineers or essential members of bottom trophic levels; therefore, the reduction of net calcification as a result of ocean acidification (OA) may have serious consequences for marine ecosystems and the ecosystem services that they provide (Andersson and Gledhill 2013; Kleypas and Yates 2009; Waldbusser et al. 2014).

In addition to atmospheric CO_2 intrusion, many other factors can influence carbonate chemistry in estuaries and coastal waters, either exacerbating or alleviating the effects of OA. These factors include net ecosystem metabolism, nutrient and organic matter loading, temperature, tides and mixing, volume of freshwater input, drainage basin mineralogy, submarine groundwater discharge, and intrusion of pollutants (NO_x and SO_x) from ocean vessels (de Weys et al. 2011; Hagens et al. 2014; Hassellöv et al. 2013; Hu and Cai 2013; Jeffrey et al. 2016; Lin et al. 2004; Ruiz-Halpern et al. 2015). Eutrophication, which often results in enhanced primary production of autochthonous organic matter in surface waters and subsequent aerobic respiration of this organic matter in bottom waters, is likely the most substantial contributor to coastal acidification on a global scale (Cai et al. 2011; Feely et al. 2010; Wallace et al. 2014; Rabalais et al. 2014). Low oxygen and acidification, which often result simultaneously from

eutrophication, are predicted to have a synergistic effect on the marine environment (Gobler et al. 2014; Gruber 2011). Nevertheless, estuarine acidification remains poorly understood because of the complex array of water chemistry drivers (e.g., river-ocean interactions, human intervention, and vegetation (Potter et al. 2010)) that result in spatial and temporal heterogeneity between and within estuarine environments.

The lagoonal estuaries of the northwestern Gulf of Mexico coast span a climactic gradient that results in freshwater balance (sum of all riverine inflow and direct precipitation minus evaporation in an estuary) that is two orders of magnitude greater in the northeast than the southwest despite the relatively narrow latitudinal range (Montagna et al. 2013). The majority of the estuaries in the region have experienced multi-decadal estuarine acidification, showing the symptoms of both alkalinity and pH decline, and this phenomenon has been attributed to long-term reduction in freshwater inflow (Hu et al. 2015). Additionally, the estuaries at the southern end of this range face increasingly negative freshwater balance (i.e., evaporation exceeds freshwater input) due to reduced precipitation and increased human water demands in recent decades (Montagna et al. 2011).

In addition to the recently discovered estuarine acidification, some estuaries in this semiarid region also experience episodic hypoxia, posing additional concern about synergistic effects of multiple stressors on overall ecosystem health (Applebaum et al. 2005; Hodges et al. 2011; McCarthy et al. 2008; Ritter and Montagna 1999; Wetz et al. 2016). To better understand the links between eutrophication and acidification in the estuarine waters in the northwestern Gulf of Mexico, multiple field surveys were used to investigate the carbonate system dynamics in Corpus Christi Bay (CCB)—a semi-arid estuary that frequently experiences summertime hypoxia.

4.2 Materials and Methods

4.2.1 Study sites

This study was carried out in CCB, located along the Texas coast in the Nueces Estuary at 27° 45' N, 97° 15' W (Fig. 4.1) in an area that experiences great climactic variability with dry and wet cycles (Montagna and Kalke 1995). CCB is the primary bay in the system due to its direct connection to the Gulf of Mexico, and it adjoins to two secondary bays, Nueces Bay and Oso Bay, which are fed by the Nueces River (43,299 km^2 drainage basin) and Oso Creek (234 km^2 drainage basin), respectively (https://maps.waterdata.usgs.gov/mapper/index.html). CCB is separated from the Gulf of Mexico by a barrier island chain with established tidal inlets—Aransas Ship Channel and Packery Channel—to the north and south of the estuary. CCB is shallow (average depth ~3.2 m), microtidal, and experiences considerable physical forcing by the high wind speeds in the region (Ritter and Montagna, 1999). Hypoxia has been found to occur in the southeastern region of the bay every summer, and potential negative effects to the benthic communities include reduced diversity, abundance, and biomass. These negative effects are observed even under oxygen concentrations as high as 3 mg L^{-1}, therefore increasing the threshold for hypoxia in the area from the broad classification of hypoxia as <2 mg L^{-1} (Ritter and Montagna, 1999).

4.2.2 Sampling and analytical methods

In the summers of 2015 and 2016, a total of 11 daytrips were conducted in southeastern CCB on board a small research vessel (i.e., two in 2015—June 9 and Aug. 25—and nine in 2016—June 1, June 14, June 28, July 11, July 22, Aug. 4, Aug. 18, Sept. 8, and Sept. 29). Fourteen stations were visited during each of the sampling trips. Note that not all stations were the same between the 2015 and 2016 sampling, so a total of 20 different stations were visited over the two

summers (Fig. 1). A calibrated YSI 6920 multisonde was used to obtain *in-situ* temperature, salinity, and dissolved oxygen (DO) concentration at both the surface (~0.5 m) and the bottom (within 0.5 m from the sediment-water interface) of the water column, and a Van Dorn water sampler was used to take water samples from both the surface and bottom of the water column.

For the two sampling trips in 2015, inorganic nutrient concentrations (nitrate + nitrite (NO_x), ammonium, orthophosphate, and silicate) were determined from the filtrate of water that passed through a 0.45 μm polycarbonate filter. The nutrient samples were frozen (-20^o C) until analysis within two weeks of collection. Samples were analyzed with an O.I. Analytical Flow Solution IV analyzer. Check standards of known concentrations as well as matrix spikes and laboratory duplicates were run after every 10 samples. Method detection limits were 0.01 μM for NO_x, 0.03 μM for ammonium, 0.01 μM for orthophosphate, and 0.07 μM for silicate. No nutrient samples were collected in 2016.

Following the standard OA operating protocol (Dickson et al. 2007), unfiltered water samples were collected in 250 mL borosilicate glass bottles for carbonate system characterization. 100 μL saturated mercuric chloride ($HgCl_2$) was added into the samples bottles and bottle stoppers were replaced after the application the Apiezon® L grease and secured with a rubber band and hose clamp. These preserved samples were used for total alkalinity (TA), total dissolved inorganic carbon (DIC), and pH analyses. TA was analyzed at 22±0.1°C using Gran titration on an automated titration system (AS-Alk2, Apollo Scitech Inc.). DIC was analyzed using infrared detection on a AS-C3 DIC analyzer (Apollo Scitech Inc.). Both DIC and TA analyses had a precision of ±0.1% based on randomly collected duplicate samples, and Certified Reference Material (CRM) was used to ensure the quality of the analysis and optimal performance of the instruments (Dickson et al. 2003). In 2015, CRM Batches 142 and 147 were

used, and in 2016, Batches 148 and 156 were used. Total scale pH was measured at 25°C using purified m-cresol purple with the method in Carter et al (2013), and all reported pH values were corrected to *in-situ* temperature. The equation in Liu et al. (2011) was used in the calculation of pH values. Recently a new equation for wider salinity range (0-40, vs. 20-40 in the Liu et al. study) was reported for spectrophotometric pH analysis (Douglas and Byrne 2017), but the two equations generated essentially the same results for our samples. Calcium concentration ($[Ca^{2+}]$) was measured (from non-preserved water samples) using an automatic titration with an ethylene glycol tetraacetic acid (EGTA) titrant on a Metrohm Titrando with a precision of ±0.2%.

Carbonate speciation calculations were done using the Excel® version CO2SYS software. Carbonic acid dissociation constants (K_1 and K_2) were from Dickson and Millero (1987), with the exception of the three samples from 2015 that had salinities of less than 20, for which the constants from Millero (2010) were used. Bisulfate dissociation constant was from Dickson (1990), and borate concentration was from Uppström (1974). Input variables for the speciation calculation included measured DIC, measured pH (at 25°C), laboratory temperature, *in-situ* temperature, pressure, and salinity. Moreover, nutrient data (ammonia, phosphate, and silicate) were used for the 2015 speciation calculations only, since no nutrient data were collected in 2016. Carbonate saturation state with respect to aragonite (Ω_{arag}) obtained from the CO2SYS output ($\Omega_{ar,CO2Sys}$) was corrected to make the calculated Ω_{arag} appropriate for estuarine waters because the river endmember has a non-zero $[Ca^{2+}]$ (Eqs. 4.1, 4.2). This correction produced Ω_{arag} values that were 0.26 ± 0.16 higher (5.7 ± 3.1% higher) than the uncorrected Ω_{arag}.

$$\Omega_{\text{arag}} = \Omega_{\text{ar,CO2Sys}} \times \frac{[Ca^{2+}]_{meas}}{[Ca^{2+}]_{theor}} \qquad (4.1)$$

where $[Ca^{2+}]_{meas}$ is the measured $[Ca^{2+}]$ and $[Ca^{2+}]_{theor}$ is the theoretical $[Ca^{2+}]$ based on salinity

$$[Ca^{2+}]_{theor} = 10.28\ mmol\ kg^{-1} \times \frac{Sal_{meas}}{35} \qquad (4.2)$$

ocean $[Ca^{2+}]$ was assumed to be 10.28 mmol kg^{-1} (Sal = 35), and Sal_{meas} is the measured salinity.

The new Excel® version CO2SYS program developed by Xu et al. (2017) was used to evaluate the effect of nutrients, especially ammonia, on calculated pH, pCO_2, and Ω_{ar}, by including the input variables of ammonia, phosphate, and silicate from the 2015 trips. Additionally, organic alkalinity (Org-Alk) was estimated using ΔTA (Yang et al. 2015) (Eq. 4.3). Operationally, ΔTA is equivalent to non-carbonate alkalinity, which normally includes contributions of both Org-Alk and nutrient-derived alkalinity (P-Alk and Si-Alk), with the latter often considered negligible. However, given the incorporation of nutrients into the calculated TA for the 2015 dataset, calculated ΔTA was equivalent to Org-Alk.

$$\Delta TA = TA_{meas} - TA_{calc} \qquad (4.3)$$

where TA_{meas} is the TA measured via titration and TA_{calc} is the TA calculated in CO2SYS using DIC, pH, salinity, *in-situ* temperature, and nutrients. For the 2016 dataset when nutrient data were unavailable, a correction of TA_{calc} from nutrient was assumed based on the 2015 results. See 3.4 for detailed discussion on the nutrient influence on TA.

Finally, to evaluate estuarine water buffer capacity, the buffer factor $ß_{DIC}$ was calculated using the expanded equation in Egleston et al. (2010) (Eq. 4.4) after a necessary correction to a sign error in the original paper (J. Orr, personal comm.).

$$\beta_{DIC} = \frac{DIC \times S - Alk_C^2}{Alk_C} \qquad (4.4)$$

where Alk_C is the carbonate alkalinity, which was calculated as $Alk_C = [HCO_3^-] + 2[CO_3^{2-}]$ from the results of CO2SYS, and $S = [HCO_3^-]+4[CO_3^{2-}]+[H+][B(OH)_4^-]/(K_b+[H^+])+[H^+]+[OH^-]$, in which K_b is the dissociation constant of boric acid.

4.2.3 Statistics

Multiple linear regression (MLR) was used to examine controlling factors of the carbonate system parameters (pH, pCO_2, and Ω_{arg}). The MuMIn package in R was used to conduct an exhaustive search of all possible models for carbonate system parameters and rank them based on AICc (with DO, salinity, temperature, and all their interactions as potential predictor variables). The best model was determined based on lowest AICc. Since there is no discernable difference between models with a difference in AICc of less than two (Burnham and Anderson 2002), multiple models may have been identified as the best model.

4.3 Results

4.3.1 Hydrologic conditions and DO

While only two trips were conducted in 2015 vs. nine trips in 2016, the timing (June 9, 2015– Aug. 25, 2015 and June 1, 2016– Sept. 29, 2016) largely overlapped. Flood influence immediately prior to the first trip in 2015 (https://maps.waterdata.usgs.gov/mapper/index.html, Fig. 2) resulted in significantly lower average salinity in 2015 than 2016 in both surface and bottom waters (t-test, $p<0.0001$, Table 4.1). Hypersaline conditions (>35) were frequently observed in 2016.

Salinity distribution in this shallow system was far from homogeneous, and higher salinity water was often observed in the southeast corner of CCB next to the Upper Laguna Madre (ULM). Despite the generally high wind speeds and the shallow basin, vertical salinity stratification was strong at times, with a bottom-surface salinity gradient (ΔS_{b-s}) of greater than 4

found (in at least one sampled station) during five of the 11 sampling trips. The greatest ΔS_{b-s} at a single station was 8.8 (observed on June 14, 2016), but stratification was not uniform throughout the sampled area, with a mean ΔS_{b-s} of only 2.8 for the same day. Stratification generally weakened by the end of the summer sampling period; for example, the greatest ΔS_{b-s} (8.8 on June 14, 2016) dropped to 2.1 by Sept. 29, 2016 (see temporal changes in surface and bottom salinity and dissolved oxygen in Fig. S4.1).

Bottom water DO concentrations were significantly lower than surface water DO concentrations for both years (paired t-test, $p<0.0001$, see temporal changes in surface and bottom salinity in Fig. S4.1). Bottom DO was highly variable, but it was significantly lower in 2015 than 2016 (t-test, $p<0.001$). Conversely, surface DO was significantly lower in 2016 than in 2015 (t-test, $p<0.0001$, Table 4.1). Hypoxic conditions (DO < 62.5 μmol kg^{-1}, or 2 mg L^{-1}) were observed in bottom waters on four of the 11 sampled days; on June 9, 2015, Aug. 4, 2016, and Aug. 18, 2016 hypoxia was found at two of the 14 sampled stations, and on June 28, 2016 hypoxia was found at four of the 14 sampled stations. Two of the 14 stations sampled in 2015 were found to have hypoxia at least once over the two sampling trips, and six of the 14 stations sampled in 2016 were found to have hypoxia at least once over the nine sampling trips. If classifying hypoxia as DO < 93.8μmol kg^{-1} (3 mg L^{-1}) as suggested by Ritter and Montagna (1999), hypoxia was observed on three additional dates, June 14, 2016, July 22, 2016, and Sept. 8, 2016 (though hypoxia was only recorded at one station for each of those dates). Hypoxia more commonly occurred when the water column showed vertical salinity stratification ($\Delta S_{b-s}>4$), but stratification was not required for hypoxia; 36% of stratified observations also had hypoxic bottom waters, while only 8% of non-stratified observations had hypoxia.

4.3.2 Carbonate system dynamics

No significant relationship (linear regression, p=0.21) was observed between bottom water salinity and TA in 2015; surface water in 2015 and bottom and surface water in 2016 all had significant positive relationships between salinity and TA (linear regression, p<0.0001). Despite substantial variations in both DIC and TA, these two parameters in both surface and bottom waters were significantly higher in 2015 than in 2016 (t-test, p<0.0001), corresponding to higher river discharge (Figs. 4.2 and 4.3, Table 4.1). Of the derived carbonate parameters (pH, Ω_{arag}, and pCO_2), the only significant differences between years were pH and Ω_{arag} in surface water (t-tests, p<0.0001 and p=0.0002, respectively) (Table 4.1).

Ca^{2+} showed a significant linear relationship with salinity for both years (Fig. 4.4, p<0.0001), but an analysis of covariance (ANCOVA) suggested a significant difference between years for both the intercept (independent variable=year, p<0.0001, df=1, mean sq=3.9, F-value=164.2) and slope (independent variable= year:salinity interaction, p<0.0001, df=1, mean sq=5.4, F-value=225.8). Regression of the 2015 data indicated a positive y-intercept of 1.631±0.176 mmol kg^{-1}, whereas the 2016 data had a negative y-intercept (-1.158±0.108 mol kg^{-1}) (Fig. 4.4).

The derived carbonate system parameters at *in-situ* conditions (pH, Ω_{arag}, and pCO_2) exhibited significant spatial and temporal variability (Table 4.1, Fig. S4.2). Of particular interest is the dynamics of pCO_2. In 2015 when surface salinity was lower, surface pCO_2 exhibited relatively smaller variation (385.4±43.3 µatm, with a range of 306.1-457.1 µatm) compared to that in the bottom water (418.5±118.3 µatm, with a range of 137.0-679.3 µatm). In 2016 however, both surface and bottom water exhibited similar magnitude of variations (Table 4.1). In addition, the lower end of pCO_2 values (~40 µatm) were significantly less than the atmospheric value (~395 µatm at the time of the fieldwork, Fig. 4.5).

The buffer factor $ß_{DIC}$ ranged 0.189-0.428 mmol kg^{-1}. Significant positive linear relationships between $ß_{DIC}$ and both salinity and temperature were observed for the entire dataset ($p<0.0001$, Fig. 4.6). There was a significant negative linear relationship between $ß_{DIC}$ and DO in the surface water ($p<0.001$), but no such relationship was observed in bottom water or the entire dataset. Additionally, there was a significant difference in $ß_{DIC}$ between surface and bottom waters (paired t-test, $p=0.002$), with bottom waters having a $ß_{DIC}$ 0.0096 ± 0.0374 higher on average.

4.3.3 Relationship between DO and the carbonate system parameters

pH had a significant positive linear relationship with DO in bottom waters ($p=0.008$, Fig. 4.7a), while Ω_{arag} did not ($p=0.26$, Fig. 4.7b). The best-fit slope indicates that a decrease of 32 µmol kg^{-1} DO corresponds to a pH decrease of ~0.02. Several parameters had significant differences in bottom waters between periods of normoxia and hypoxia, including salinity, DIC, TA, Ca^{2+}, pH, and pCO_2 (Table 4.2).

The best MLR models for pH and pCO_2 in surface waters according to AICc both required salinity, DO, and their interaction, but not temperature (Table 4.3). The best models to fit Ω_{arag} in surface or bottom and pH and pCO_2 in bottom waters all required more independent variables, often including temperature and its interactions with other variables.

4.3.4 Non-carbonate alkalinity

ΔTA for the 2015 data alone (when nutrient concentrations were used in calculations) was 43.5±20.7 µmol kg^{-1}, or 1.7±0.8% of measured TA. Nutrient contribution to the calculated TA had small variation, at 4.9±1.2 µmol kg^{-1}, with the most contribution coming from silicate (4.4±1.1 µmol kg-1). TA contribution from phosphate and ammonia were 0.4±0.2 and 0.1±0.2 µmol kg^{-1}, respectively. Omitting the nutrients in the 2015 CO2SYS calculation resulted in ΔTA of 48.3±21.3 µmol kg^{-1}. However, calculated *in-situ* pH, pCO_2, and Ω_{arag} differed by only -

0.00009±0.00005, -0.10±0.08 µatm, and 0.0009±0.0004, respectively, when calculated with and without the nutrient data. These differences were sufficiently small compared to analytical precision (for example pH had ±0.0004), and propagated errors calculated from the measured values were two orders of magnitude higher than the calculated differences. ΔTA for the 2016 data alone (when nutrient samples were not collected) was 29.0 ± 18.4 µmol kg^{-1}, or 1.2 ± 0.7 % of measured TA. Given that nutrient contributions to TA was uniformly small in 2015 despite the larger salinity gradient in 2015 (Table 4.1), the calculated ΔTA in 2016 was corrected by the mean nutrient-derived TA (4.9 µmol kg^{-1}) to better represent Org-Alk, which reduced ΔTA to 24.1 ± 18.4 µmol kg^{-1}, or 1.0±0.8% of measured TA. Overall, ΔTA showed negative correlation with salinity in the 2015 samples ($p<0.0001$, Fig. 4.8), while a positive correlation was observed in the 2016 samples ($p=0.02$, Fig. 4.8).

4.4 Discussion

4.4.1 Hydrologic conditions and estuarine solute distribution

Due to both the restricted exchange between CCB and the coastal waters (i.e., through the Aransas Ship Channel, Packery Channel, and the ULM) and limited freshwater discharge from Nueces River and Oso Creek, the transition from freshwater to saltwater is very abrupt in this estuary compared to typical river-dominated estuaries and does not exhibit substantial temporal variability. For example, a recent study that examined both Nueces Bay (NB) and CCB during the July 2013-July 2016 period had salinity of 32.8±5.0 across both bays (Montagna et al. 2018). Similarly, in an earlier work that spanned from May 1990-December 1994, salinity in CCB was 32.1, with a range of 28.6-37.9 (Pennock et al. 1999). Nevertheless, fluctuations in freshwater inflow conditions can still periodically exert an important control on the short-term salinity variability and carbonate chemistry. In 2015, greater freshwater influence can be clearly seen

(Table 4.1, Figs. 4.2, 4.3, and 4.4) as more freshwater discharge occurred due to heavy precipitation events between May and July prior to the sampling trips. Because of the more positive freshwater balance in 2015, relationships between carbonate system parameters as well as between carbonate system parameters and salinity often differed between years, and therefore interpretations often differed between 2015 and 2016. AICc of MLR models revealed that both salinity and DO are necessary to best model the derived carbonate system parameters (Table 4.3); therefore, freshwater inflow and aerobic respiration were likely both important controllers on the carbonate system. However, it is apparent that Ω_{arag} and $ß_{DIC}$ were more closely associated with salinity than DO level (Figs. 4.6 and 4.7).

As estuarine water residence time varies depending on the amount of freshwater inflow (Solis and Powell 1999), it is likely CCB was "flushed" faster or to a greater extent in 2015 than in 2016, as reflected by the higher salinity in 2016 (Table 4.1). For a typical river-ocean mixing scenario, TA (or other non-reactive solutes) and salinity would exhibit a linear relationship based on a conservative mixing line with the intercept of zero salinity falling on the river-endmember concentration of the solute (Hu et al. 2015). While most rivers contain lower TA than ocean waters resulting in a positive slope of the conservative mixing line, the rivers in south Texas have relatively high alkalinity due to both weathering of limestone in the watersheds and evaporation (Zeng et al. 2011; Montagna et al. 2018), resulting in a negative slope of the conservative mixing line.

To better understand factors influencing alkalinity, the expected conservative mixing lines and an evaporation-precipitation line of seawater (E-P line, Fig. 4.3 a&b) for TA were both examined. For the conservative mixing, two potential mixing lines were established based on average Nueces River TA collected by both our Carbon Cycle Lab (CCL; 3842±307 μmol kg^{-1}

with a range of 3242-4324 μmol kg^{-1}, n= 9, 2015-2016; Hu, unpublished data) and the Texas Commission on Environmental Quality (TCEQ; 2881±250 μmol kg^{-1}, n=33, 1981-1989, https://www.tceq.texas.gov/agency/data/records-services). The ocean endmember was established using average northern Gulf of Mexico (nGoM) surface water values (salinity = 36.4, TA = 2428 μmol kg^{-1}, Hu et al. 2015). The seawater E-P line was then established by holding the TA:S ratio of the ocean endmember constant across all salinities (since evaporation or precipitation would cause TA and salinity to change concurrently, but without changing the TA:S ratio). If there is no reaction that consumes TA, the TA:S ratio of any location in an estuary should fall above the seawater E-P line since river water has infinitely high TA:S ratio if assuming its salinity is zero (Hu et al. 2015). The clear majority of the data points in both 2015 and 2016 (surface and bottom combined) fell above the seawater E-P line (Fig. 4.3a&b); therefore, the dominant controls on TA were mixing and evaporation. However, for the few data points that fell below the seawater E-P line, definitive consumption must have occurred (2016 data in Fig. 4.3a&b). The linear relationship between TA and salinity (using observations with S<30) in surface waters in 2016 (Fig. 4.3a) had a y-intercept of 826 μmol kg^{-1}, much lower than the CCL and TCEQ measurements of Nueces River TA, further suggesting that TA consumption occurred, and this consumption is further suggested by the fact that the majority of data points fell below the river-ocean mixing line (dotted lines in Fig. 4.3 a&b).

While there was no immediately evident TA:S relationship, even in the better-flushed 2015, higher alkalinity was observed during periods of higher freshwater inflow (2015; Figure 4.3a). Estuarine TA-S relationship formed somewhat of a concave pattern in both the surface (Fig. 4.3a) and bottom waters (Fig. 4.3b). Despite the large variability that has been observed in the TA of the river endmember, both TCEQ and CCL river TA data were consistently higher than

CCB surface TA values (and further, the concave pattern in the TA-S relationship was observed during individual sampling trips), meaning that concave pattern in the TA-S relationship could not have occurred as result of changing TA of the freshwater endmember. While tidal flushing also has the potential to exert control on TA in an estuary, tidal flushing is minimal in this system. In addition, the increasing TA/DIC with increasing salinity indicates that high salinity waters have reduced CO_2, which is likely attributed to evaporation-induced CO_2 loss during longer residence times (Fig. 4.3c&d, Yao and Hu, 2017) as well as seagrass uptake of CO_2 (see Section 4.4.3).

An E-P line was also used to investigate the $[Ca^{2+}]$:S relationship. The same nGoM salinity (36.4) and a slope of the empirical relationship between $[Ca^{2+}]$ and salinity in ocean surface waters (10.28 mmol kg^{-1} : 35) were used to plot an E-P line, and two potential conservative mixing lines were plotted using average Nueces River $[Ca^{2+}]$ collected by CCL (1.85±0.47 mmol kg^{-1}, n= 9, 2015-2017; Hu, unpublished data) and TCEQ (1.45±0.23 mmol kg^{-1}, n=33, 1981-1989) (dotted lines in Fig. 4.4). In 2015, the $[Ca^{2+}]$ at zero salinity extrapolated from the linear relationship between $[Ca^{2+}]$ and salinity (1.63±0.18 mmol kg^{-1}) is similar to the Nueces River measurements. However, the 2016 linear regression for $[Ca^{2+}]$:S had a negative intercept (-1.16±1.11). Such negative intercepts are not uncommon in the marine environment. For example, while not addressing Ca^{2+} *per se*, Jiang et al. (2014) attributed a negative TA:S intercept to either TA removal at low salinities or TA addition at high salinities. Given that Ω_{arag} values were all greater than 3.3 in high salinity waters (S>35, Fig. 4.7), no carbonate dissolution (i.e., Ca^{2+} addition) would be expected there. The most plausible explanation for this negative intercept would be Ca^{2+} removal at lower salinities. Lower salinity (<30) waters were mostly observed in early and mid-June (June 1 and June 14, 2016), and low $[Ca^{2+}]$/S ratios during this

period were observed in the west end of our sampling area, despite that the values were never lower than that of the ocean endmember (0.294, Fig. 4.4). It is likely that reduced freshwater flushing and subsequent increased residence time of estuarine water in 2016 allowed TA and Ca^{2+} consumption signals from calcification processes to be preserved. The reduced $[Ca^{2+}]/S$ is likely a result of oyster calcification in Nueces Bay or other benthic calcifiers in the region. There are other processes that may concurrently lower alkalinity, such as ammonia uptake, but they would not consume $[Ca^{2+}]$.

4.4.2 Hypoxia formation and destruction in CCB

In a study that assessed Oso Bay outflow, which partially originates from the Barney Davis Power Plant (near the end of Oso Bay) that draws cooling water from the more saline ULM, Hodges et al. (2011) suggested that high salinity water could create a gravity flow that enters CCB bottom waters. This high salinity water would create a strong vertical salinity gradient that prevents efficient wind-driven mixing, allowing the development of hypoxia in the CCB bottom waters. However, Hodges et al. (2011) only examined a small area at the mouth of the Oso Bay. Our study had greater spatial coverage, and our 'composite' figure of salinity and pCO_2 in both surface and bottom water (i.e., average of all data at each sampling station from all 2016 data) revealed that saline water inflow to SE CCB directly from the ULM, rather than Oso Bay (Fig. 4.9b), probably played an important role in hypoxia formation. Bottom waters moving into SE CCB that originated from the ULM were both high in salinity and very low in pCO_2 (Fig. 4.9). As additional evidence that low pCO_2 waters are being transported into the bottom waters of CCB, significantly higher $ß_{DIC}$ was found in bottom waters compared to surface waters (paired t-test, p=0.002), indicating that the bottom waters are better buffered. Despite having very low pCO_2, reaching as low as about ~40 µatm in these waters, the DO level of this water plume from

the ULM was also relatively low (though not as low as some areas outside of Oso Bay, Fig. 4.9f).

There is a range of benthic respiration rate measurements in the literature. Sell and Morse (2006) reported sediment oxygen consumption rate of 13.5±3.8 mmol-O_2 m^{-2} d^{-1}. In a global synthesis, CCB was reported to have amongst the highest benthic respiration rate of studied estuaries, as high as 115 mmol-C m^{-2} d^{-1} (Hopkinson and Smith 2005). Assuming a respiration quotient of 1, this CCB respiration rate can be converted to 114 mmol-O_2 m^{-2} d^{-1}. In comparison, our own measurements using whole core incubation technique (cf. Wang et al. 2018) indicated that benthic DO consumption rate was on the order of 40-60 mmol-O_2 m^{-2} d^{-1} (Hu, unpublished data). The effect of such benthic respiration on hypoxia formation was calculated; for example, starting with the conditions at our southernmost sampled station (bottom water S = 38.6, T = 30.64˚C, DO = 190.1 μmol kg^{-1}, or 102.7% saturation), and assuming that the hypersaline layer was 0.14 m as suggested by Hodges et al. (2011), benthic respiration alone could cause hypoxia (<93.8μmol kg^{-1}, Ritter and Montagna 1999) after only ~3-25 hours if there was no vertical mixing. While the thickness of the hypoxic layer was not directly measured at stations that were hypoxic, doubling of the thickness would still make the hypoxia formation a faster process compared to that in the nGoM (Hu et al. 2017). Therefore, the formation and wind-driven destruction of hypoxia in the SE CCB bottom waters can be ephemeral, which is reflected by observed sporadic low oxygen conditions during sampling (Fig. S4.1).

4.4.3 Enhanced buffering caused by seagrasses and evaporation

While CCB pH decreased with decreasing DO, as has been observed in many other scenarios of hypoxia, the decrease in pH was substantially less than what would be expected on aerobic respiration of coastal water in the shelf of western Gulf of Mexico (Fig. 4.7). Based on the best-

fit regression between DO and pH in CCB, a decrease in DO of 200 μmol kg^{-1} would have led to roughly a pH decrease of 0.14, while the same change in DO would lead to pH decreases of 0.42 and 0.56 in the nGoM (Hu et al. 2017) and Long Island Sound seawater (Wallace et al. 2014), respectively. Theoretically, wind influence could disrupt hypoxia and thus alter the pH-DO relationship. However, given the different air-water exchange rates between oxygen and CO_2 (Williams and Follows, 2011), DO would be replenished much faster than CO_2 could degas. During subsequent stratification (given the fast DO consumption kinetics, Section 4.4.2), the reoccurrence of hypoxia would effectively increase the pH-DO slope, producing even lower pH at low DO levels (vs. our observed lowest pH of 7.93 in hypoxic conditions), similar to what Cai et al (2011) suggested (although this suggestion was based on some inadvertently incorporated deep water data, see Hu et al. 2017 for details). Therefore, the high wind speeds coupled with the difference in gas exchange rates could not be responsible for the difference between this pH-DO relationship and others in the literature.

The resistance of CCB waters to aerobic respiration-induced CO_2 production is likely due to its exceptionally high buffer capacity. The buffer factor $ß_{DIC}$ ranged 0.19-0.43 mmol kg^{-1} in CCB waters (Table 4.1, Fig. 4.6). In comparison, nGoM shelf water had a $ß_{DIC}$ range of 0.16-0.36 mmol kg^{-1} (Hu et al. 2017), and the global surface ocean had a $ß_{DIC}$ range of 0.16-0.28 mmol kg^{-1} in 1994 (Egleston et al. 2010). The high $ß_{DIC}$ values indicate that CCB water is less sensitive to pH changes for a given amount of CO_2 addition compared to other coastal areas in the literature. There was no significant difference for either year in bottom water $ß_{DIC}$ between hypoxic (DO < 93.8μmol kg^{-1}, i.e., based on Ritter and Montagna criteria in CCB) and normoxic (DO > 93.8μmol kg^{-1}) conditions (Table 4.2), indicating that respiration-induced hypoxia also did not significantly alter this high buffer capacity.

It is known that the ULM is subject to negative freshwater balance due to high evaporation and low freshwater inflow, thus hypersalinity (S>seawater salinity) is a frequent occurrence (Montagna et al. 2013; Solis and Powell 1999; Wilson and Dunton 2018). Thermodynamic calculations using CO2SYS indicate that evaporation would increase pCO_2 due to decreased CO_2 solubility (Yao and Hu 2017). Therefore, to counteract the evaporation effect and reach the low pCO_2 levels observed in the saline bottom waters in this study, substantial CO_2 consumption would have to take place, and the consumption likely comes from the seagrasses that live throughout the ULM (Fig 4.1.).

The ULM is home to vast meadows of two seagrass species, *Halodule wrightii* and *Syringodium filiforme*, and the former is more tolerant to high salinity waters (Wilson and Dunton 2018). On a global scale, seagrass meadows are a CO_2 sink because their high productivity generally results in local net consumption of CO_2 as well as increased buffer capacity, especially during the daytime (Anthony et al. 2013; Anthony et al. 2011; Duarte et al. 2010; Hendriks et al. 2014). Regardless of whether the seagrasses take up CO_2 directly (Hemminga and Duarte 2000; Zimmerman et al. 1997) or assimilate bicarbonate (HCO_3^-) indirectly through the use of carbonic anhydrase (Björk et al. 1997; Uku et al. 2005), inorganic carbon utilization can drive down both DIC and pCO_2, creating a carbon-limited environment. Meanwhile, it is also important to note that there can be substantial spatial heterogeneity and regional variability in net ecosystem metabolism in seagrass ecosystems, with some seagrass beds actually having observations of photosynthesis: respiration (P:R) ratios less than one (Duarte et al. 2010). Our interpretation assumes that this region of the ULM remains net autotrophic during summer months (Copeland and Nixon, 1974), although there have been studies reporting that gross primary production and respiration can be nearly balanced on an

annual scale in the ULM (Ziegler and Benner, 1998). Additionally, the diel cycle of photosynthesis and respiration of seagrasses locally increases the extremes in the carbonate system, and these extremes are expected to increase in areas that are acidifying (Challener et al. 2016; Pacella et al. 2018).

In addition to seagrass-induced pCO_2 drawdown and subsequent pH increase, higher salinity water also has higher $[Ca^{2+}]$ due to the concentrating effect. For example, the high salinity water coming from ULM (S = 39.85) can have ~18% higher $[Ca^{2+}]$ compared to the nwGOM shelf water. Since evaporation may exert some control on $[Ca^{2+}]$, it may also have the potential to increase Ω_{arag}. In 2016, $[Ca^{2+}]$ was significantly higher in hypoxic bottom waters than normoxic bottom waters ($p= 0.003$, Table 4.2), potentially because the same stratification that allowed the hypoxia to develop also prevented the higher $[Ca^{2+}]$ bottom waters that came from the ULM from mixing with the water column. While Ω_{arag} was still significantly lower in these hypoxic bottom waters, the source water likely had higher Ω_{arag}. The entire process (evaporation, carbon uptake by seagrasses, and hypoxia formation) that is likely occurring in the CCB system during our two years of summer sampling is illustrated in Fig. 4.10.

The highly buffered CCB waters currently have Ω_{arag} and pCO_2 levels remaining higher than 2 (supersaturation) and less than 1000 μatm (hypercapnia), respectively. Given that supersaturation and hypercapnia are the two indicators that are important for calcifiers (Feely et al. 2018; McNeil and Sasse 2016), CCB has seemingly suitable carbonate chemistry conditions for growth and preservation of calcium carbonate skeletons even under very low DO levels. Unfortunately, freshwater shortages are expected to worsen in this region (Cook et al. 2015) and could potentially yield a twofold threat to the ability of this system to naturally buffer against hypoxia-associated acidification and sustain calcifiers. Reduced freshwater inflow would worsen

the hypersaline conditions, subsequently deteriorating the seagrass coverage (Wilson and Dunton 2018), and reduced freshwater inflow would also reduce the alkalinity delivery to the bay (Hu et al. 2015). In both of these ways, potential future reductions in freshwater inflow could reduce this unique buffer capacity in Corpus Christi Bay. The effects of the reduced freshwater inflow may also be compounded by the influence of the ongoing acidification of the ocean endmember.

4.4.4 Organic alkalinity in CCB waters

Given the proximity to land masses and freshwater influence, estuarine TA is expected to include substantial Org-Alk. However, contrary to previous observations that non-carbonate alkalinity has a negative relationship with salinity (Cai et al. 1998; Hunt et al. 2011), ΔTA exhibited an initial decrease followed by an increase with salinity (Fig. 4.8). Based on an ANOVA to compare two models ($F=13.07$, $p<0.001$), ΔTA:S relationship for all data is better fit by a second order polynomial ($p<0.0001$, $R^2_{adj} = 0.0970$, root mean square = 19.38) than a linear model ($p<0.0001$, $R^2_{adj} = 0.0495$, rse = 19.77). Such a salinity dependence of ΔTA was similar to the observations in the nearby, semiarid Mission-Aransas Estuary (Yao and Hu 2017). When the two years were examined individually, 2015 (the high river inflow year) data showed a negative relationship between ΔTA and salinity (linear regression, $p<0.0001$), as has been seen in other river-dominated estuaries. This relationship is expected because river inflow is the source of Org-Alk. However, during 2016 there was a significant positive relationship between ΔTA and salinity (linear regression, $p=0.02$), likely because evaporation exerted more control than freshwater inflow, concentrating both salinity and Org-Alk during longer water residence time (Fig. 4.8).

4.5 Conclusions

Carbonate chemistry in semi-enclosed lagoonal estuaries such as CCB is strongly affected by hydrologic conditions. Greater freshwater inflow in 2015 introduced higher levels of alkalinity despite lower salinity, and lower freshwater inflow in 2016 allowed carbonate removal signals (both TA and Ca^{2+}) to become evident.

CCB exhibited a stronger buffer against respiration-induced acidification than has been observed in many other estuaries. Despite periodic summer hypoxia, CCB bottom waters did not reach critically low Ω_{arag} or critically high pCO_2. Aquatic vegetation and evaporation both likely contributed to the elevated buffer capacity by introducing low pCO_2, high pH, and high Ω_{arag} waters. While sampling only took place in summer months, this study cannot fully explain annual carbonate system dynamics, but it likely captures the majority of annual occurrences of hypoxia. CCB's unique buffer capacity may be threatened in the future by reduced freshwater inflows and seagrass decline. Based on this study compared with other regions examined in the literature, the extent of hypoxia induced estuarine and coastal acidification clearly is not one-size-fits-all, and systems may respond differently due to the intrinsic buffer capacity of the water bodies under examination.

References

Andersson, A.J., and D. Gledhill. 2013. Ocean acidification and coral reefs: effects on breakdown, dissolution, and net ecosystem calcification. *Annual Review of Marine Science* 5: 321-348.

Anthony, K.R.N., G. Diaz-Pulido, N. Verlinden, B. Tilbrook, and A.J. Andersson. 2013. Benthic buffers and boosters of ocean acidification on coral reefs. *Biogeosciences* 10: 4897-4909.

Anthony, K.R.N., J.A. Kleypas, and J.-P. Gattuso. 2011. Coral reefs modify their seawater carbon chemistry –implications for impacts of ocean acidification. *Global Change Biology* 17: 3655-3666.

Applebaum, S., P.A. Montagna, and C. Ritter. 2005. Status and trends of dissolved oxygen in Corpus Christi Bay, Texas, U.S.A. *Environmental Monitoring and Assessment* 107: 297-311.

Björk, M., A. Weil, S. Semesi, and S. Beer. 1997. Photosynthetic utilisation of inorganic carbon by seagrasses from Zanzibar, East Africa. *Marine Biology* 129: 363-366.

Burnham, K.P., and D.R. Anderson. 2002. *Model Selection and Multimodel Inference: A Practical Information-Theoretic Approach*. New York: Springer-Verlag

Cai, W.-J., X. Hu, W.-J. Huang, M.C. Murrell, J.C. Lehrter, S.E. Lohrenz, W.-C. Chou, W. Zhai, J.T. Hollibaugh, Y. Wang, P. Zhao, X. Guo, K. Gundersen, M. Dai, and G.-C. Gong. 2011. Acidification of subsurface coastal waters enhanced by eutrophication. *Nature Geoscience* 4: 766-770.

Cai, W.-J., W. Yongchen, and R.E. Hodson. 1998. Acid-base properties of dissolved organic matter in the estuarine waters of Georgia, USA. *Geochimica et Cosmochimica Acta* 62: 473-483.

Carter, B.R., J.A. Radich, H.L. Doyle, and A.G. Dickson. 2013. An automatic system for spectrophotometric seawater pH measurements. *Limnology and Oceanography: Methods* 11: 16-27.

Challener, R.C., L.L. Robbins, and J.B. McClintock. 2016. Variability of the carbonate chemistry in a shallow, seagrass-dominated ecosystem: implications for ocean acidification experiments. *Marine and Freshwater Research* 67: 163-172.

Copeland, B.J. and Nixon, S.W., 1974. Hypersaline lagoons. In: H.T. Odum, B.J. Copeland and E.A. McMahan (Editors), Coastal Ecoogical Systems of the United States. The Conservation Foundation, Washington D.C., pp. 312-330.

Cook, B.I., T.R. Ault, and J.E. Smerdon. 2015. Unprecedented 21st century drought risk in the American Southwest and Central Plains. *Science Advances* 1: e1400082.

de Weys, J., I.R. Santos, and B.D. Eyre. 2011. Linking groundwater discharge to severe estuarine acidification during a flood in a modified wetland. *Environmental Science & Technology* 45: 3310-3316.

Dickson, A.G. 1990. Standard potential of the reaction: AgCl(s) + 12H_2(g) = Ag(s) + HCl(aq), and and the standard acidity constant of the ion HSO4− in synthetic sea water from 273.15 to 318.15 K. *The Journal of Chemical Thermodynamics* 22: 113-127.

Dickson, A.G., J.D. Afghan, and G.C. Anderson. 2003. Reference materials for oceanic CO_2 analysis: a method for the certification of total alkalinity. *Marine Chemistry* 80: 185-197.

Dickson, A.G., and F.J. Millero. 1987. A comparison of the equilibrium constants for the dissociation of carbonic acid in seawater media. *Deep Sea Research* 34: 1733-1743.

Dickson, A.G., C.L. Sabine, and J.R. Christian. 2007. Guide to Best Practices for Ocean CO_2 Measurements. PICES Special Publication 3, 191.

Douglas, N.K., and R.H. Byrne. 2017. Spectrophotometric pH measurements from river to sea: Calibration of mCP for 0≤S≤40 and 278.15≤T≤308.15K. *Marine Chemistry* 197: 64-69.

Duarte, C.M., N. Marbà, E. Gacia, J.W. Fourqurean, J. Beggins, C. Barrón, and E.T. Apostolaki. 2010. Seagrass community metabolism: Assessing the carbon sink capacity of seagrass meadows. *Global Biogeochemical Cycles* 24: GB4032

Egleston, E.S., C.L. Sabine, and F.M.M. Morel. 2010. Revelle revisited: buffer factors that quantify the response of ocean chemistry to changes in DIC and alkalinity. *Global Biogeochemical Cycles* 24: doi:10.1029/2008GB003407.

Feely, R.A., S.R. Alin, J. Newton, C.L. Sabine, M. Warner, A. Devol, C. Krembs, and C. Maloy. 2010. The combined effects of ocean acidification, mixing, and respiration on pH and carbonate saturation in an urbanized estuary. *Estuarine, Coastal and Shelf Science* 88: 442-449.

Feely, R.A., R.R. Okazaki, W.-J. Cai, N. Bednaršek, S.R. Alin, R.H. Byrne, and A. Fassbender. 2018. The combined effects of acidification and hypoxia on pH and aragonite saturation in the coastal waters of the California current ecosystem and the northern Gulf of Mexico. *Continental Shelf Research* 152: 50-60.

Feely, R.A., C.L. Sabine, K. Lee, W. Berelson, J. Kleypas, V.J. Fabry, and F.J. Millero. 2004. Impact of anthropogenic CO_2 on the $CaCO_3$ system in the oceans. *Science* 305: 362-366.

Gobler, C.J., E.L. DePasquale, A.W. Griffith, and H. Baumann. 2014. Hypoxia and acidification have additive and synergistic negative effects on the growth, survival, and metamorphosis of early life stage bivalves. *PLoS ONE* 9: e83648.

Gruber, N. 2011. Warming up, turning sour, losing breath: ocean biogeochemistry under global change. *Philosophical Transactions of the Royal Society A: Mathematical, Physical and Engineering Sciences* 369: 1980-1996.

Hagens, M., K.A. Hunter, P.S. Liss, and J.J. Middelburg. 2014. Biogeochemical context impacts seawater pH changes resulting from atmospheric sulfur and nitrogen deposition. *Geophysical Research Letters* 41: 2013GL058796.

Hassellöv, I.-M., D.R. Turner, A. Lauer, and J.J. Corbett. 2013. Shipping contributes to ocean acidification. *Geophysical Research Letters* 40: 2731-2736.

Hemminga, M.A., and C.M. Duarte. 2000. *Seagrass Ecology*: Cambridge University Press.

Hendriks, I.E., Y.S. Olsen, L. Ramajo, L. Basso, A. Steckbauer, T.S. Moore, J. Howard, and C.M. Duarte. 2014. Photosynthetic activity buffers ocean acidification in seagrass meadows. *Biogeosciences* 11: 333-346.

Sell, K.S. and Morse, J.W., 2006. Dissolved Fe^{2+} and ΣH_2S Behavior in Sediments Seasonally Overlain by Hypoxic-to-anoxic Waters as Determined by CSV Microelectrodes. *Aquatic Geochemistry* 12: 179-198.

Hopkinson, C.S., and E.M. Smith. 2005. Estuarine respiration: an overview of benthic, pelagic, and whole system respiration. In *Respiration in Aquatic Ecosystems*, ed. P.A. del Giorgio and P.J.l.B. Williams, 122-146: Oxford University Press.

Hu, X., J. Beseres Pollack, M.R. McCutcheon, P.A. Montagna, and Z. Ouyang. 2015. Long-term alkalinity decrease and acidification of estuaries in Northwestern Gulf of Mexico. *Environmental Science & Technology* 49: 3401–3409.

Hu, X., and W.-J. Cai. 2013. Estuarine acidification and minimum buffer zone—A conceptual study. *Geophysical Research Letters* 40: 5176-5181.

Hu, X., Q. Li, W.-J. Huang, B. Chen, W.-J. Cai, N.N. Rabalais, and R.E. Turner. 2017. Effects of eutrophication and benthic respiration on water column carbonate chemistry in a traditional hypoxic zone in the Northern Gulf of Mexico. *Marine Chemistry* 194: 33-42.

Hunt, C.W., J.E. Salisbury, and D. Vandemark. 2011. Contribution of non-carbonate anions to river alkalinity and overestimation of pCO_2. *Biogeosciences* 8: 3069-3076.

Jeffrey, L.C., D.T. Maher, I.R. Santos, A. McMahon, and D.R. Tait. 2016. Groundwater, acid and carbon dioxide dynamics along a coastal wetland, lake and estuary continuum. *Estuaries and Coasts* 39: 1325-1344.

Jiang, Z.-P., T. Tyrrell, D.J. Hydes, M. Dai, and S. Hartman. 2014. Variability of alkalinity and the alkalinity-salinity relationship in the tropical and subtropical surface ocean. *Global Biogeochemical Cycles* 28: 729-742.

Kleypas, J.A., and K.K. Yates. 2009. Coral reefs and ocean acidification. *Oceanography* 22: 109-117.

Lin, C., M. Wood, P. Haskins, T. Ryffel, and J. Lin. 2004. Controls on water acidification and de-oxygenation in an estuarine waterway, eastern Australia. *Estuarine Coastal and Shelf Science* 61: 55-63.

Liu, X., M.C. Patsavas, and R.H. Byrne. 2011. Purification and characterization of meta-cresol purple for spectrophotometric seawater pH measurements. *Environmental Science & Technology* 45: 4862-4868.

Mazarrasa, I., N. Marbà, C.E. Lovelock, O. Serrano, P.S. Lavery, J.W. Fourqurean, H. Kennedy, M.A. Mateo, D. Krause-Jensen, A.D.L. Steven, and C.M. Duarte. 2015. Seagrass meadows as a globally significant carbonate reservoir. *Biogeosciences* 12: 4993-5003.

McCarthy, M., K. McNeal, J. Morse, and W. Gardner. 2008. Bottom-water hypoxia effects on sediment–water interface nitrogen transformations in a seasonally hypoxic, shallow bay (Corpus Christi Bay, TX, USA). *Estuaries and Coasts* 31: 521-531.

McNeil, B.I., and T.P. Sasse. 2016. Future ocean hypercapnia driven by anthropogenic amplification of the natural CO_2 cycle. *Nature* 529: 383-386.

Millero, F.J. 2010. Carbonate constants for estuarine waters. *Marine and Freshwater Research* 61: 139-142.

Montagna, P., T.A. Palmer, and J. Beseres Pollack. 2013. *Hydrological Changes and Estuarine Dynamics*. New York: Springer.

Montagna, P., B. Vaughan, and G. Ward. 2011. The importance of freshwater inflows to Texas estuaries. In *Water Policy in Texas: Responding to the Rise of Scarcity*, ed. R.C. Griffin, 107-127. Washington D.C.: The RFF Press.

Montagna, P.A., X. Hu, T.A. Palmer, and M.S. Wetz. 2018. Effect of hydrological variability on the biogeochemistry of estuaries across a regional climatic gradient. *Limnology & Oceanography* in press.

Montagna, P.A., and R.D. Kalke. 1995. Ecology of infaunal Mollusca in south Texas estuaries. *American Malacological Bulletin* 11: 163-175.

Pacella, S.R., C.A. Brown, G.G. Waldbusser, R.G. Labiosa, and B. Hales. 2018. Seagrass habitat metabolism increases short-term extremes and long-term offset of CO_2 under future ocean acidification. *Proceedings of the National Academy of Sciences* 115: 3870-3875.

Pennock, J.R., J.N. Boyer, J.A. Herrera-Silveira, R.L. Iverson, T.E. Whiteledge, B. Mortazavi, and F.A. Comin. 1999. Nutrient behavior and phytoplankton production on Gulf of

Mexico estuaries. In *Biogeochemistry of Gulf of Mexico Estuaries*, ed. T.S. Bianchi, J.R. Pennock and R.R. Twilley, 109-162: John Willey & Sons, Inc.

Potter, I.C., B.M. Chuwen, S.D. Hoeksema, and M. Elliott. 2010. The concept of an estuary: A definition that incorporates systems which can become closed to the ocean and hypersaline. *Estuarine, Coastal and Shelf Science* 87: 497-500.

Rabalais, N.N., W.-J. Cai, J. Carstensen, D.J. Conley, B. Fry, X. Hu, Z. Quiñones-Rivera, R. Rosenberg, C.P. Slomp, R.E. Turner, M. Voss, B. Wissel, and J. Zhang. 2014. Eutrophication-driven deoxygenation in the coastal ocean. *Oceanography* 27: 172-183.

Ritter, C., and P. Montagna. 1999. Seasonal hypoxia and models of benthic response in a Texas Bay. *Estuaries and Coasts* 22: 7-20.

Ruiz-Halpern, S., D.T. Maher, I.R. Santos, and B.D. Eyre. 2015. High CO_2 evasion during floods in an Australian subtropical estuary downstream from a modified acidic floodplain wetland. *Limnology and Oceanography* 60: 42-56.

Solis, R.S., and G.L. Powell. 1999. Hydrography, mixing characteristics, and residence times of Gulf of Mexico Estuaries. In *Biogeochemistry of Gulf of Mexico Estuaries*, ed. T.S. Bianchi, J.R. Pennock and R.R. Twilley, 29-61: John Willey & Sons, Inc.

Uku, J., S. Beer, and M. Björk. 2005. Buffer sensitivity of photosynthetic carbon utilisation in eight tropical seagrasses. *Marine Biology* 147: 1085-1090.

Uppström, L.R. 1974. The boron/chlorinity ratio of deep-sea water from the Pacific Ocean. *Deep Sea Research and Oceanographic Abstracts* 21: 161-162.

Waldbusser, G.G., B. Hales, C.J. Langdon, B.A. Haley, P. Schrader, E.L. Brunner, M.W. Gray, C.A. Miller, and I. Gimenez. 2014. Saturation-state sensitivity of marine bivalve larvae to ocean acidification. *Nature Climate Change* 5: 273-280.

Wallace, R.B., H. Baumann, J.S. Grear, R.C. Aller, and C.J. Gobler. 2014. Coastal ocean acidification: The other eutrophication problem. *Estuarine, Coastal and Shelf Science* 148: 1-13.

Wang, H., Hu, X., Wetz, M.S. and Hayes, K.C., 2018. Oxygen consumption and organic matter remineralization in two subtropical, eutrophic coastal embayments. Environmental Science & Technology, 55: 13004-13014.

Wetz, M.S., K.C. Hayes, K.V.B. Fisher, L. Price, and B. Sterba-Boatwright. 2016. Water quality dynamics in an urbanizing subtropical estuary (Oso Bay, Texas). *Marine Pollution Bulletin* 104: 44-53.

Williams, R.G. and Follows, M.J., 2011. Ocean Dynamics and the Carbon Cycle. Cambridge University Press, New York.

Wilson, S.S., and K.H. Dunton. 2018. Hypersalinity during regional drought drives mass mortality of the seagrass Syringodium filiforme in a subtropical lagoon. *Estuaries and Coasts* 41: 855-865.

Yang, B., Byrne, R. H., & Lindemuth, M. 2015. Contributions of organic alkalinity to total alkalinity in coastal waters: A spectrophotometric approach. *Marine Chemistry*, 176: 199–207.

Yao, H., and X. Hu. 2017. Responses of carbonate system and CO_2 flux to extended drought and intense flooding in a semiarid subtropical estuary *Limnology & Oceanography* 62: S112-S130.

Zeng, F.-W., Masiello, C. and Hockaday, W., 2011. Controls on the origin and cycling of riverine dissolved inorganic carbon in the Brazos River, Texas. *Biogeochemistry* 104: 275-291.

Ziegler, S. and Benner, R., 1998. Ecosystem metabolism in a subtropical, seagrass-dominated lagoon. *Marine Ecology Progress Series* 173: 1-12.

Zimmerman, R.C., D.G. Kohrs, D.L. Steller, and R.S. Alberte. 1997. Impacts of CO_2 enrichment on productivity and light requirements of eelgrass. *Plant Physiology* 115: 599-607.

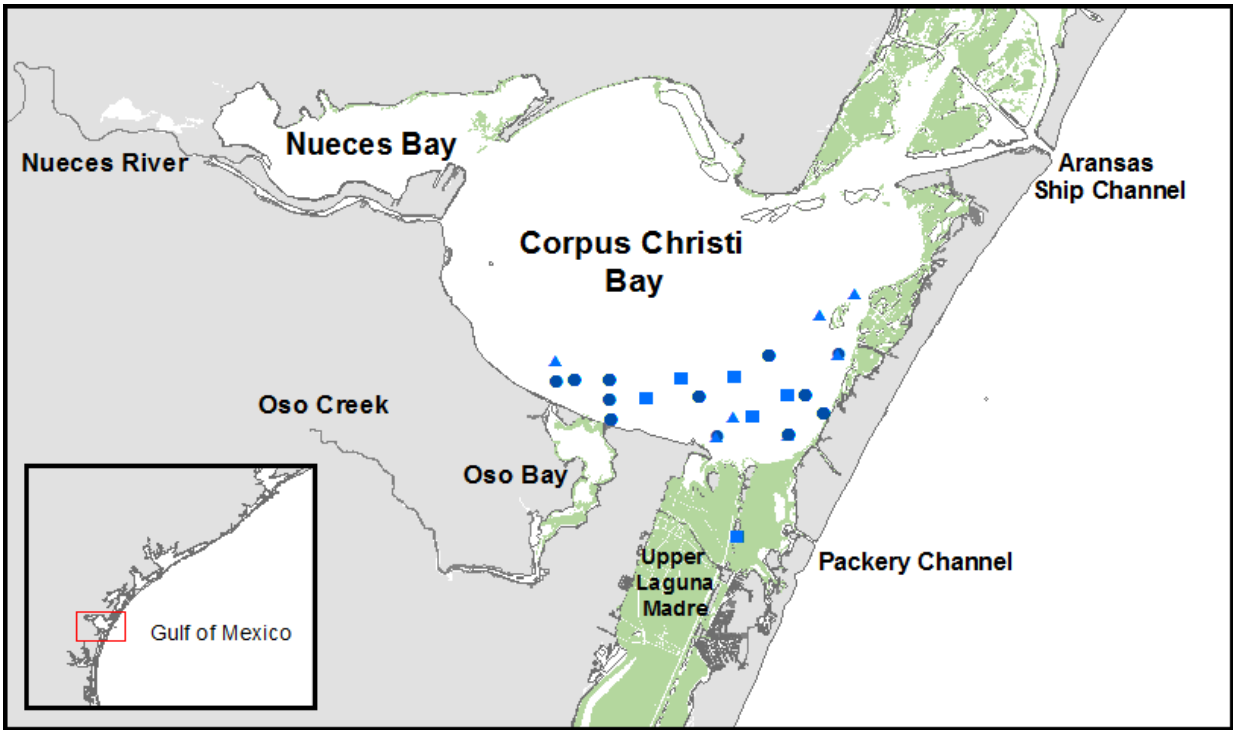

Figure 4.1. Sampling stations in southeastern Corpus Christi Bay (CCB). Stations marked with dark blue circles were sampled in both 2015 and 2016. Stations with blue triangles and squares were sampled during 2015 and 2016, respectively. Areas shaded in light green indicate seagrass habitats according to Texas Parks and Wildlife Department spatial data (https://tpwd.texas.gov/gis/)

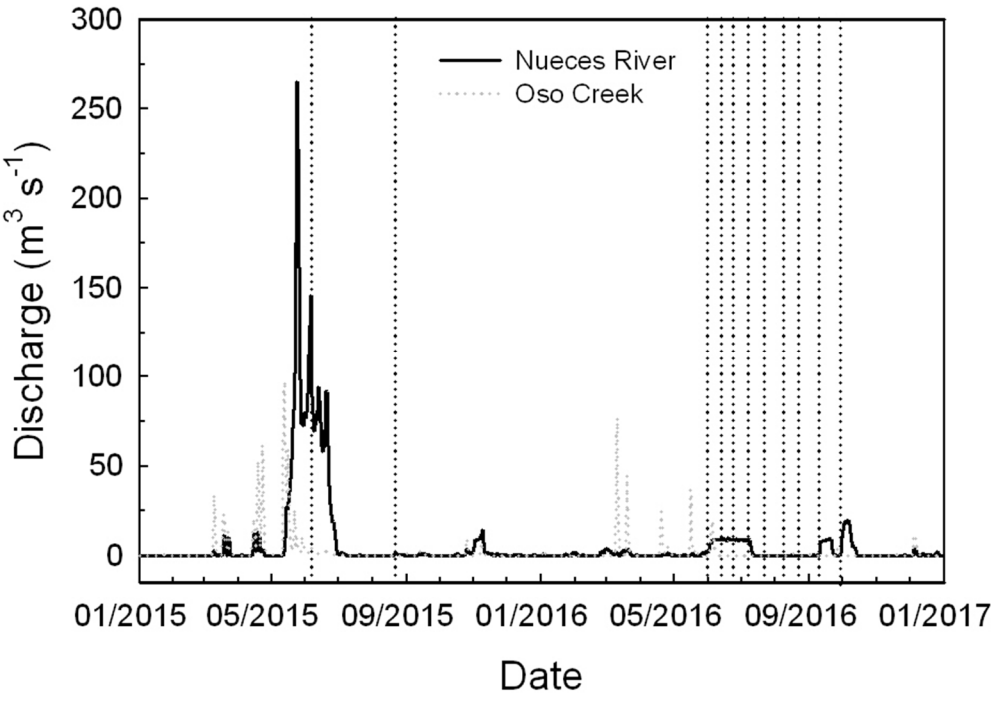

Figure 4.8. Daily discharge (m^3 s^{-1}) from the Nueces River (black) and Oso Creek (gray) into the Nueces Estuary system (https://maps.waterdata.usgs.gov/mapper/index.html). Vertical dotted lines denote the dates of sampling trips.

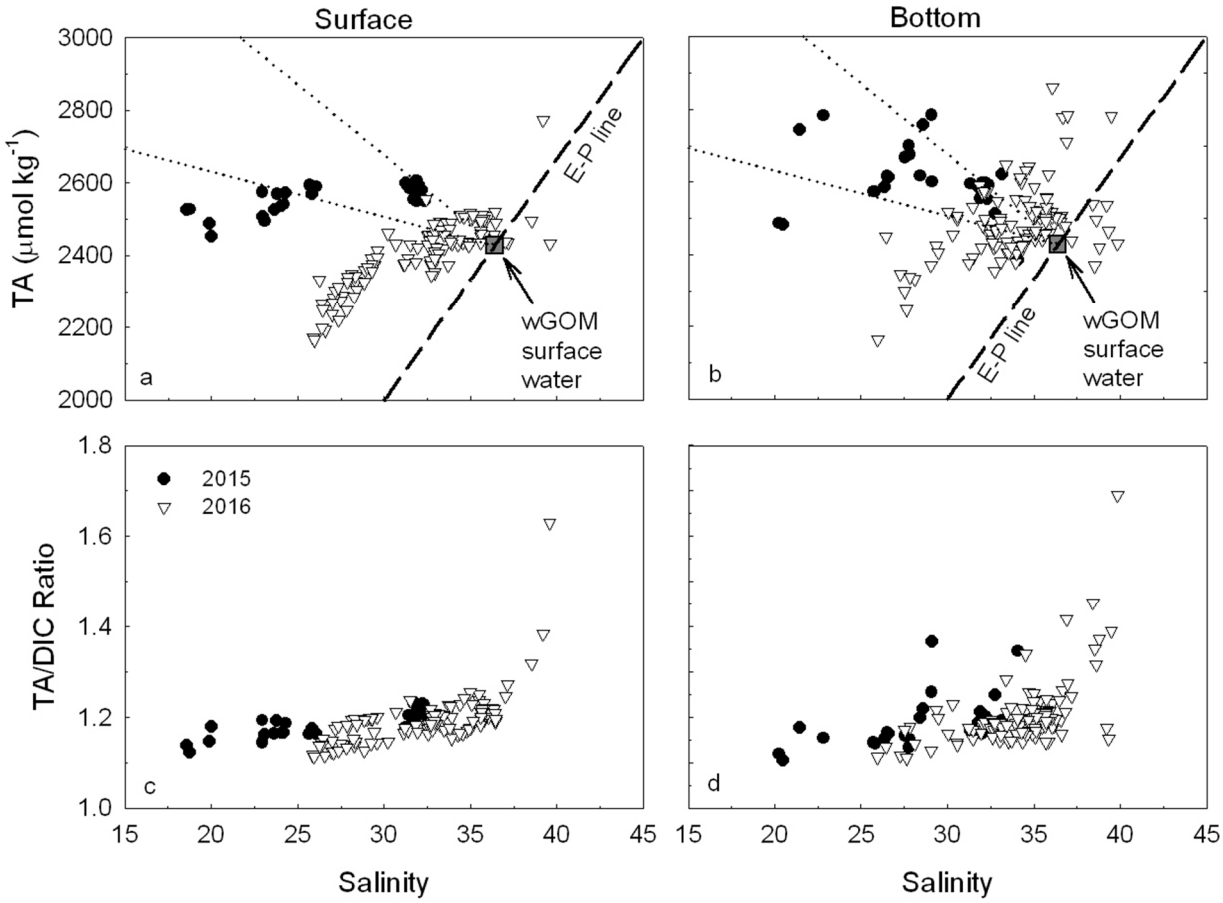

Figure 4.3. TA and TA:DIC vs. salinity in surface and bottom waters in CCB in 2015 and 2016. In a and b, the black square denotes the TA and salinity of the ocean endmember (nGoM), and the dashed line represents the evaporation-precipitation line, and the dotted lines represent potential conservative mixing lines.

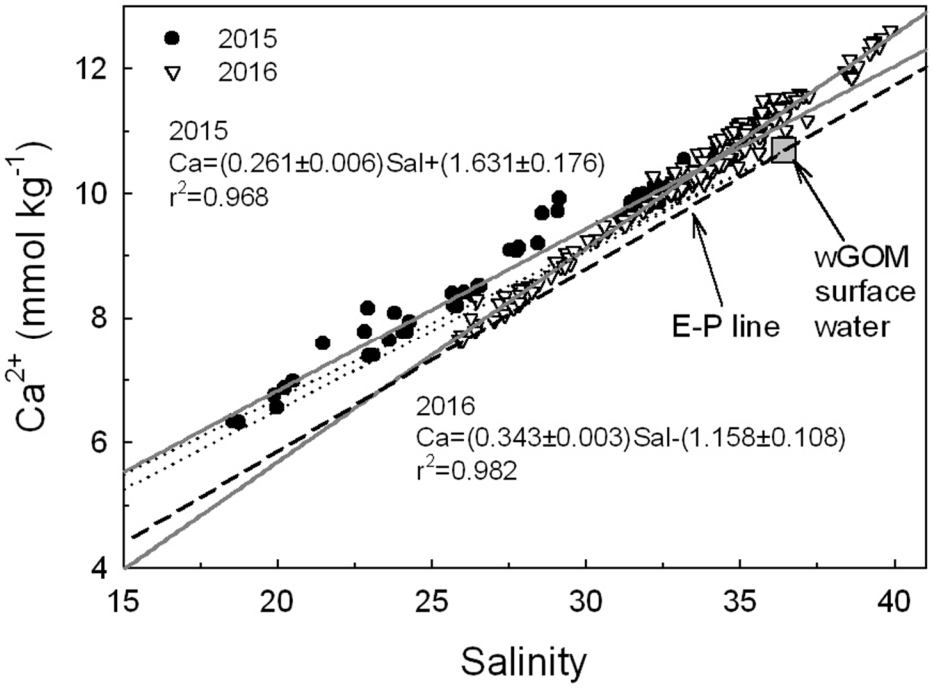

Figure 4.4. [Ca^{2+}] vs. salinity in CCB in 2015 and 2016 (both surface and bottom samples shown). The black square denotes the TA and salinity of the ocean endmember (nGoM), the dashed line represents the evaporation-precipitation line, the two dotted lines represent potential conservative mixing lines (both CCL and TCEQ river data), and the solid grey lines are the linear regression associated with each year.

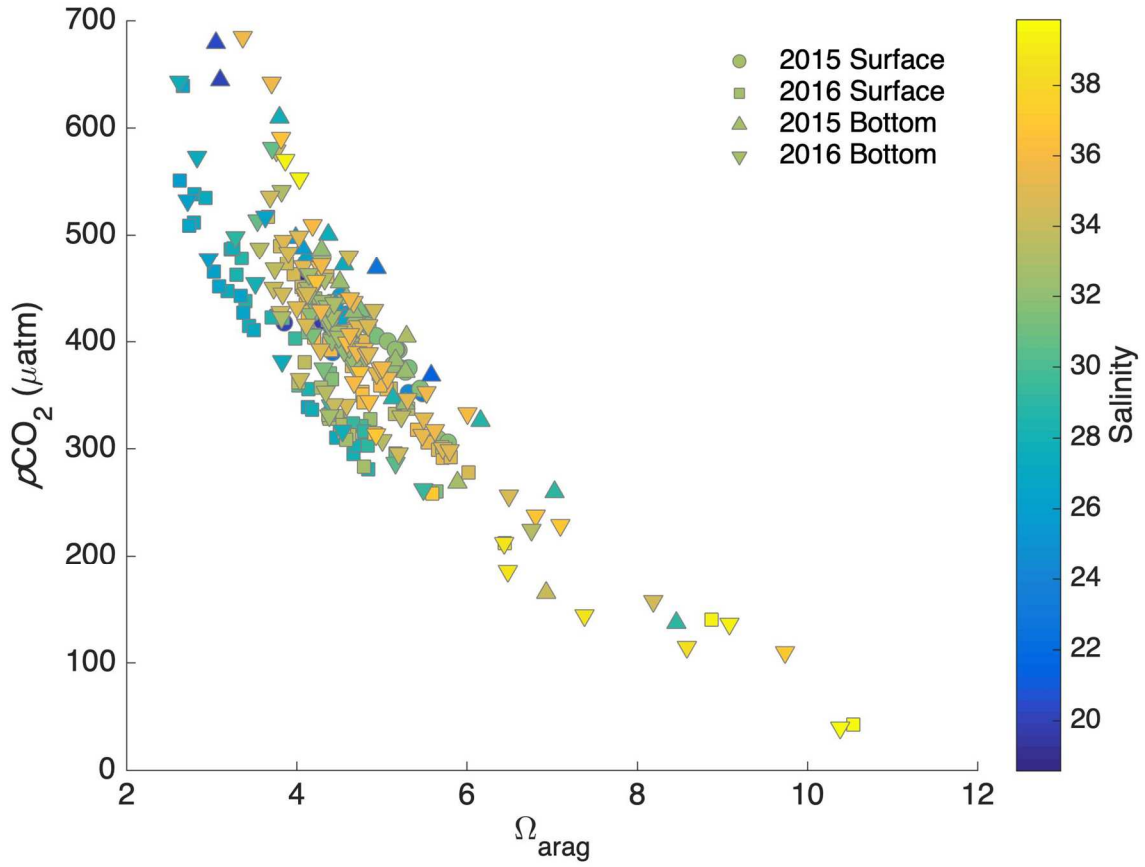

Figure 4.5. pCO_2 vs. Ω_{arag} in CCB in 2015 and 2016.

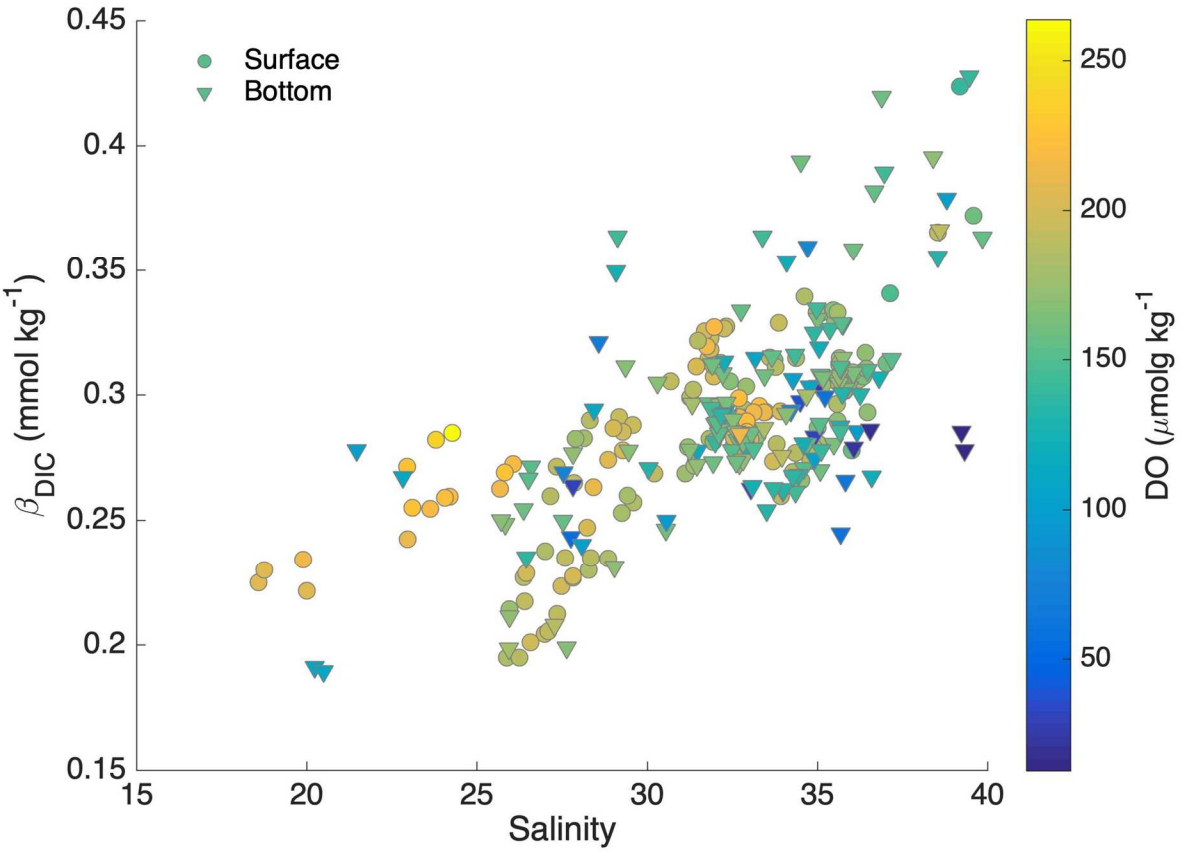

Figure 4.6. ß$_{DIC}$ in CCB surface and bottom waters in 2015 and 2016.

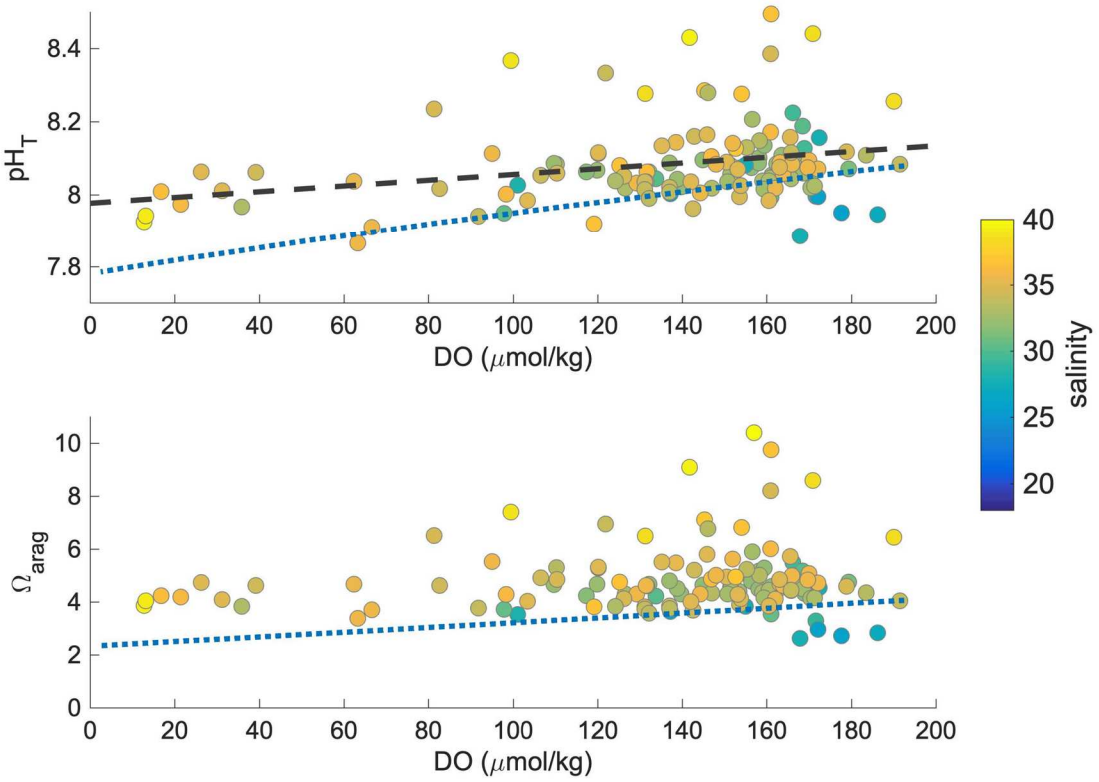

Figure 4.7. Correlation between carbonate parameters (pH and Ω_{arag}) vs. DO in bottom water of CCB in 2015 and 2016. The dotted lines represent a simulation of Texas shelf water (upper 30 m) with the starting condition: S = 36.4, TA = 2425 µmol kg^{-1}, DIC = 2063 µmol kg^{-1}, and DO = 192 µmol kg^{-1}.

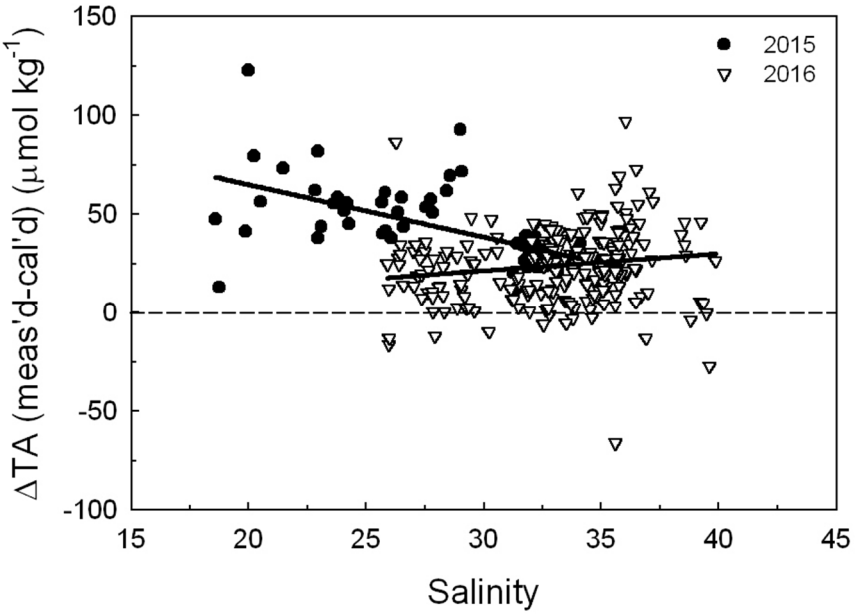

Figure 4.8. Difference between measured and calculated TA ($\Delta TA = TA_{meas'd}-TA_{calc'd}$) vs. salinity in CCB in 2015 and 2016. The 2016 ΔTA data were subtracted by 4.9 μmol kg^{-1} to account for average nutrient contribution. See text for details. Significant regression lines for each year are shown.

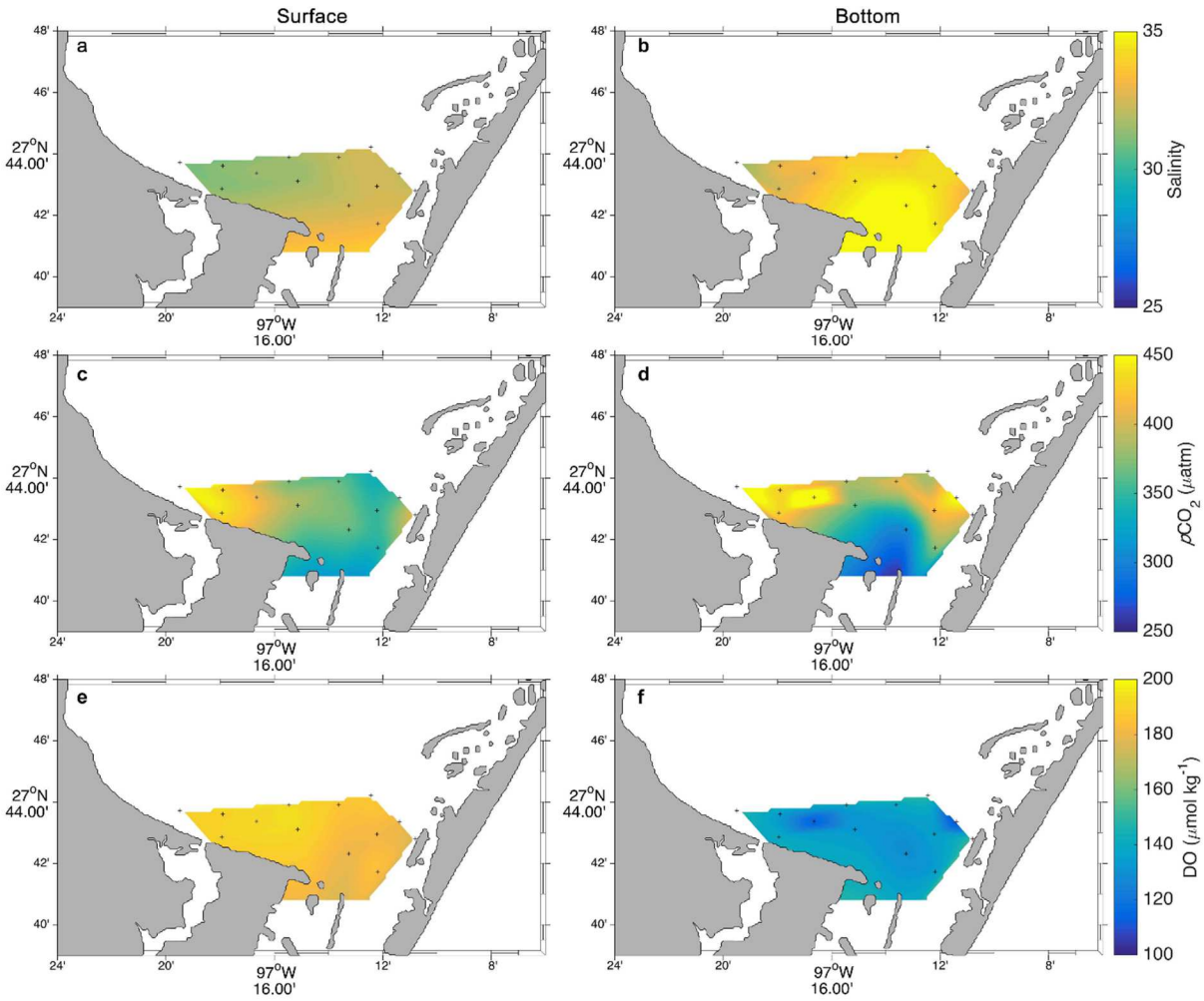

Figure 4.9. Composite spatial distribution of salinity, pCO_2, and DO in both surface (a, c, e) and bottom (b, d, f) waters in 2016.

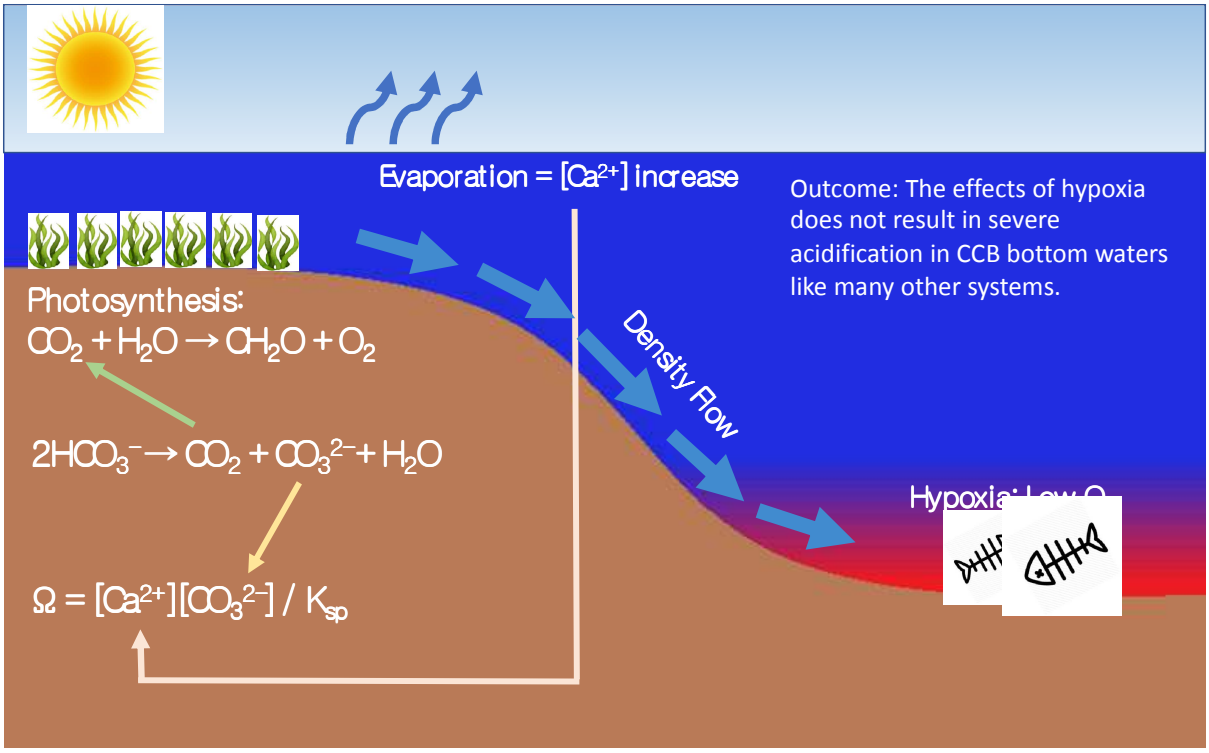

Figure 4.10. Conceptual model of seagrass meadow induced enhanced buffer and hypoxia formation in CCB.

Table 4.3. Mean hydrologic conditions (salinity and temperature), nutrients, carbonate chemistry, and dissolved oxygen conditions in the southeastern Corpus Christi Bay in a relatively wet period (2015) and relatively dry period (2016). Uncertainty represents standard deviation of the mean (including all 14 sampled stations each year and all trips conducted each year). Values inside the parentheses are the ranges of the values. NH_x is total ammonia, DSi is silicate, and DIP is dissolved phosphate.

	2015 (Wet Period)		2016 (Dry Period)	
	Surface	*Bottom*	*Surface*	*Bottom*
Temperature (˚C)	30.5±0.9 (29.2-32.2)	29.6±0.9 (28.2-31.6)	29.4±1.3 (24.4-31.1)	29.5±1.2 (26.7-31.8)
Salinity	27.7±4.8 (18.6-32.3)	28.9±3.9 (20.2-34.1)	32.3±3.3 (25.9-39.6)	33.9±2.8 (25.9-39.8)
NH_x (µmol kg^{-1})	0.51±1.23 (0-6.79)	2.36±4.37 (0.16-19.81)	-	-
DSi (µmol kg^{-1})	73.65±0.18 (61.76±90.55)	78.26±11.94 (54.18-101.35)	-	-
DIP (µmol kg^{-1})	0.23±0.16 (0.10-0.71)	0.38-0.23 (0.13-1.09)	-	-
DIC (µmol kg^{-1})	2159.1±46.7 (2071.7-2249.5)	2199.6±126.2 (1770.7-2410.6)	2023.0±72.5 (1492.9-2151.6)	2073.3±107.2 (1437.2-2323.9)
TA (µmol kg^{-1})	2561.1±37.8 (2453.4-2606.3)	2606.6±87.3 (2383.3-2784.3)	2409.4±91.4 (2164.9-2773.0)	2485.2±102.6 (2163.7-2860.6)

Ca^{2+} (mmol kg^{-1})	8.78±1.28 (6.32-9.99)	9.24±1.02 (6.87-10.63)	9.89±1.13 (7.64-12.49)	10.50±0.99 (7.64-12.61)
Ω_{arag}	4.93±0.53 (3.85-5.)	4.94±1.12 (3.05-8.46)	4.47±1.01 (2.63-10.54)	4.73±1.27 (2.62-10.39)
pH_T	8.118±0.031(8.081-8.172)	8.102±0.107 (7.935-8.445)	8.090±0.092 (7.797-8.710)	8.083±1.024 (7.866-8.721)
pCO_2 (µatm)	384.7±42.2 (305.7-448.4)	418.6±118.3 (136.9-679.1)	378.3±80.6 (42.5-639.5)	398.4±110.9 (39.4-685.5)
DO (µmol kg^{-1})	209.2±16.6 (187.4-263.6)	129.1±36.2 (29.8-179.4)	184.7±13.6 (140.2-223.1)	137.7±42.1 (12.8-191.4)
$ß_{DIC}$	0.284±0.034 (0.222-0.327)	0.287±0.040 (0.189-0.364)	0.283±0.037 (0.195-0.424)	0.294±0.040 (0.199-0.428)

Table 4.2. Comparison of hydrologic conditions and carbonate system parameters between hypoxic (DO < 93.8µmol $kg^{-}1$) and normoxic (DO > 93.8µmol kg^{-1}) bottom water conditions in Corpus Christi Bay in 2015 and 2016. Uncertainty represents standard deviation of the mean. The p-values for t-test for the comparison of the hypoxic and normoxic conditions are included, and * indicates a significant difference based on α=0.05.

	2015			2016		
	Bottom Hypoxic (n=4)	*Bottom Normoxic (n=26)*	*p-value*	*Bottom Hypoxic (n=10)*	*Bottom Normoxic (n=103)*	*p-value*
Temperature (˚C)	28.6 ± 0.3	29.7 ± 0.9	0.0001*	30.1 ± 0.4	29.5 ± 1.2	0.0007*
Salinity	27.9 ± 0.5	29.0 ± 4.2	0.2039	35.6 ± 1.8	33.7 ± 2.9	0.0023*
DIC (µmol kg^{-1})	2317.4 ± 50.0	2181.5 ± 124.9	0.0029*	2156.8 ± 49.7	2061.9 ± 108.0	<0.0001*
TA (µmol kg^{-1})	2700.3 ± 39.8	2592.1 ± 83.8	0.0030*	2542.3 ± 54.3	2477.4 ± 105.3	<0.0001*
Ca^{2+} (mmol kg^{-1})	9.25 ± 0.29	9.23 ± 1.09	0.9649	11.12 ± 0.66	10.42 ± 1.00	0.0033*
Ω_{arg}	4.72 ± 1.01	4.97 ± 1.15	0.6738	4.30 ± 0.76	4.78 ± 1.32	0.0119*
pH_T	8.065 ± 0.093	8.107 ±0.110	0.4479	7.996 ±0.090	8.095 ± 0.123	0.0002*
pCO_2 (µatm)	477.1 ± 116.9	409.6 ± 118.2	0.3431	499.9 ± 108.3	384.6 ± 104.3	0.0007*
DO (µmol kg^{-1})	59.1 ± 21.2	139.9 ± 23.7	<0.0001*	46.1± 27.8	150.2 ± 22.5	<0.0001*
$ß_{DIC}$	0.274 ± 0.033	0.288 ± 0.042	0.4802	0.278 ± 0.019	0.288 ± 0.040	0.1583

Table 4.3. Multiple linear regression (MLR) models for carbonate system parameters in Corpus Christi Bay during all 2015 and 2016 sampling events ranked by AICc. For each model, variables considered include salinity, temperature, dissolved oxygen, and all of their interactions. Only those models with a delta AICc less than 10 are shown. Models in bold are considered the best fit, and when multiple models are in bold, they are equally plausible based on the common practice of delta AICc > 2 as a threshold.

Dependent Variable	Water Depth	Independent Variables and interactions Incorporated into each model	df	logLik	AICc	delta AICc	AICc weight
pH	Surface	**DO, Sal, DO:Sal**	**5**	**177.302**	**-344.184**	**0.000**	**0.609**
		DO, Sal, Temp, DO:Sal,	6	177.313	-342.034	2.149	0.208
		DO, Sal, Temp, DO:Sal, Sal:Temp	7	177.331	-339.869	4.315	0.070
		DO, Sal, Temp, DO:Sal, DO:Temp	7	177.319	-339.843	4.341	0.069
		DO, Sal, Temp, DO:Sal, DO:Temp, Sal:Temp	8	177.335	-337.641	6.543	0.023
		DO, Sal, Temp, DO:Sal, DO:Temp, Sal:Temp, DO:Sal:Temp	9	178.338	-337.380	6.803	0.020
	Bottom	**DO, Sal, Temp, DO:Sal, Sal:Temp**	**7**	**123.283**	**-231.760**	**0.000**	**0.547**
		DO, Sal, Temp, DO:Sal, DO:Temp, Sal:Temp	**8**	**123.425**	**-229.807**	**1.953**	**0.206**
		DO, Sal, DO:Sal	5	119.383	-228.341	3.419	0.099
		DO, Sal, Temp, DO:Sal, DO:Temp, Sal:Temp, DO:Sal:Temp	9	123.456	-227.599	4.161	0.068
		DO, Sal, Temp, DO:Sal	6	119.553	-226.507	5.254	0.040
		DO, Sal, Temp, DO:Temp, Sal:Temp	7	120.023	-225.239	6.521	0.021
		DO, Sal, Temp, DO:Sal, DO:Temp	7	119.641	-224.476	7.284	0.014
		DO, Sal, DO:Sal	**5**	**-829.005**	**1668.430**	**0.000**	**0.586**
		DO, Sal, Temp, DO:Sal	6	-828.981	1670.553	2.123	0.203

pCO_2	Surface	DO, Sal, Temp, DL:Sal, DO:Temp	7	-828.782	1672.358	3.928	0.082
		DO, Sal, Temp, DO:Sal, Sal:Temp	7	-828.962	1672.718	4.288	0.069
		DO, Sal, Temp, DO:Sal, DO:Temp, Sal:Temp	8	-828.738	1674.505	6.075	0.028
		DO, Sal	4	-833.914	1676.105	7.675	0.013
		DO, Sal, Temp, DO:Sal, DO:Temp, Sal:Temp, DO:Sal:Temp	9	-828.583	1676.462	8.031	0.011
		DO, Sal, Temp	5	-833.839	1678.098	9.668	0.005
	Bottom	**DO, Sal, DO:Sal**	**5**	**-875.132**	**1760.689**	**0.000**	**0.303**
		DO, Sal, Temp, DO:Sal, Sal:Temp	**7**	**-873.031**	**1760.867**	**0.178**	**0.278**
		DO, Sal, Temp, DO:Sal	**6**	**-874.931**	**1762.462**	**1.774**	**0.125**
		DO, Sal, Temp, DO:Sal, DO:Temp, Sal:Temp	**8**	**-872.749**	**1762.542**	**1.853**	**0.120**
		DO, Sal, Temp, DO:Sal, DO:Temp	7	-874.709	1764.223	3.535	0.052
		DO, Sal, Temp, DO:Temp, Sal:Temp	7	-874.890	1764.586	3.897	0.043
		DO, Sal, Temp, DO:Sal, DO:Temp, Sal:Temp, DO:Sal:Temp	9	-872.702	1764.717	4.028	0.040
		DO, Sal, Temp, DO:Temp	6	-876.983	1766.567	5.878	0.016
		DO, Sal	4	-879.634	1767.550	6.861	0.010
		DO, Sal, Temp, Sal:Temp	6	-877.574	1767.749	7.060	0.009
		DO, Sal, Temp	5	-879.533	1769.491	8.802	0.004
Ω_{ar}	Surface	**DO, Sal, Temp, DO:Sal**	**6**	**-152.599**	**317.789**	**0.000**	**0.354**

		DO, Sal, Temp, DO:Sal, DO:Temp, Sal:Temp, DO:Sal:Temp	**9**	**-149.449**	**318.192**	**0.403**	**0.289**
		DO, Sal, Temp, DO:Sal, Sal:Temp	**7**	**-152.326**	**319.446**	**1.657**	**0.154**
		DO, Sal, Temp, DO:Sal, DO:Temp	**7**	**-152.434**	**319.662**	**1.873**	**0.139**
		DO, Sal, Temp, DO:Sal, DO:Temp, Sal:Temp	8	-152.083	321.194	3.405	0.064
	Bottom	**DO, Sal, Temp, DO:Sal, Sal:Temp**	**7**	**-214.459**	**443.725**	**0.000**	**0.592**
		DO, Sal, Temp, DO:Sal, DO:Temp, Sal:Temp	**8**	**-214.335**	**445.713**	**1.988**	**0.219**
		DO, Sal, Temp, DO:Sal, DO:Temp, Sal:Temp, DO:Sal:Temp	9	-214.272	447.858	4.133	0.075
		DO, Sal, Temp, DO:Sal	6	-217.778	448.156	4.431	0.065
		DO, Sal, Temp, DO:Sal, DO:Temp	7	-217.701	450.208	6.483	0.023
		DO, Sal, DO:Sal	5	-219.998	450.421	6.696	0.021
		DO, Sal, Temp, DO:Temp, Sal:Temp	7	-219.207	453.220	9.495	0.005

Supplementary Materials

Figure S4.1. Spatial distributions of dissolved oxygen (DO) and salinity and surface and bottom waters of the southeastern Corpus Christi Bay during the 2015 and 2015 trips.

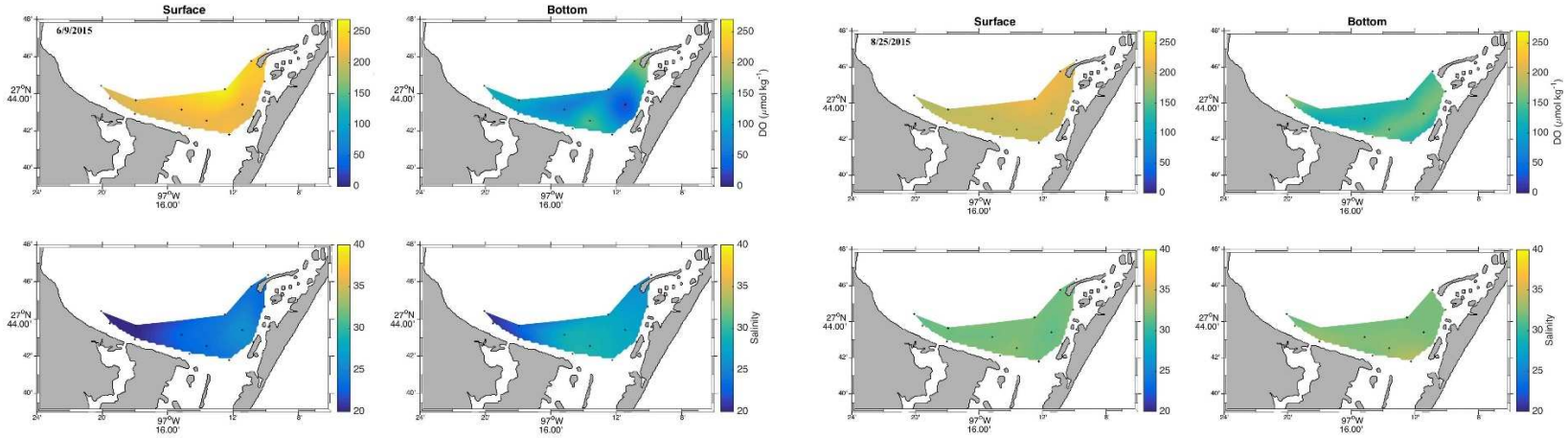

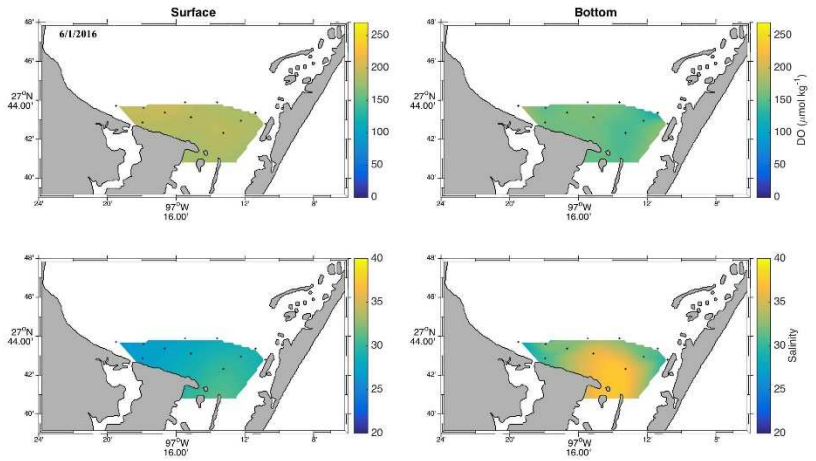
Surface
Bottom
6/1/2016
DO (μmol kg⁻¹)
Salinity
27°N
44.00'
97°W
16.00'

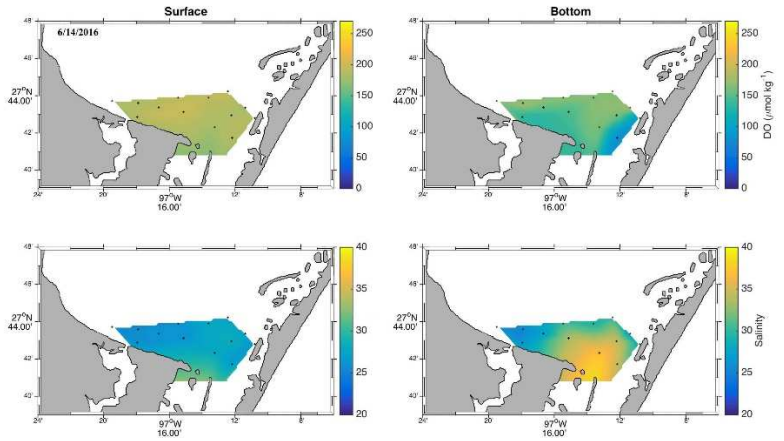
Surface
Bottom
6/14/2016
DO (μmol kg⁻¹)
Salinity
27°N
44.00'
97°W
16.00'

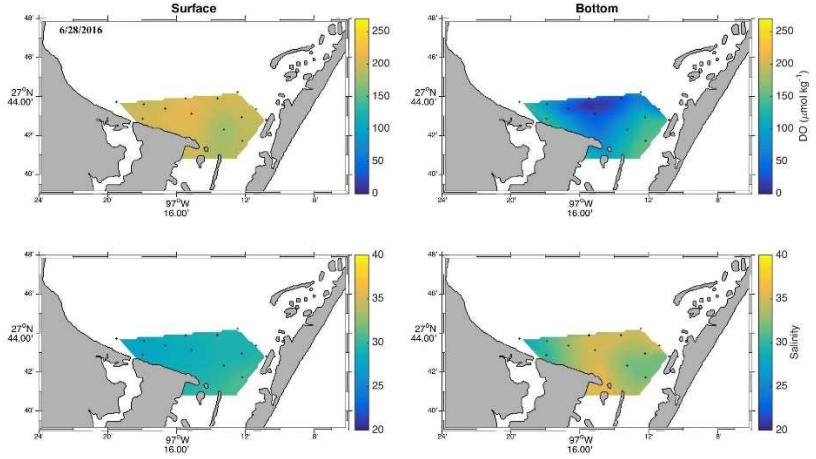
Surface
Bottom
6/28/2016
DO (μmol kg⁻¹)
Salinity
27°N
44.00'
97°W
16.00'

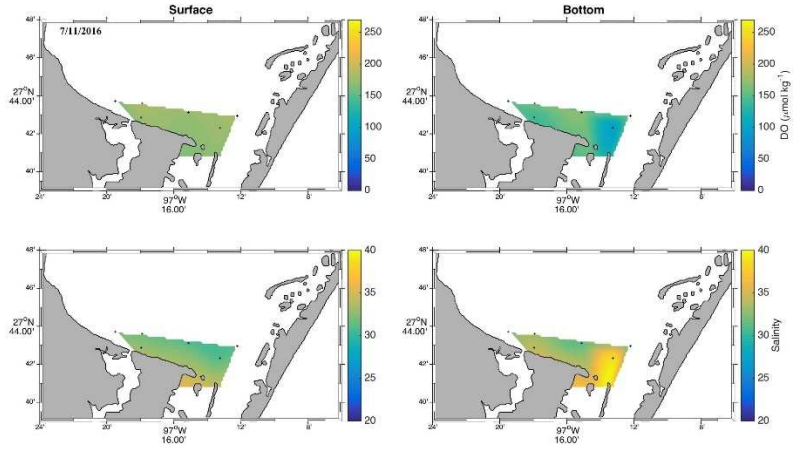
Surface
Bottom
7/11/2016
DO (μmol kg⁻¹)
Salinity
27°N
44.00'
97°W
16.00'

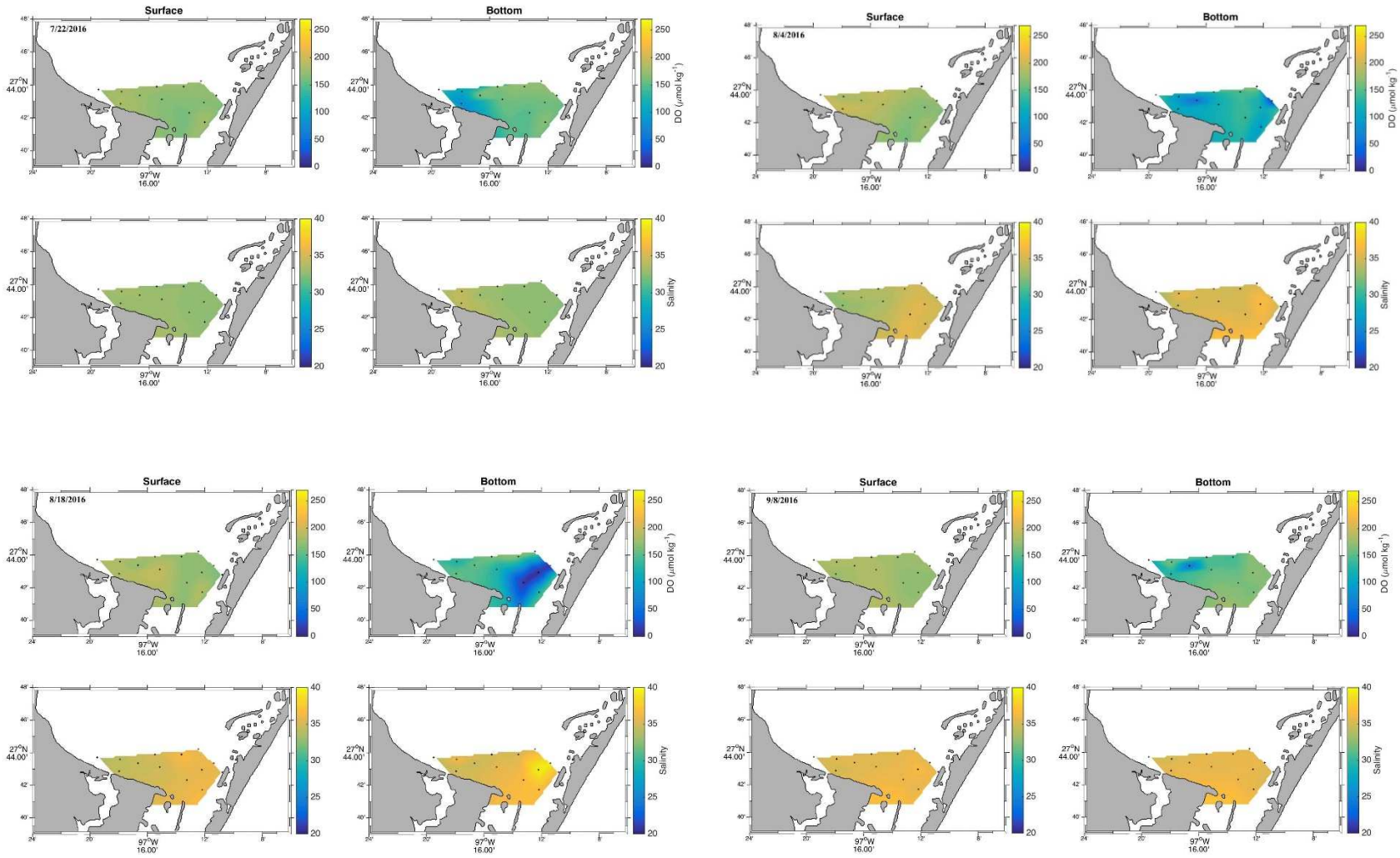
Surface
Bottom
7/22/2016
8/4/2016
8/18/2016
9/8/2016
27°N
44.00'
97°W
16.00'
DO (μmol kg⁻¹)
Salinity

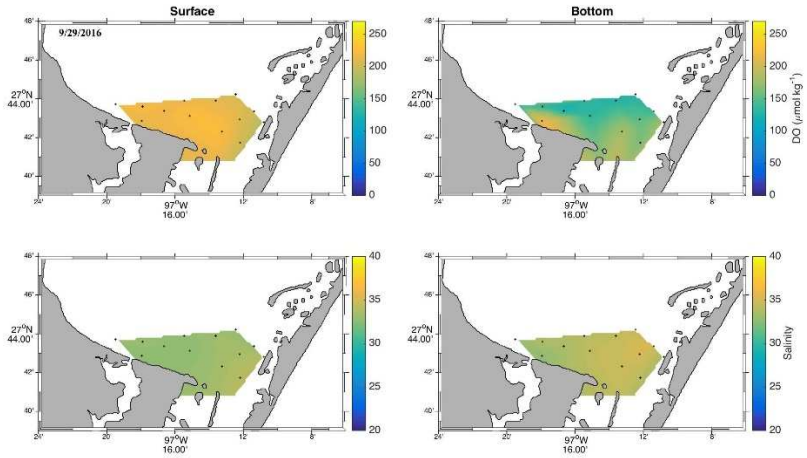
Surface
Bottom
9/29/2016
27°N
44.00'
97°W
16.00'
DO (μmol kg⁻¹)
Salinity

Figure S4.2. Spatial distributions of pCO_2, pH, and Ω_{arag} in surface and bottom waters of the southeastern Corpus Christi Bay during the 2015 and 2016 trips.

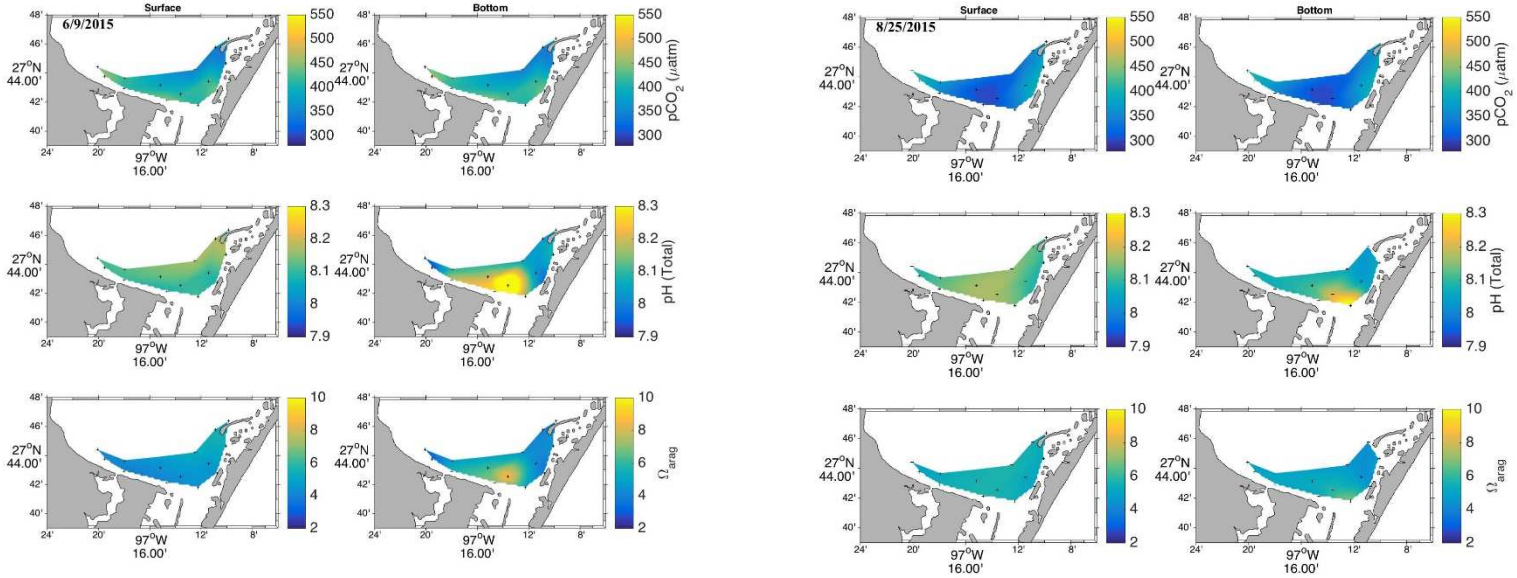

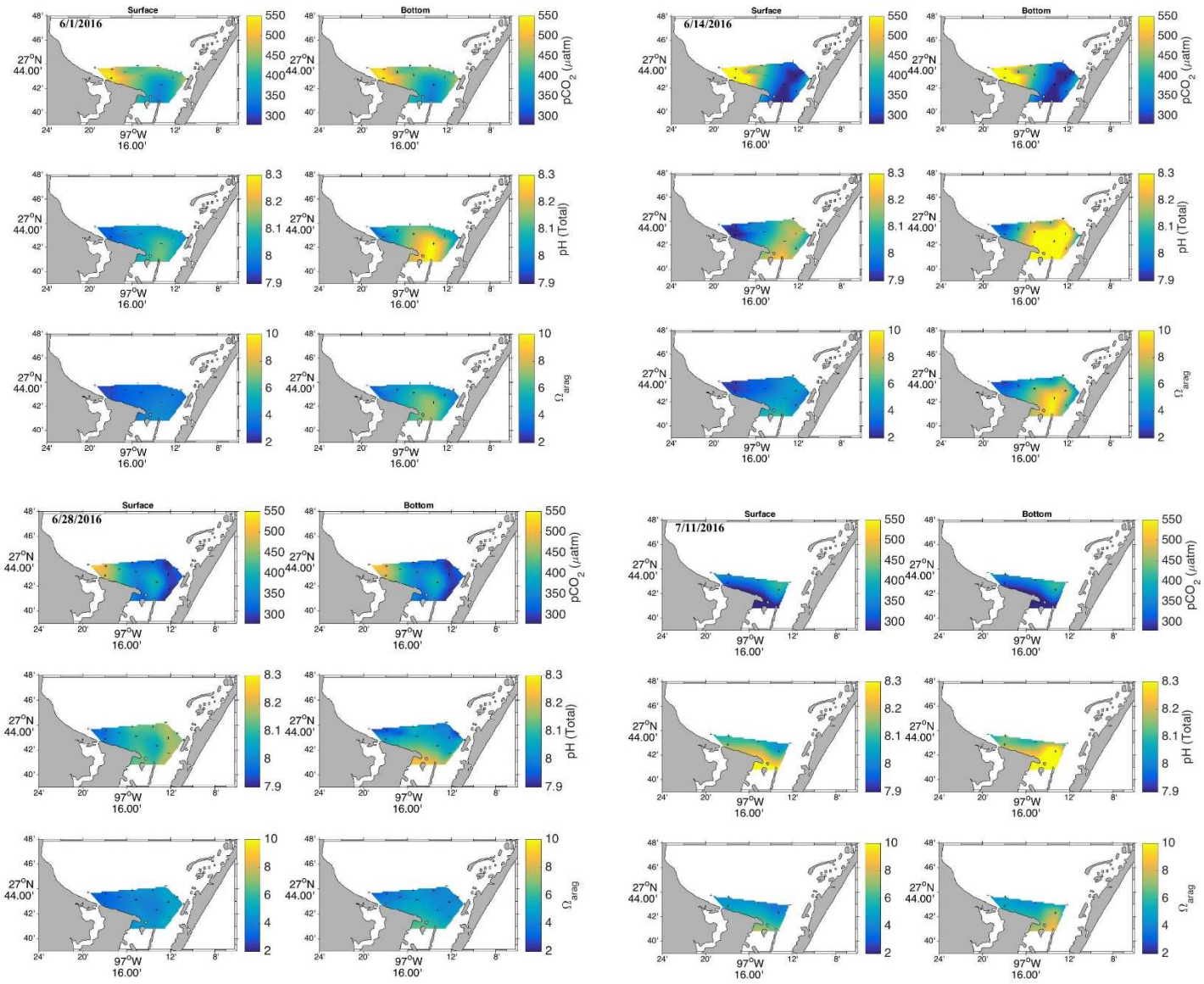
Surface
Bottom
6/1/2016
6/14/2016
6/28/2016
7/11/2016
27°N 44.00'
97°W 16.00'
pCO2 (μatm)
pH (Total)
Ωarag

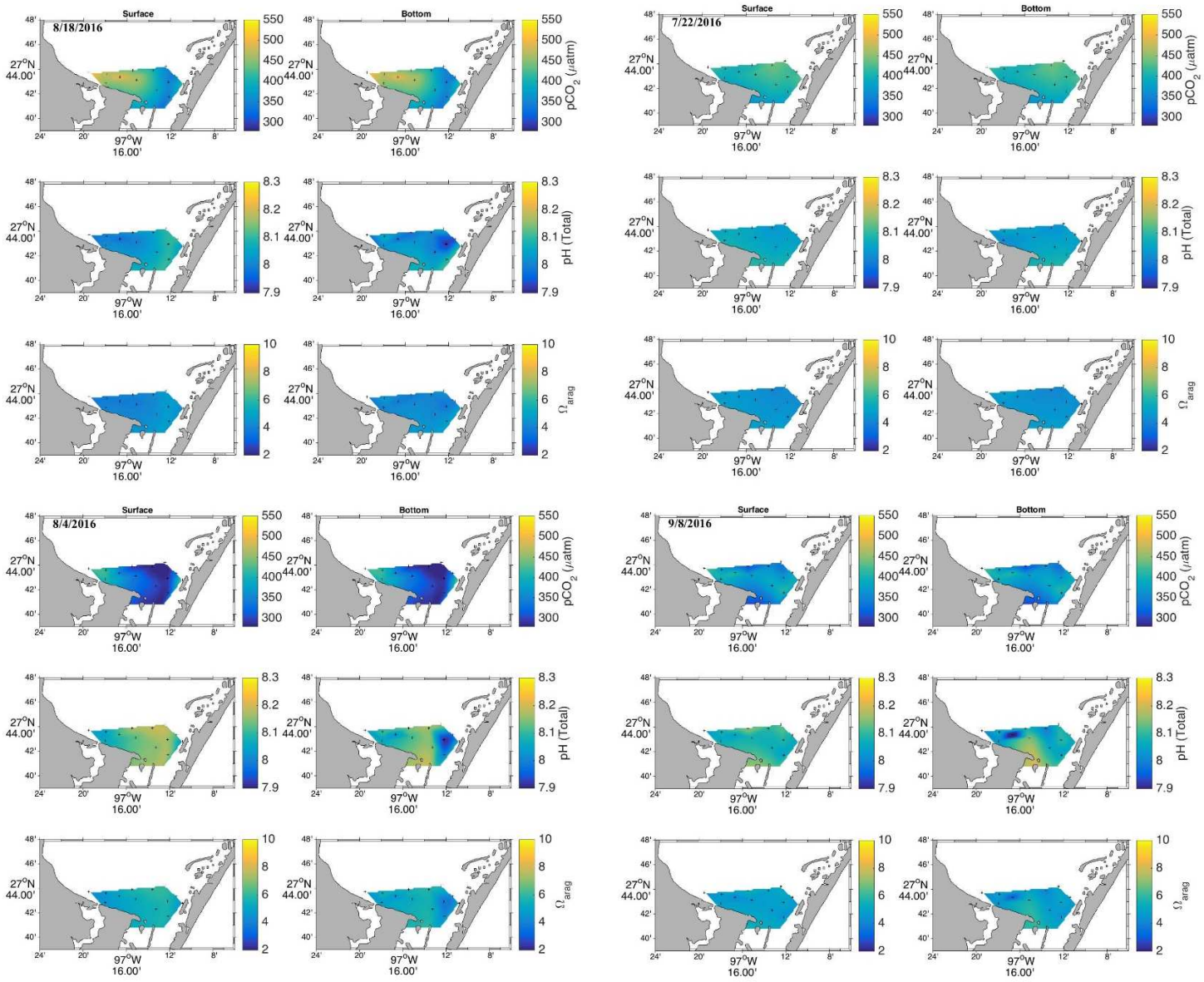
Surface
Bottom
8/18/2016
7/22/2016
8/4/2016
9/8/2016
27°N 44.00'
97°W 16.00'
pCO2 (μatm)
pH (Total)
Ωarag

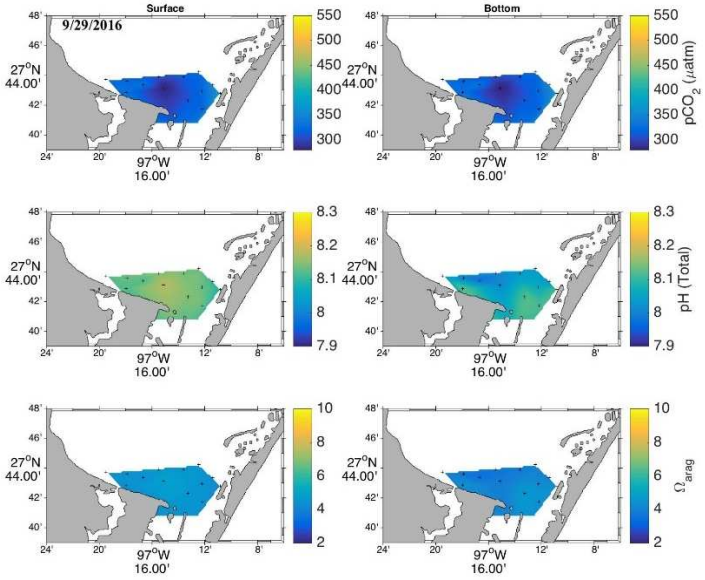
Surface
Bottom
9/29/2016
27°N 44.00'
97°W 16.00'
24' 20' 12' 8'
48' 46' 42' 40'
550 500 450 400 350 300
pCO2 (μatm)
8.3 8.2 8.1 8 7.9
pH (Total)
10 8 6 4 2
Ωarag

CHAPTER V: CONCLUDING SUMMARY

This dissertation investigated variability in carbonate chemistry in estuaries of the northwestern Gulf of Mexico (nwGOM), including both temporal variability from diel to decadal timescales and spatially variability within and between estuaries. In addition, relationships between the carbonate system and other environmental parameters were investigated. This type of work is applicable to the health of coastal ecosystems and economies, as suitable carbonate chemistry is required by calcifying organisms, e.g., Eastern oysters, which are both ecosystem engineers and the products of a profitable industry in the estuaries of the nwGOM.

Using one of the longest-running estuarine datasets that includes routine measurements of adequate parameters to calculate the full carbonate system, Chapter II revealed long-term trends in the most biologically relevant—saturation state of aragonite (Ω_{Ar}) and partial pressure of CO_2 (pCO_2)—and the most carbon budget-relevant—pCO_2 and dissolved inorganic carbon (DIC)—parameters at 54 stations in seven estuaries across a latitudinal gradient in the nwGOM. With the notable exceptions of the northernmost and southernmost estuaries and individual stations near direct freshwater input, nwGOM estuaries generally experienced long-term increases in pCO_2 and decreases in DIC and Ω_{Ar} (both tied to decreasing alkalinity) over past decades, with the magnitude of change generally increasing from south to north. Despite the relatively coarse analytical precision of parameters used in calculations and the resulting, high propagated error associated with calculated parameters, simulation analyses that accounted for the propagated error generally confirmed the direction and magnitude of long-term trends.

Given that the rates of pCO_2 were greater than that of the atmosphere, this study implies that nwGOM estuaries have become a greater source of CO_2 to the atmosphere over past

decades. The decreasing Ω_{Ar}, while currently remaining mostly above the saturation level across the region, suggests that carbonate chemistry of the region may have become less suitable for biological calcification. Additionally, long-term decreases in the buffer factor β_{DIC} were detected in many stations across nwGOM estuaries, indicating that the pH response of estuaries to DIC addition has become more sensitive over time.

Chapter III used pH and pCO_2 data from both sensor deployments (10 months) and discrete sample collection (5+ years) to characterize carbonate system variability in a tidal inlet in the nwGOM (Aransas Ship Channel). Significant seasonal variability and diel variability in carbonate system parameters were both present at the location, though the magnitude of both types of temporal fluctuations were not as large as other coastal areas that have been studied. The diel pattern in pCO_2 was not consistent across the sensor deployment; summer months displayed the expected, biologically driven day-night difference, while winter months showed a reversal of this pattern. Multiple analyses using data from co-located environmental sensors gave insight to driving forces of the carbonate chemistry at this location, which appear to include temperature, freshwater influence, biological activity, and tide level (despite the small tidal range in the area).

Additionally, it was concluded that carbonate chemistry (particularly pCO_2) is an important contributor to overall system variability on both diel and seasonal scales. These insights to system variability and drivers support the need for carbonate chemistry sensor deployments in estuarine environments (where high-frequency data has been extremely limited) and the utility of co-locating with other environmental sensors. However, comparisons between continuous data and discrete bottle samples suggested—despite known temporal variability on shorter timescales—that discrete sampling was generally representative of the average carbonate system (including the average CO_2 flux) on a seasonal and annual basis. This validates the use of

discrete sample collection for carbonate system characterization when sensors are unable to be deployed.

Chapter IV investigated carbonate chemistry in a semi-enclosed lagoonal estuary in the nwGOM (Corpus Christi Bay, CCB) that experiences periodic summertime hypoxia. The study incorporated data from two different years that experienced very different hydrological conditions, which highlighted that freshwater inflow is also an important control of carbonate chemistry. In conjunction with occurrences of hypoxia, the bay experienced respiration-induced acidification. However, the magnitude of decline in pH and Ω_{Ar} associated with hypoxia was much less than other coastal regions in previous literature, never reaching critically low levels. This high buffer capacity was attributed to a combination of high-alkalinity river inflow, high productivity in seagrass meadows, evaporation, and water flow patterns. The mild response of the carbonate system to hypoxia is a unique response that highlights the importance of intrinsic buffer capacity for system response.

Estuaries deserve continued attention in carbonate system studies, as estuaries are densely populated with organisms that rely on suitable water chemistry, and there is great heterogeneity in conditions between and within estuaries (e.g., Chapter II illustrated opposite-sign long-term trends in close proximity within estuaries). Together, the chapters of this dissertation demonstrate that the carbonate chemistry of the nwGOM estuaries remains in fair condition, with relatively high mean pH, TA, Ω_{Ar} and β_{DIC}. These well buffered estuaries, which also experienced less intense diel and seasonal fluctuations, have the potential to provide an important refuge for sustainable shellfish production in the United States when compared to the higher latitudes that have experienced deteriorating conditions. As Texas expands its oyster aquaculture industry following the passage of Senate Bill 682 in 2019 and capitalizes on the suitable

conditions for oyster reef restoration, there is a need to improve project siting by including carbonate chemistry data (specifically Ω_{Ar} and its temporal fluctuations) into existing oyster restoration and aquaculture suitability indices. Current data are not yet adequate to fully support such an effort. While the work in this dissertation is a small step toward filling the substantial gaps in carbonate chemistry data coverage that remain in estuaries (which are particularly prominent in GOM estuaries), additional spatial coverage in needed, especially of diel fluctuations in carbonate chemistry. Additional experimentation to clearly define thresholds of negative effects to oyster larvae may also be needed to appropriately include Ω_{Ar} in suitability indices.

Despite that estuarine conditions in the nwGOM are currently suitable for calcifiers, the long-term decreases in Ω_{Ar} and β_{DIC} as well as hypoxia-associated, respiration-driven acidification that have been revealed by this dissertation indicate that future mitigation efforts may be necessary to ensure that these estuaries maintain their relatively suitable conditions. Climate change is expected to lead to drier conditions in the southwestern United States, and human populations are continually growing in the coastal region, leading to increased demand for freshwater resources. Together, these issues may worsen the long-term deterioration of carbonate chemistry as the unique, high-TA rivers in the region will deliver less TA to estuaries. Future studies are needed to clearly define desirable carbonate chemistry outcomes and tie those outcomes to specific management actions. Based on the observations in this dissertation that freshwater inflow and net community metabolism are both important drivers of carbonate chemistry, regulation of freshwater inflow (i.e., requiring minimum flow levels) and reduction of nutrient loading into estuaries (i.e., leveraging the Environmental Protection Agency's Total

Maximum Daily Loads (TMDLs) to reduce nutrient delivery to estuaries) may be important management avenues.

LIST OF APPENDICES

APPENDICES PAGE

Appendix 1 - Copyright release of Chapter IV

SPRINGER NATURE LICENSE
TERMS AND CONDITIONS
Apr 01, 2021

This Agreement between Ms. Melissa McCutcheon ("You") and Springer Nature ("Springer Nature") consists of your license details and the terms and conditions provided by Springer Nature and Copyright Clearance Center.

License Number	5040291316283
License date	Apr 01, 2021
Licensed Content Publisher	Springer Nature
Licensed Content Publication	Estuaries and Coasts
Licensed Content Title	Characteristics of the Carbonate System in a Semiarid Estuary that Experiences Summertime Hypoxia
Licensed Content Author	Melissa R. McCutcheon et al
Licensed Content Date	Jun 13, 2019
Type of Use	Thesis/Dissertation
Requestor type	academic/university or research institute
Format	print and electronic
Portion	full article/chapter
Will you be translating?	no
Author of this Springer Nature content	yes
Title	Spatial and temporal trends and controlling factors of CO2 chemistry in the estuaries of the northwestern Gulf of Mexico
Institution name	Texas A&M University-Corpus Christi
Expected presentation date	Apr 2021
Order reference number	5020330327029